PROPERTIES OF TRAPPED ELECTRONS

Bruce C. R. Ewan

Chemistry Department

Glasgow University

October 1974

ProQuest LLC.
789 East Eisenhower Parkway
P.O. Box 1346
Ann Arbor, MI 48106 – 1346

ABSTRACT

The current experimental evidence relating to absorption spectra, spontaneous decay and photobleaching of electrons trapped in non-ionic media is reviewed and the present state of the trapped electron theories which have been applied to these systems is discussed.

Localised molecular orbital studies are performed on the hydrogen bonding interaction and the results are discussed in relation to present semi-continuum theories.

The relevance of photoionisation spectra to trapped electron absorption in ice is investigated by considering the sensitivity of spectral features to well parameters for some simple potentials.

The spontaneous short term decay of electrons at low temperature is investigated by means of a tunneling model which incorporates electron-scavenger distribution features. Electron-parent cation distributions are also considered and the results discussed in relation to the 'spur' model.

A general photobleaching scheme is presented and quantum efficiencies are evaluated for ice and two organic media. In the former the wavelength dependence is reproduced by means of a mobile electron capture model whilst in the latter, bleaching by means of tunneling from long lived excited states is considered.

Acknowledgements

I would like to extend my thanks to Dr. Brian Webster for his many helpful suggestions during the course of this work.

I also thank my wife for her assistance in the typing, and the Science Research Council for their financial support.

CONTENTS

CHAPTER 1

INTRODUCTION

Trapped electrons in liquids and solids are electrons which are localised in particular regions of the medium but whose properties cannot be described in terms of conventional molecular ions. The concept of such a species arose initially from the need to explain some of the unusual physical properties associated with solutions of alkali metals in ammonia (1). Such properties included the large volume expansion accompanying solution and its behaviour with concentration and the relatively high electrical conductivity.

These observations suggested that alkali metal atoms behaved as 'salts', dissociating in solution into cations and electrons, the latter becoming solvated and occupying a finite volume. From the volume expansion measurements, the radius of the ammoniated electron was estimated as 3.0-3.4A^{o} and it was envisaged that the electron was maintained in a state of localisation by the well provided by surrounding solvent molecules (2) and long range polarisation of the medium (3). In addition, the intense visible absorption which these solutions exhibited was regarded as arising from transitions to higher states of such a polarisation potential.

The notion that electrons could play a role as'anions' had much success in accounting for the origin of colour centres in alkali halide crystals (4) following irradiation. In these the electron was regarded as occupying an anion vacancy, being bound by an effective positive charge at the centre of the cavity.

The possibility that solvated electrons may exist in water was first suggested by Stein and Platzman (5) on the basis of the observed reduction products following X irradiation. Later ionic strength studies of reaction rates revealed that one of the

reducing species had a unit negative charge (6). With the development of the electron pulse radiolysis technique, the hydrated electron was finally identified by means of its visible absorption spectrum which was similar to that of the ammoniated species (7).

Following these early observations it has since been found that trapped electrons may be produced in a wide variety of media (8) ranging from alkane glasses to the polar alkaline ices. Methods of production include irradiation by high energy light or particles, chemical reaction and photoionisation of impurity solutes.

The various aspects of excess electrons which have received much investigation concern both macroscopic and microscopic properties. In the former category are such features as volume expansion and surface tension changes (1). Microscopic properties are naturally divided between those relating to pre-trapped electrons and those which are a feature of the trapped state.

Since electrons resulting from an external radiation source are trapped in a liquid in a time less than psecs, and since their high reactivity toward oxidising agents gives them a lifetime of the order of usecs at ordinary temperatures, early models for the behaviour of pre-trapped electrons were based on the relative yields of their long term reaction products (9). Such models depicted an initial distribution of trapped electrons and reactive solutes from which the various reaction products were obtained by application of diffusion kinetics. From these considerations there developed the spur model of Samuel and Magee (10,11) in which it was envisaged that mobile electrons, resulting from primary and secondary ionisation, lost their excess energy to electronic and vibrational excitations in the medium, becoming trapped relatively close to their parent cations. For well sep-

arated primary events, the passage of radiation was thus regarded as giving rise to local regions of radiation damage or spurs.

Properties which relate to the trapped state include visible and e.s.r. absorption spectra, energies of formation, reactivities and lifetimes, formation times and photobleaching.

Optical absorption maxima for various systems lie in the 0.5-2.0ev range and associated half widths range from 0.5-1.0 ev. Spectra are unsymmetrical having a high energy tail extending to several ev, and many exhibit a temperature dependence, shifting to the blue and narrowing as the temperature is lowered.

Lifetimes for the trapped species are also strongly affected by temperature and in most systems effective stability is reached at temperatures around 70^{o}K. Such a state of stability may be removed however by the action of light lying within the absorption range of the electron, the process being termed photobleaching, and the energy threshold for such bleaching within the absorption band has had important consequences in the assignment of the excited states of the trapped species. The above properties are described in some detail in Chapter 3.

The theoretical account of microscopic properties has been largely directed toward a description of the nature of the ground and excited states as reflected in energies of formation and absorption spectra. In many of these, the notion that bound excited states are involved has had much success within various models in reproducing observed transition energies, whilst current estimates of the band width remain underestimated. The similarity of spectra to ionisation profiles has prompted others to suggest that delocalised excited states are involved (12) and band shapes calculated within such a model are capable of reproducing many

of the observed features. A review of the recent theories which have been applied to non-ionic media is presented in Chapter 4.

With the refinement of pulse techniques, times of the order of psec have now become accessible for study, making possible the observation of solvent relaxation processes in liquids. These have revealed in the case of liquid water that trapped electrons exist within 2psec (13) and solvent relaxation proceeds for a further 2psec. It is expected that a more detailed description of the electron-solvent interaction will provide an explanation for such short relaxation times.

Short term studies in low temperature solids have revealed similar relaxation phenomena (14,15) and in addition, that a substantial fraction of electrons are lost through recombination with scavengers following their formation.

Following from the discussion of Chapter 4, calculations are presented in Chapter 5.1 on the hydrogen bonding interaction within a localised molecular orbital framework in an attempt to discover the extent to which molecular interactions at the surface of an electron cavity are likely to modify the well parameters in present semi-continuum theories. In addition the nature of the charge redistribution is elucidated and the possible effect of an excess electron on molecular relaxation is discussed.

In 5.2 the properties of photoionisation spectra are investigated for some simple potentials to discover the sensitivity of spectral features to well parameters. A range of potentials are chosen to reproduce the observed spectral maxima in pure and alkaline ice, and for the additional spectral properties of energy threshold, half width and intensity, it is shown that for particular potentials parameters can be chosen to represent alkaline ice.

Following from the discussion in Chapter 3.2 on the short term decay characteristics of electrons in low temperature solids, a tunneling decay scheme is considered in 5.3 with the incorporation of electron scavenger distribution features. The model is applied to the observed decay in pure ice, 3 methyl pentane and methyl-tetrahydrofuran.

In 5.4 a general method is presented to represent the quantum efficiency for photobleaching. The model is firstly applied within a mobile electron capture scheme to the wavelength dependence of bleaching in pure ice and secondly to the decay of long lived bound excited states by a tunneling mechanism. In Chapter 2 a review is presented of the theories used in the calculations.

REFERENCES

1 G. Lepoutre, M. J. Sienko 'Metal Ammonia Solutions' W. A. Benjamin (1964)

2 R. A. Ogg Phys. Rev. 69,668,(1946)

3 J. Jortner J. Chem. Phys. 30(3),839,(1959)

4 W. B. Fowler 'Physics of Colour Centres' Academic Press 1968

5 G. Stein Disc. Faraday Soc. 12,227,(1952)

6 G. Czapski, H. A. Schwarz J. Phys. Chem. 68,1169,(1964)

7 E. J. Hart, J. W. Boag J. Amer. Chem. Soc. 84,4090,(1962)
E. J. Hart, M. Anbar 'The Hydrated Electron' Wiley-Interscience (1970)

8 L. Kevan 'Radiation Chemistry of Aqueous Systems' Ed. G.Stein
T. Shida J. Phys. Chem. 73(12),4311,(1969)

9 J. L. Magee, M. Burton J. Amer. Chem. Soc. 73,523,(1951)
P. J. Dyne, J. M. Kennedy Can. J. Chem. 36,1518,(1958)

10 J. L. Magee J. Amer. Chem. Soc. 73,3270,(1951)
A. H. Samuel, J. L. Magee J. Chem. Phys. 21(6),1080,(1953)
A. K. Ganguly, J. L. Magee J. Chem. Phys. 25(1),129,(1956)

11 A. Mozumder, J. L. Magee Rad. Res. 28,203,(1966)
H. A. Schwarz J. Phys. Chem. 73(6),1928,(1969)

12 T. Kajiwara, K. Funabashi, C. Naleway Phys. Rev. 6,808,(1972)

13 P. M. Rentzepis, R. P. Jones, J. Jortner J. Chem. Phys. 59(2),766,(1973)

14 K. Kawabata, H. Horii, S. Okabe Chem. Phys. Lett. 14(2), 223,(1972)
G. Nilsson J. Chem. Phys. 56(7),3427,(1972)

15 J. T. Richards, J. K. Thomas J. Chem. Phys. 53(1),218,(1970)
J. T. Richards, J. K. Thomas Chem. Phys. Lett.8(1),13,(1971)

C H A P T E R 2

SOME THEORIES REVIEWED

1 Localisation Theory

(i) Invariant Molecular Properties

For a closed shell molecule represented by a Slater determinant of N orthonormalised one electron orbitals, application of the variation method yields the set of coupled Hartree-Fock equations (1)

$$F\Phi_k = \sum_n \lambda_{kn}\Phi_n \qquad k = 1,2 \ldots\ldots N \qquad (1)$$

where

$$F = H + \sum_j (2J_j - K_j) \qquad (2)$$

subject to the definitions

$$H = \sum_p \left(-\tfrac{1}{2}\nabla_p^2 - \sum_A \frac{Z_A}{r_{pA}}\right)$$

$$J_j(1) = \int \Phi_j^*(2)\, \frac{1}{r_{12}}\, \Phi_j(2)\, \partial\tau_2 \qquad (3)$$

$$K_j(1)\Phi_i(1) = \left[\int \Phi_j^*(2)\, \frac{1}{r_{12}}\, \Phi_i(2)\, \partial\tau_2\right]\Phi_j(1) \qquad (4)$$

The orbitals Φ_k are not the unique solutions to the above calculations (2), and alternative solutions χ_n may be obtained by applying an orthogonal transformation

$$\chi_n = \sum_m T_{nm}\Phi_m \qquad (5)$$

such that $\sum_m T_{\ell m}T_{nm} = \delta_{\ell n}$

The new set of matrix elements H_{kn} and λ_{kn} are related to the previous set by

$$H_{kn} = \sum_{i,j} T_{ik}^{-1} H_{ij} T_{nj} \qquad (6)$$

$$\lambda_{kn} = \sum_{i,j} T^{-1}_{ik} \lambda_{ij} T_{nj} \qquad (7)$$

Two properties of the above matrices which are invariant to such a transformation are the trace and determinant. Since the total electronic energy is given by

$$E = \sum_{n} (\lambda_{nn} + H_{nn})$$

the invariance of the trace of these two matrices is equivalent to the invariance of the total energy.

The invariance of the Slater determinant representing the total electronic wave function leads to the invariance of the first and second order density matrices

$$\rho(ij) = \sum_{n} \Phi_n(x_{i1}) \Phi_n(x_{j1})$$

$$\rho(ijk\ell) = \sum_{m,n} \Phi_m(x_{i1}) \Phi_n(x_{k2}) \Phi_m(x_{j1}) \Phi_n(x_{\ell 2})$$

If the total electron interaction energy is represented by the difference between the coulomb and exchange terms defined by

$$C = \sum 2J_{mn} \qquad (8)$$

$$X = \sum_{m,n} K_{mn} \qquad (9)$$

then the above properties of the density matrices leads to the invariance of $\underline{C}$ and $\underline{X}$ (2). Solution of the diagonal form of the Hartree-Fock equations, for which $\lambda_{kn} = 0 \quad k \neq n$, leads to the delocalised molecular orbitals belonging to the irreducible representations of the molecular symmetry group (4).

The use of these orbitals is necessary in the description of such properties as the ionisation of the molecule. An alternative description in other cases is in terms of equivalent orbitals (3), which are related to each other by the symmetry operations of the molecule. Such orbitals are localised in

particular regions of space and may be useful in the description of local regions of the molecule.

(ii) Energy Localised Orbitals

It was pointed out by Lennard-Jones and Pople (3) that such localised orbitals should exhibit maximum self repulsion energy and shown in the case of a two electron system. Although the total coulomb C and exchange X interaction are invariant under an orthogonal transformation, their individual components are not. The maximisation of self repulsion energy, therefore, is equivalent to the maximisation of the trace of the matrices J and K and minimisation of the off diagonal interorbital repulsion and exchange. Such a property furnishes an external criterion which may be used to localise the molecular orbitals even in cases where no symmetry exists.

A method of obtaining such energy localised orbitals has been developed by Edmiston and Ruedenberg (5,6). For a two molecular orbital system, the self repulsion energy $D(\Phi)$ is given by

$$D(\Phi) = \langle \Phi_1^2 | \Phi_1^2 \rangle + \langle \Phi_2^2 | \Phi_2^2 \rangle$$

If a two dimensional transform is defined by

$$T = \begin{bmatrix} \cos\gamma & \sin\gamma \\ -\sin\gamma & \cos\gamma \end{bmatrix}$$

then the new set of orbitals is given by

$$u_1 = \Phi_1 \cos\gamma + \Phi_2 \sin\gamma$$

$$u_2 = -\Phi_1 \sin\gamma + \Phi_2 \cos\gamma$$

The self energy $D(u)$ is then

$$D(u) = \langle u_1^2 | u_1^2 \rangle + \langle u_2^2 | u_2^2 \rangle$$

Expansion of the new functions yields

$$D(u) = D(\Phi) + A_{12} + (A_{12}^2 + B_{12}^2)^{\frac{1}{2}} \cos 4(\gamma - \alpha)$$

where $A_{12} = \langle \Phi_1\Phi_2 | \Phi_1\Phi_2 \rangle - \frac{1}{4}\langle \Phi_1^2 - \Phi_2^2 | \Phi_1^2 - \Phi_2^2 \rangle$

$$B_{12} = \langle \Phi_1^2 - \Phi_2^2 | \Phi_1\Phi_2 \rangle$$

and 4α is defined by

$$\cos 4\alpha = - \frac{A_{12}}{(A_{12}^2 + B_{12}^2)^{\frac{1}{2}}}$$

$$\sin 4\alpha = \frac{B_{12}}{(A_{12}^2 + B_{12}^2)^{\frac{1}{2}}}$$

$$\tan 4\alpha = - \frac{B_{12}}{A_{12}}$$

The values of γ which maximise $D(u)$ are given by

$$\gamma = \alpha + \frac{n\pi}{2} \qquad n = 0, 1 \ldots\ldots$$

For $n = 0$, $\cos\alpha$ and $\sin\alpha$ may be obtained from $\cos 4\alpha$, using

$$x_{\pm} = + \left[\tfrac{1}{2} \pm (\tfrac{1}{2}(1 + \cos 4\alpha))^{\frac{1}{2}} \right]^{\frac{1}{2}}$$

$$y_{\pm} = + (1 - x_{\pm}^2)^{\frac{1}{2}}$$

This yields two pairs of values $(x_+ y_+)$ and $(x_- y_-)$, the required pair $(x_k y_k)$ being obtained by the further requirement that

$$4 x_k y_k (x_k^2 - y_k^2) = \sin 4\alpha$$

For an N orbital system the above method may be used for each of the $N(N-1)/2$ orbital pairs. Since each pair transformation maximises the self repulsion energy, the total self energy converges.

(iii) Alternative Methods

The choice of the transformation matrix in the above energy localisation method was based on the general self repulsion properties of the orbitals. The localised nature of the orbitals, however, has generated alternative criteria from which the matrix may be derived (7 - 10). Typical of these is the method of Magnasco and Perico (11) which uses the fact that for a localised orbital describing two 'bonded' atoms in a molecule, the atomic orbital overlap population between the two atoms is maximum. This is expressed quantitatively by requiring that, for localised orbital Φ_i,

$$2P_i = 2\sum_{u\subset A}\sum_{v\subset B} C_{ui}C_{vi}S_{uv} \qquad (12)$$

is a maximum, where atomic orbitals u and v belong to the set associated with atoms A and B respectively and S_{uv} is the overlap integral

$$S_{uv} = \int \chi_u \chi_v \partial\tau$$

Within this scheme, the final localised orbitals are chosen to represent the m bonds, n inner shells and p lone pairs. For a particular pair transformation involving molecular orbitals Φ_i and Φ_j, the atomic orbitals selected for the sum of eq. (12) will depend on the nature of the localised orbital which Φ_i' or Φ_j' have been chosen to represent, whether bond, lone pair or inner shell. The elements $\sin\gamma$ and $\cos\gamma$ of the transformation matrix are obtained from the condition

$$\cot 2\gamma = \frac{\sum_{u,v\subset\Gamma_i}(C_{ui}C_{vi}-C_{uj}C_{vj})S_{uv} + \sum_{k,n\subset\Gamma_j}(C_{kj}C_{nj}-C_{ki}C_{ni})S_{kn}}{\sum_{u,v\subset\Gamma_i}(C_{ui}C_{vj}+C_{uj}C_{vj})S_{uv} - \sum_{k,n\subset\Gamma_j}(C_{ki}C_{nj}+C_{kj}C_{ni})S_{kn}}$$

where u, v and k, n refer to the set of orbitals Γ_i and Γ_j respectively of which orbitals Φ_i and Φ_j will ultimately be composed. This method has been termed 'uniform localisation' and it has the advantage over the energy localisation scheme that only the molecular orbitals and atomic overlap matrix are required. Its main disadvantage however, has been pointed out by Trindle and Sinanoglu (12) and concerns the fact that for equivalent molecular orbitals, the above transformation equation is zero even although such molecular orbitals are delocalised.

2 Photoionisation Theory

(i) The Photoionisation Cross Section

If ψ_a and ψ_b are respectively the ground state and an excited state of the Hamiltonian

$H_o = -\frac{\hbar^2}{2m}\nabla^2 + V(r)$ and Ψ is a solution of the time dependent equation $i\hbar\frac{d\Psi}{dt} = (H_o + H')\Psi$

where H' is a perturbation, then the coefficient $a_b(t)$ of ψ_b in the eigenfunction expansion of Ψ at some time t is given to a first order approximation by (13)

$$a_b(t) = -\frac{i}{\hbar}\int\langle b|H'|a\rangle \exp(i\omega_{ab}t)\partial t$$

where $\omega_{ab} = (E_b - E_a)/\hbar$

For a radiation produced transition the perturbation is given to first order by

$H' = -\frac{e}{mc}A.\hat{p} = \frac{ie\hbar}{mc}A.\nabla$ where A is the vector potential describing the radiation

$A = 2|A_o(\omega)|\cos(k.r-\omega t+\alpha)$ where $|A_o(\omega)|$ is the real polarisation vector and α a phase factor.

Expressing the radiation in complex form gives

$$a_b(t) = -\frac{H'_{ab}}{\hbar}\cdot\frac{\exp[i(\omega_{ab}-\omega)t]}{(\omega_{ab}-\omega)}$$ with only absorption considered and $H'_{ab} = \frac{ie\hbar}{mc}\langle b|e^{ik.r}A_o(\omega).\nabla|a\rangle$

For the ionisation process, ψ_b describes a continuum function. Since the radiation covers a finite frequency range, a range of continuum states must be counted. If the number of continuum states in the energy range dE is $\rho(E)dE$ then the transition probability becomes $\int a_b^2(t)\rho(E)\partial E$

The latter is :

$$4\int \left|H'_{ab}\right|^2 \frac{\sin^2 \frac{1}{2}(\omega_{ab}-\omega)t}{\hbar^2(\omega_{ab}-\omega)^2}\, \rho(E)\hbar\partial\omega$$

Assuming that $A_o(\omega)$ and $\rho(E)$ are slowly varying functions of energy this becomes

$$\frac{2\pi t}{\hbar}\, \rho(E)\left|H'_{ab}\right|^2 \int \delta(\omega_{ab}-\omega)\partial\omega$$

$$= \frac{2\pi t}{\hbar}\, \rho(E)\left|H'_{ab}\right|^2$$

Thus the transition probability per unit time is

$$P_b = \frac{2\pi e^2\hbar}{m^2c^2}\, \rho(E)\left|\langle b|e^{ik.r}A_o(\omega).\nabla|a\rangle\right|^2$$

Since the total intensity in the range $\Delta\omega$ is $I(\omega)$

where $I(\omega) = \dfrac{\omega^2\left|A_o(\omega)\right|^2}{2\pi c}$

then $P_b = \dfrac{4\pi^2e^2\hbar}{m^2\omega^2c}\, \rho(E)I(\omega)\left|\langle b|e^{ik.r}\ \nabla_A|a\rangle\right|^2$

where ∇_A is the component of the gradient operator in the polarisation direction.

For wavelengths much larger than atomic dimensions $e^{ik.r}$ can be replaced by unity (14)

$$\therefore\quad P_b = \frac{4\pi^2e^2\hbar^2}{m^2\omega c}\, \rho(E)\Omega(\omega)\left|\langle b|\nabla_A|a\rangle\right|^2$$

where $\Omega(\omega)$ is the photon flux $\Omega(\omega) = I(\omega)/\hbar\omega$

Since $\langle b|\text{grad}_A|a\rangle = \frac{i}{\hbar}\langle b|\hat{p}_A|a\rangle$ and

$$\langle b|\hat{p}_A|a\rangle = im\omega_{ab}\langle b|r_A|a\rangle \text{ then}$$

$$\langle b|\text{grad}_A|a\rangle = -\frac{m\omega_{ab}}{\hbar}\langle b|r_A|a\rangle$$

$$\therefore\quad P_b = \frac{4\pi^2e^2\omega_{ab}}{c}\, \rho(E)\Omega(\omega)\left|\langle b|r_A|a\rangle\right|^2$$

For isotropic radiation $|\langle b|r_A|a\rangle|^2$ can be replaced by its average $|\langle b|r|a\rangle|^2/3$

$$\therefore \quad P_b = \frac{4\pi^2 \alpha E_{ab}}{3} \rho(E)\Omega(\omega) |\langle b|r|a\rangle|^2 \qquad (1)$$

$$\alpha = \frac{e^2}{\hbar c} \qquad E_{ab} = E_b - E_a$$

$\rho(E)$, the number of continuum states per unit volume per unit energy can be found by counting the states in a box. It has the value $k/2\pi$ where k is the wave vector of the electron in au.

$$\therefore \quad P_b = \frac{4\pi}{3} \alpha k a_o^2 E_{ab} |\langle b|r|a\rangle|^2 \Omega(\omega)$$

in which the energy E_{ab} is in Rydbergs and the transition moment is in atomic units and a_o is the Bohr radius.

Since $P_b = \sigma\Omega(\omega)$, where σ = cross section for the transition, then, evaluating the constants (15) yields

$$\sigma = 8.56 \times 10^{-19} k E_{ab} |\langle b|r|a\rangle|^2 \ \text{cm}^2$$

The above analysis can be applied to the radiative capture of electrons by a potential well. If the above continuum function is normalised to unit amplitude, representing one particle per unit volume and the radiation is represented by $\Omega(\omega)/c$ photons per unit volume, then equation (1) can be rearranged to

$$P_b = \frac{4\pi^2 \alpha c E_{ab}}{3v} \rho_p(E) \frac{\Omega(\omega)}{c} v |\langle b|r|a\rangle|^2$$

where v is the electron velocity and can be taken to represent the incident electron flux, and $\rho_p(E)$ refers now to the density of final states of the outgoing photon. This can be shown to be:

$$\rho_p(E) = \frac{\omega^2}{\pi^2 \hbar c^3}$$

From this it follows that (16)

$$\sigma_{att.} = \frac{2\hbar^2\omega^2}{m^2 v^2 c^2} \sigma_{det} \qquad (2)$$

(ii) The Continuum Solution

The expression (1) must be summed over all possible final configurations of the system with the usual dipole selection rules applying. In terms of the radial functions only $\langle b|r|a\rangle^2$

$$|\langle b|r|a\rangle|^2 = \sum_{\ell=\ell'\pm1} C_\ell \left| \int P_{n\ell'}(r) r G_{k\ell}(r)\, \partial r \right|^2$$

where $P_{n\ell'}(r)$ is the ground state radial solution and $G_{k\ell}(r)$ is a solution of (19, 20)

$$\frac{d^2}{dr^2} G_\ell + \left\{ k^2 - 2U(r) - \frac{\ell(\ell+1)}{r^2} \right\} G_\ell = 0 \qquad (3)$$

k being the wave vector of the continuum electron in au.

The coefficients C_ℓ are derived from summations over angular integrals. For initial s state configurations, the coefficients are unity. (17)

For potential functions U(r) for which $r^2U(r)$ decreases as $r \longrightarrow \infty$, the solutions of (3) for large r are combinations of spherical Bessel and Neumann functions (18)

$$G_\ell = B_c r(\cos\delta j_\ell(kr) - \sin\delta n_\ell(kr))$$

in which δ is the phase shift.

In particular for $\ell = 1$

$$G_1 = B_c r \left\{ \cos\delta \left(\frac{\sin t}{t^2} - \frac{\cos t}{t} \right) + \sin\delta \left(\frac{\cos t}{t^2} + \frac{\sin t}{t} \right) \right\}$$

where $t = kr$ and B_c is an amplitude factor.

Alternatively

$$G_1 = B_c r \left(\frac{\sin(t+\delta)}{t^2} - \frac{\cos(t+\delta)}{t} \right)$$

For continuum functions normalised to unit amplitude, required by the above cross section formulae, B_c must be set to unity.

The above asymmptotic behaviour of G_1 can be used as a

normalisation condition providing the phase shift can be obtained. This can be found at two large radial values t_1 and t_2 since if:

$$Q = \frac{t_1}{t_2} \cdot \frac{G_1(t_1)}{G_1(t_2)} \qquad \text{then}$$

$$\tan\delta = \frac{\sin t_1 - t_1\cos t_1 - Q(\sin t_2 - t_2\cos t_2)}{Q(\cos t_2 + t_2\sin t_2) - (\cos t_1 + t_1\sin t_1)}$$

The value of δ thus obtained will be indefinite by an integral multiple of π(18). This is resolved by specifying that the phase shift should tend to zero as the particle velocity tends to infinity. Hence by choosing an initially large free particle energy, δ can be fixed absolutely at that energy. By allowing δ to change continuously through lower energies its absolute value can be found in the appropriate energy region.

3 Theory of Vibrational Excitation by Electrons

(i) The Excitation Cross Section

To investigate the possibility of a molecule undergoing a vibrational transition through interacting with a beam of electrons, the wave function for the system - molecule + electron is expanded as a sum of products, each term representing a possible state of the system (16, 18, 21).

$$\Phi = \sum_{v_1 v_2 \ldots JKM} \Gamma_{v_1 v_2 \ldots}(X_1, X_2 \ldots)\, \Omega_{JKM}(\theta, \chi, \varphi)\, F_{v_1 v_2 \ldots JKM}(R, \Upsilon, \phi) \quad (1)$$

where

(i) $\Gamma_{v_1 v_2 \ldots}(X_1, X_2 \ldots)$ represents a vibrational state of the molecule defined by the quantum numbers v_i, and X_i represent the coordinates of each vibration

(ii) $\Omega_{JKM}(\theta, \chi, \varphi)$ represents a rotational state of the molecule defined by the quantum numbers J, K and M, and θ, χ, φ are the angles defining the orientation of the molecule

(iii) $F_{v_1 v_2 \ldots JKM}(R, \Upsilon, \phi)$ is the electron wave function corresponding to the molecular state defined by the quantum numbers v_i and J, K, M and R, Υ, ϕ are electron coordinates.

Neglecting coupling between vibration and rotation, the Hamiltonian for the system can be written as:

$$H = H_v(X_1, X_2, \ldots) + H_r(\theta, \chi, \varphi) + H_e(R, \Upsilon, \phi) + V(X_1, X_2, \ldots, \theta, \chi, \varphi, \ldots, R, \Upsilon, \phi) \quad (2)$$

where H_v, H_r and H_e are the vibrational, rotational and single electron Hamiltonians. V is the interaction potential between molecule and electron.

If a molecule has permanent dipole u and the induced dipole for the i^{th} vibrational state is A_iX_i then the interaction is approximated by the long range form (22)

$$V = V^I + V^{II}$$

$$V^I = \frac{ue}{r^2}\,(\cos\theta\cos\gamma+\sin\theta\sin\gamma\cos(\varphi-\phi))$$

$$V^{II} = \sum_i V^i_{II} = \sum_i \frac{A_iX_ie}{R^2}\,(\cos\theta\cos\gamma+\sin\theta\sin\gamma\cos(\varphi-\phi))$$

Substituting the wave function (1) into the Schroedinger equation for the system $H\Phi = E\Phi$, multiplying by $\Gamma_{v_1v_2\ldots}(X_1,X_2\ldots)\Omega_{JKM}(\theta,\chi,\varphi)$ and integrating over the molecular coordinates yields:

$$\left[\nabla^2 + \frac{2m}{\hbar^2}\,(E-E_v-E_{JKM})\right] F_{v_1v_2\ldots JKM}(R,\gamma,\phi) =$$

$$\frac{2m}{\hbar^2}\sum_{v_1'v_2'\ldots J'K'M'} V(v_1v_2\ldots JKM;v_1'v_2'\ldots J'K'M')F_{v_1'v_2'\ldots J'K'M'}(R,\gamma,\phi) \quad (3)$$

and $V(v_1v_2\ldots JKM;v_1'v_2'\ldots J'K'M')$

$$= \int \Gamma^*_{v_1'v_2'\ldots}\,\Omega^*_{J'K'M'}(V^I+V^{II})\,\Gamma_{v_1v_2\ldots}\Omega_{JKM}\partial X_1\ldots\partial X_n\partial\cos\theta\partial\chi\partial\varphi \quad (4)$$

In the above, use has been made of the fact that

$$H_v\Gamma_{v_1v_2\ldots}(X_1,X_2\ldots) = E_v\Gamma_{v_1v_2\ldots}(X_1,X_2\ldots)$$

and

$$H_r\Omega_{JKM}(\theta,\chi,\varphi) = E_{JKM}\Omega_{JKM}$$

Due to the nature of V^I and V^{II} the selection rules for the matrix elements in (4) are:

for V^{I} $\Delta v_i = 0 (i=1 \rightarrow n)$, $\Delta J = \pm 1$, $\Delta K = 0$, $\Delta M = 0, \pm 1$

for V^{II} $\Delta v_i = \pm 1$, $\Delta v_j = 0 (i \neq j = 1 \rightarrow n)$ $\Delta J = \pm 1$, $\Delta K = 0$, $\Delta M = 0, \pm 1$

If the suffix $a_i pqr$ refers to the wave function pertaining to the molecular state with the i^{th} vibrational quantum number = a and rotational quantum numbers J,K,M, equal to p, q and r respectively, then the single electron state which relates to the i^{th} vibration having $v_i = 1$ is $F_{1_i pqr}$. If a molecule is initially in its ground state then the terms in the expansion of (3) which contribute mostly to this final state will be those involving the $F_{0_i 000}$ term. In this case the major process will be the excitation of a vibration. This will be the main source of the $F_{1_i pqr}$ state providing the interaction is weak i.e. providing the dipole and induced dipole moment (in atomic units) are small compared to unity. The only non-zero term in the summation (3) which derives from the $F_{0_i 000}$ term and involves the appropriate vibrational transition is the $F_{1_i 100}$ term, i.e. a simultaneous rotational transition must take place (22).

In this case:

$$\left[\nabla^2 + k^2_{1_i 100} \right] F_{1_i 100} = \frac{2m}{\hbar^2} V_i^{II}(1_i 100;\ 0_i 000) F_{0_i 000} \qquad (5)$$

and

$$V_i^{II}(1_i 100; 0_i 000) = \frac{\langle v' | u | v \rangle \cos\gamma}{\sqrt{3}.R^2}$$

where $\langle v' | u | v \rangle$ is the transition moment for the vibrational change.

(ii) The Born Approximation

If Born's approximation is applied to the incident electron the $F_{0_i 000}$ is represented by a plane wave $\exp(ik_o.R)$ and solving (5) yields for the asymmptotic expression for $F_{1_i 100}$

$$F_{l_i 100} = \frac{2\pi m\langle v'|u|v\rangle}{\sqrt{3}\,\hbar^2}\,\frac{\exp(ik_{l100}\cdot R)}{R}\int\exp[i(k_o-k_{l100}).R]\cos\gamma\partial R\partial\cos\gamma\partial\phi$$

Since the correct asymmptotic expression for the final electron state is:

$$F_{l_i 100} = f(\gamma)\,\frac{\exp(ik_{l100}R)}{R}$$

$$R\longrightarrow\infty$$

and the total cross section for the transition is:

$$Q_{l_i 100} = \int|f(\gamma)|^2\sin\gamma\partial\gamma\partial\phi$$

the angular factor in the expression for $F_{l_i 100}$ yields (22,23)

$$Q_{l_i 100} = \frac{8\pi}{3k^2}|\langle v'|u|v\rangle|^2\ell n\,\frac{k+k'}{k-k'} \qquad (6)$$

where k and k' are the initial and final wave vectors for the electron (24,25).

The validity of the above analysis requires that

(i) the distortion of the free electron function is small enough to allow the Born approximation to be used

(ii) the long range form of the interaction can be used throughout all ranges

(iii) quadrupole and higher terms are unimportant

(iv) the interaction is small enough to allow a first order treatment.

(iii) Transition Moments from Experiment

The transition moment in (6) can be obtained from the infra-red absorption spectrum of the substance since

$$\text{Absorbance} = \ell n\,\frac{I_o}{I} = \varepsilon(\nu)c\ell$$

where $\varepsilon(\nu)$ = molar extinction coefficient, c and ℓ are concentration and path length respectively.

Also $K(\nu) = \varepsilon(\nu)c$ is defined as the absorptivity.

The integrated absorption intensity A is defined as

$$A = \frac{1}{c\ell}\int \ell n\left(\frac{I_o}{I}\right)\partial\nu = \int \varepsilon(\nu)\partial\nu = \frac{1}{c}\int K(\nu)\partial\nu$$

This quantity is related to the transition moment by:

$$A = \frac{8\pi^3 N_o \nu e^2}{3hc^2} \left|\langle v'|u|v\rangle\right|^2$$

where ν = light frequency and c = light velocity.

From this it follows that

$$\left|\langle v'|u|v\rangle\right|^2 = 1.7293\times10^{-23}\ \frac{Ac}{\nu} \quad (cm^2)$$

4 Electron Tunneling Theory

(i) Resonant Transfer

The spontaneous transfer of particles between bound states separated by a potential barrier falls into the general category of radiationless transitions and as such may be analysed in the same way as excitation transfer (26,27,28).

Theories concerned with the latter, regard the initial state as an eigenstate of some incomplete Hamiltonian H_o and observe the evolution of the system under the perturbing influence of the correction to the Hamiltonian H' which causes transitions to other eigenstates of the system (29). Treating the initial state as non-stationary is valid (30) providing the measurement is rapid compared to the evolution time of the system.

For initial and final states, ψ_1 and ψ_2, which are discrete and of the same energy the wavefunction for the system Φ oscillates between these two states such that

$$\Phi^2 = (\cos^2\beta t/\hbar)\ \psi_1^2 + (\sin^2\beta t/\hbar)\psi_2^2 \qquad (1)$$

where β is the perturbation between initial and final states

$$\beta = \int \psi_2^* H' \psi_1 \partial\tau$$

In such a case the average time for total transfer is $h/4\beta$. For times which are short compared to $h\beta^{-1}$ the above resonance can be represented in terms of a transfer probability per unit time P_t.

From (1) $P_t = \beta^2 t/\hbar^2$

(ii) Non-Resonant Transfer

When the initial and final states differ in energy by an amount F, a first order perturbation treatment yields

$$P_t t = \frac{4\beta^2}{(4\beta^2+F^2)} \sin^2\left[\tfrac{1}{2}(4\beta^2+F^2)^{\frac{1}{2}}\right] t/\hbar \qquad (2)$$

Equation (2) forms the starting point in the analysis by Robinson and Frosch of the transfer of molecular electronic excitation in solids (30,33).

The initial state is taken to be the zero vibrational level of an electronically excited state whilst the final state consists of a high vibrational level of a lower electronic state with the addition of a few low lying lattice vibrations. The coupling between the molecular and lattice vibrations is regarded as being sufficiently weak to allow the treatment of the molecular vibrations separately. If the coupling between the molecular and lattice vibrations is greater than the coupling between the two electronic states, however, the excitation is unlikely to return to the initial state since the molecule will have relaxed vibrationally, giving its energy to the surrounding lattice during the time the excitation exists in the final state (31,32). If the initial and final states are almost degenerate, the energy difference F is regarded as arising from the weak coupling between the molecular vibration and the lattice in the final state. If this coupling is greater than the electronic coupling as is assumed then (2) becomes

$$P_t t = \frac{4\beta^2}{F^2} \sin^2(\tfrac{1}{2}Ft/\hbar) \qquad (F \gg \beta) \qquad (3)$$

The ability of the final state to lose energy to the lattice, effectively introduces a large number $\underline{N}$ of final states arising from the distribution of a few quanta from the molecular vibration among several lattice modes. Since the energy of the final state is regarded as being broadened by the weak coupling between molecular and lattice vibration of the order $\underline{d}$ then the final states can be incorporated in the form of an average density of states $\rho(F) \approx N/d$ allowing the integration of (3) over F giving

$$P_t t = 4 \int \frac{\beta^2}{F^2} \rho(F) \sin^2 \tfrac{1}{2} Ft/\hbar \partial F \qquad (4)$$

When the electronic matrix element β^2 is normalised to the number of final states N then for times greater than $4\hbar d^{-1}$ the integral (4) becomes

$$P_t = \frac{2\pi\beta^2}{d\hbar} \qquad (5)$$

The quantity $\underline{d}$ which represents the average coupling energy between a molecular vibration and the surrounding lattice is related to the quantity $\hbar d^{-1}$ which is of the order of a vibrational relaxation time t_{vib}. This gives

$$P_t = \frac{2\pi\beta^2 t_{vib}}{\hbar^2}$$

The total wave function for the initial and final states is taken as a product of electronic and vibrational terms.

$\Phi_i = \Psi_i(R,X)\,\Gamma_i(X)$ with $\Gamma_i(X)$ the vibrational function associated with the i^{th} electronic state of the system.

The initial vibrational state is the product of all modes of the system comprising molecule and lattice and is considered

to be a ground state.

$$\Gamma_1(X) = \Theta_{01}(X_1)\Theta_{01}(X_2)\,\Theta_{01}(X_3)\ \ldots$$

whilst the final state is a summation over such states, consistent with the near degeneracy of the two total states.

$$\Gamma_2(X) = \sum\Theta_{a2}(X_1)\Theta_{b2}(X_2)\Theta_{c2}(X_3)\ldots$$

where a, b, c... define the vibrational quantum numbers.

The electronic matrix element is taken as being independent of nuclear coordinate which gives

$$\beta = \int\Psi_2^*(R,X)H'\Psi_1(R,X)\partial\tau.\langle\Gamma_2(X)\,|\,\Gamma_1(X)\rangle \qquad (6)$$

where $\langle\Gamma_2(X)\,|\,\Gamma_1(X)\rangle = \int\Theta_{01}(X_1)\Theta_{01}(X_2)\ldots\left[\sum\Theta_{a2}(X_1)\Theta_{b2}(X_2)\Theta_{c2}(X_3)\ldots\right.$
$\left.\ldots\right]\partial X_1\partial X_2\ldots$

and is the product of the Franck-Condon factors for each vibrational mode summed over all final vibrational states.

When the initial and final electronic states are nearly degenerate the Franck-Condon factors are expected to be around unity since the vibrational quantum numbers will change to a smaller extent.

(iii) Approximate Methods

The above analysis has previously been applied to the problem of electron tunneling (34,35). In such cases the perturbation which makes the initial state non-stationary is the centre to which the particle tunnels and associated with which therefore is the final electronic state. Particle tunneling has recently been reviewed (36). The problem was first solved for a double minimum potential by Dennison and Uhlenbeck (37) who

calculated the matrix element β in a one-dimensional analysis using the W.K.B. approximation.

They obtained

$$\beta = h\nu_o \exp\left\{-\hbar^{-1}\int_a^b [2m(V-E)]^{\frac{1}{2}}\partial x\right\} \qquad (7)$$

where ν_o is the frequency in one well, E is the particle energy, a and b are the points of intersection of the energy level E with the potential function. V is the potential between a and b.

Brocklehurst has used the above expression for β (34) equating $h\nu_o$ with the ionisation potential of the electron, giving for the tunneling rate constant, P_t, the expression

$$P_t = (\hbar d)^{-1}(V_o-E)^2\sigma \exp\left\{-2\hbar^{-1}\int_a^b [2m(V-E)]^{\frac{1}{2}}\partial x\right\} \qquad (8)$$

where V_o is the potential at long distances from the electron. Equation (8) has a similarity in form to the rate obtained for free particles tunneling through a rectangular barrier of width a

$$k_t = \frac{16\nu E(V_o-E)}{V_o^2} \cdot \exp\left\{-2\hbar^{-1}[2m(V_o-E)]^{\frac{1}{2}}a\right\} \qquad (9)$$

where ν is the collision frequency, which has been used by Miller (38) and Mikhailov (39) to calculate tunneling properties.

A similar 'free particle' equation has been used for non-rectangular barriers by Dexter (40) for which a W.K.B. solution gives

$$k_t = \nu \exp\left\{-2\hbar^{-1}\int_a^b [2m(V(x)-E)]^{\frac{1}{2}}\partial x\right\} \qquad (10)$$

Dexter attempted to improve the applicability of a one dimensional calculation to a three dimensional system by multiplying (10) by the solid angle subtended at the trapped electron by the centre to which the electron was tunneling.

It has been pointed out by Brocklehurst that for the H_2^+ ion, β is half the g-u splitting, and at large R has the leading term

$$\beta = \frac{0.736e^2}{a_o^2} R \exp\left\{-\left[\frac{2m}{\hbar^2}(V_o-E)\right]^{\frac{1}{2}}R\right\}$$

where E is the particle energy and V_o is the maximum in the barrier potential. The similarity in the exponent in this formula and that of equation (9) suggests that the use of a rectangular barrier approximation may reduce the error involved in a one dimensional analysis.

The similarity in the simple formulae for free and bound particle tunneling, however, cannot conceal the different premises on which they are based, a fact which can give rise to differences of the order 10^3 in the pre-exponential factors, depending for example on the choice of frequency factors, vibrational relaxation times or overlap factors.

REFERENCES

1 V. Fock Z. Physik 61, 126, (1930)

2 G. G. Hall, J. Lennard-Jones Proc. Roy. Soc. (London) A202, 155, (1950)

3 J. Lennard-Jones, J. A. Pople Proc. Roy. Soc. (London) A202, 166, (1950)

4 G. G. Hall Proc. Roy. Soc. (London), A202, 336, (1950)

5 C. Edmiston, K. Ruedenberg Rev. Mod. Phys. 35(3), 457 (1963)

6 C. Edmiston, K. Ruedenberg J. Chem. Phys. 43(10),S97 (1965)

7 J. M. Foster, S. F. Boys Rev. Mod. Phys. 32, 300, (1960)

8 W. von Niessen Theoret. Chim. Acta. 27, 9, (1972)

9 D. Peters J. Chem. Soc. 2003, 4017, (1963)

10 W. H. Adams J. Chem. Phys. 34(1),89, (1961) J. Chem. Phys. 37(9), 2009, (1962) J. Chem. Phys. 42(11), 4030, (1965)

11 V. Magnasco, A. Perico J. Chem. Phys. 47(3), 971, (1967)

12 C. Trindle, O. Sinanoglu J. Chem. Phys. 49(1), 65, (1968)

13 L. I. Schiff 'Quantum Mechanics' McGraw-Hill, 3rd ed.

14 E. Merzbacher 'Quantum Mechanics' Wiley (New York)

15 A. L. Stewart Adv. in Atomic and Molecular Physics 3, 1, (1967)

16 H. S. W. Massey, E. H. S. Burhop 'Electronic and Ionic Impact Phenomena' Vols. 1 & 2 Clarendon Press

17 D. R. Bates (Ed.) 'Atomic and Molecular Processes' Academic Press (New York)

18 H. S. W. Massey "Theory of Atomic Collisions" Clarendon Press

19 R. L. Smith, R. W. Labahn Phys. Rev. A2(6), 2317, (1970)

20 J. C. Weisheit Phys. Rev. A5(4), 1621, (1972)

21 H. S. W. Massey Proc. Camb. Phil. Soc. 28, 99, (1932)

22 Ta-You Wu Phys. Rev. 71(2), 111, (1947)

23 K. Takayanagi J. Phys. Soc. Japan 21(3), 507, (1966)

24 A. M. Arthurs, A. Dalgarno Proc. Roy. Soc. A256, 540, (1960)

25 A. Dalgarno, O. H. Crawford, A. C. Allison Chem. Phys. Lett. 2(6), 381, (1968)

26 J. Jortner, S. A. Rice, R. M. Hochstrasser Adv. in Photochem. 7, 149, (1969)

27 B. R. Henry, M. Kasha Ann. Rev. Phys. Chem. 19, 161, (1968)

28 A. S. Davydov Phys. Stat. Soc. 30, 357, (1968)

29 D. L. Dexter J. Chem. Phys. 21(5), 836, (1953)

30 G. W. Robinson, R. P. Frosch J. Chem. Phys. 38(5), 1187,(1963)

31 D. L. Dexter, T. H. Förster, R. S. Knox Phys. Stat. Sol. 34, K159, (1969)

32 D. L. Dexter, W. B. Fowler J. Chem. Phys. 47(4), 1379,(1967)

33 G. W. Robinson, R. P. Frosch J. Chem. Phys. 37(9), 1962, (1962)

34 B. Brocklehurst Chem. Phys. 2, 6, (1973)

35 J. Bardeen Phys. Rev. Lett. 6, 57, (1961)

36 M. D. Harmony Chem. Soc. Rev. 1, 211, (1972)

37 D. M. Dennison, G. E. Uhlenbeck Phys. Rev. 41, 313, (1932)

38 J. R. Miller J. Chem. Phys. 56(10), 5173, (1972)

39 A. I. Mikhailov Doklady Phys. Chem. 197, 223, (1971)

40 D. L. Dexter Phys. Rev. 93(5), 985, (1954)

CHAPTER 3

EXPERIMENTAL OBSERVATIONS

1 Optical Absorption Spectra

The optical absorption spectra of electrons trapped in solid media exhibit similarities over a range of properties including band position, half width, temperature coefficient, extinction coefficient, band shape and time development. Some of these are listed in Table 3.1.

	E_{max}	Threshold	$W_{\frac{1}{2}}$	e_{max}(/M cm)	T(^{o}K)
Ice	1.90	1.50	0.50	1.85×10^{4}	77
Alk. Ice	2.12	1.48	1.03	2.0×10^{4}	77
MTHF	1.0	0.63	0.58	1.94×10^{4}	77
3MH	0.75	0.54	0.68		76
3MP	0.73	0.54	0.55	3.0×10^{4}	76

TABLE 3.1 Energies in ev, $W_{\frac{1}{2}}$ = half width

The band maxima exhibit a blue shift with decreasing temperature (typically 10^{-3} ev/deg.) and in some systems stability has been reported below certain temperatures (1, 5). Increasing the temperature causes broadening of the spectra of a similar magnitude, with a resultant loss of maximum intensity. The similarity in band shapes includes a high energy tail extending several ev beyond the maximum, and the need to extrapolate spectra has introduced some uncertainty into the values of oscillator strengths, where estimation of these has been made, and their behaviour with temperature.

(i) Analysis of Spectra

The fundamental questions which must be answered in relation to light absorption by localised electrons, concern the nature of the excited state and the origin of the band width.

The nature of the medium appears to be important in deciding the first of these questions with a division occurring between those for which the excited state is localised and those for which it is a conduction band state. Evidence comes from a study of spectra, to discern any fine structure implying higher discrete states, photoconductivity and photobleaching. Photobleaching is a property of trapped electrons in which repeated irradiation of the sample with light lying within the absorption range of the electron, causes eventual loss of trapped electrons. A summary of the evidence relating to the nature of the absorption spectrum in various media is presented below.

Crystalline Ice

The position of the absorption maximum in pure ice remains constant at 1.90 ev until 140°K (1, 6, 15) beyond which it shifts to the red, reaching a value of 1.82 ev at the melting point (14). The small yield of electrons in ice (10^{-4} - 10^{-3}/100 ev) has prevented an accurate estimate of the extinction coefficient and oscillator strength for the transition. Values of $\underline{f}$ between 0.33 and 0.71, that for water, have been described (1).

The electron spectrum in D_2O ice shows exactly the same temperature variation, with the D_2O ice maximum lying 0.04 ev above that for H_2O ice throughout the whole range (77 - 300°K).

Recently, more accurate pure ice spectra have revealed a shoulder on the absorption band between 5000 - 5600A° (7).

This feature is also present in D_2O ice. According to Dye et. al. (8), the low energy portion of the spectrum up to and beyond the maximum can be represented by the Gaussian $F=\exp(-0.0313x^2)$ where $x=31.39(E_{max}-E)$ with energy in ev. Using this function the spectrum has been separated into the two components shown in Figure 3.1. The higher energy curve has a maximum at 2.24 ev.

Trapped electron concentrations are too small to permit photoconductivity studies but detailed photobleaching studies have been made (1). They reveal that the photobleaching quantum efficiency Q varies with the bleaching wavelength used. Between 3.2 ev and 2.6 ev Q decreases linearly from 0.22 to 0.06 and thereafter tends to zero around the spectrum maximum.

It is the generally held view that the spectrum in ice arises from transitions to a bound state, with the higher energy portion representing transitions to higher bound states and the continuum. If the loss of electrons through photobleaching is regarded as taking place from a 'free' state then the onset of bleaching at the high energy side of the band coupled with the resolved bands of Figure 3.1 lend support to this view.

Alkaline Ice

As with the pure ice spectrum, that of alkaline ice is stable in position below 140°K (5). Excitation of the electron in the presence of an applied voltage produces a photocurrent, the wavelength dependence of which is the same as the absorption spectrum itself (3). This fact, along with the temperature dependence of the Hall mobility of the upper state suggest that the excited state is a delocalised one. Photobleaching results are complex but suggest that two types of trap exist (4) since

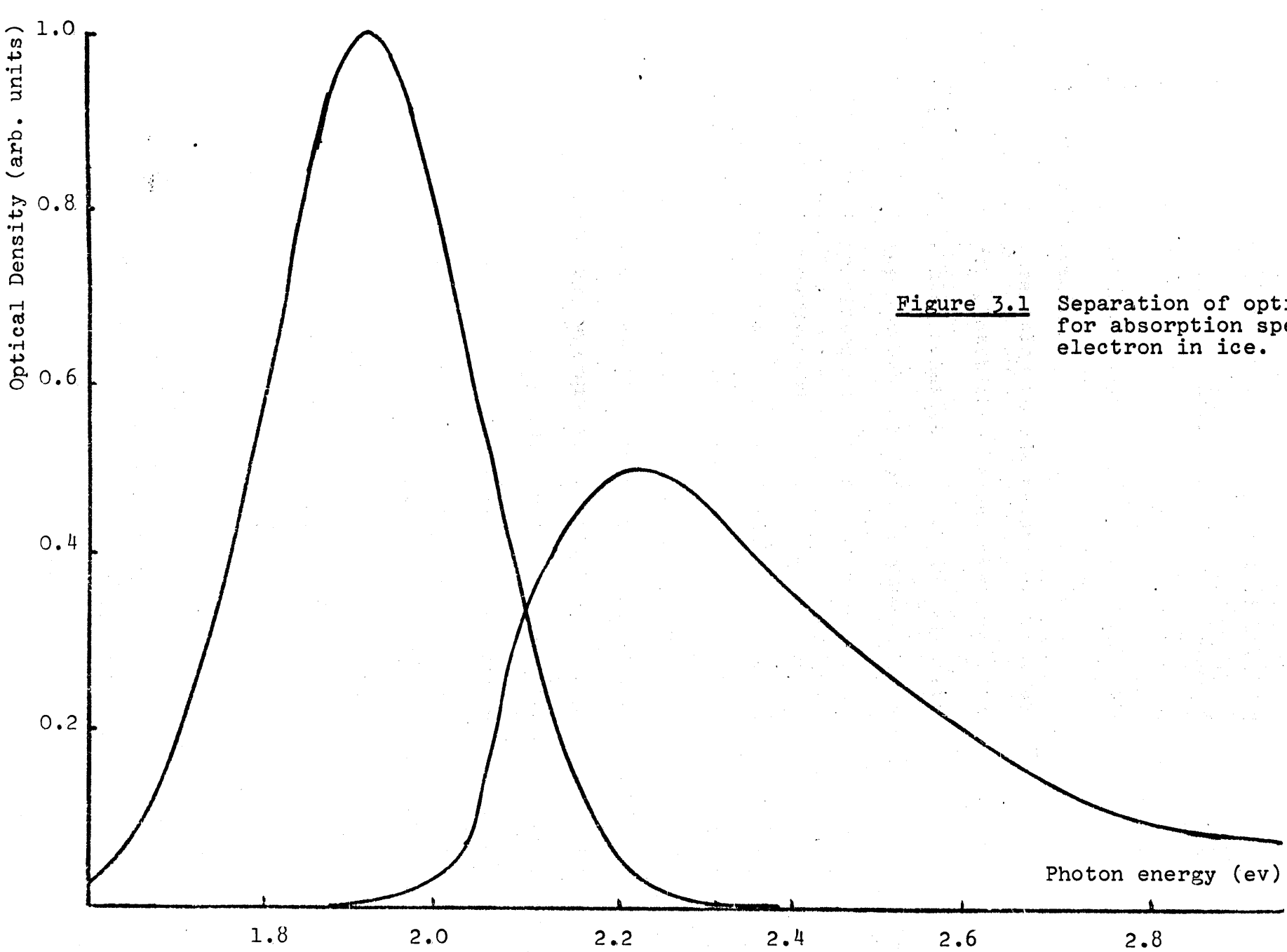

Figure 3.1 Separation of optical components for absorption spectrum of electron in ice.

irradiating on the low energy side (700nm) causes a blue shift which stabilises and is followed by uniform decay across the band. From this it is further concluded that 30% of electrons are in a shallow trap with a maximum at 660nm, the remainder having a maximum at 585nm. The above trap interconversion is assumed to take place via a mobile electron state.

Methyltetrahydrofuran

Evidence relating to the nature of the excited state in MTHF comes from photobleaching and photoconductivity studies. The photobleaching behaviour is similar to that of pure ice, a threshold being observed around the absorption maximum 520nm (3,9). The wavelength dependence of the photocurrent shows the same variation (3) supporting the view that direct ionisation begins beyond the spectrum maximum. The photocurrent, however, shows a second maximum around 950nm which is found to involve a two photon process. This is thought to represent photoionisation from a long lived excited state derived from the directly excited state by internal conversion (3). The slight temperature dependence of photobleaching in this wavelength region (E_{act}= 0.001 ev) is taken to be consistent with a thermally aided conversion process.

Further support for a bound excited state comes from the temperature dependence of the excited state mobility which is more consistent with a 'hopping' model (10, 11, 16) than a band state.

3 Methylhexane

The energy level structure of the electron trapped in 3MH is considered to be similar to that of MTHF on the basis of

similar photobleaching and photocurrent behaviour. Above the spectral maximum the photocurrent dependence on wavelength shows a maximum around 1000nm as does the photobleaching efficiency. With lower energy light around the spectral maximum the photocurrent depends on the square of the light intensity whilst the photobleaching efficiency shows a second maximum in the 1650 - 1700nm range as well as a slight temperature dependence.

Evidence on the nature of the excited state in 3 methylpentane appears inconclusive since contrary to early investigations (12), recent studies have shown the photobleaching efficiency to retain a significant value to the threshold of the absorption spectrum (13). However, mobility studies on the excited state (3) suggest a 'hopping' mechanism similar to MTHF.

2 Decay of Trapped Electrons

The decay of electrons trapped in solid media occurs in a time scale ranging from nanoseconds to several hours and represents one aspect of the re-attainment of chemical equilibrium altered by the interaction of the medium with radiation. In a particular medium the decay rate is influenced by such factors as temperature, the method of trapped electron production, the presence of impurity scavengers and the presence of solutes capable of immobilising hole centres. The decay can be followed:

(a) by monitoring the intensity of the trapped electron's optical absorption

(b) by observing the intensity of the electron's e.s.r. absorption

(c) by measuring the intensity of light emitted in those systems which exhibit luminescence

(d) by monitoring the intensity of light absorption by a primary product of the neutralisation process.

A study of the decay of trapped electrons in both polar and non-polar matrices suggest four possible modes of decay:

1 Diffusion of positive hole centres

2 Diffusion of trapped electron centres

3 Thermal detrapping of electrons and scavenging by capture from a conduction state

4 Tunneling of trapped electrons to adjacent scavenging centres.

The assignment of one or more of these modes in particular cases is made by observing the order of the kinetics and the way in which it is influenced by the above factors.

Presented below is a summary of the decay characteristics of trapped electrons in various solid media.

Crystalline Ice

Shubin and co-workers (15, 18) have examined the decay of trapped electrons produced by microsecond electron pulses by following the optical absorption in the temperature range 213 - 273°K and have found that the decay can be represented by two temperature dependent modes, one first order the other second order. The rate constants for these processes have been estimated to be:

$$k_1 = (5.2 \pm 0.7) \times 10^{10} \exp\left[- \frac{(7500 \pm 1300)\text{cal/mole}}{RT} \right]$$

$$k_2 = (3.5 \pm 0.6) \times 10^{13} \exp\left[- \frac{(3500 \pm 500)\text{cal/mole}}{RT} \right]$$

k_2 has been assigned to a recombination with H^+ whilst it is believed that k_1 relates to detrapping of electrons.

Similar experiments by Taub and Eiben (6) with electron pulses have produced trapped electron concentrations in the range 10^{-6} - 10^{-7}M. They have found that above 260°K the decay is predominantly second order whilst between 203 - 233°K it is mainly first order. At lower temperatures (110 - 173°K) the decay is found to separate into a slow first order process and a fast decay portion of no simple order, the latter taking place on a msec time scale and occupying a major role as the temperature is decreased implying a much smaller temperature dependence.

A similar rapid decay has been found by Kawabata (20,21) in pulsed samples at 110°K who has shown the optical absorption spectrum to decay uniformly in 2 msec to a stable value following 0.5 usec pulses.

The decay behaviour in the 200 - 273°K range has been confirmed by other workers (1).

Alkaline Ice

Buxton and co-workers (22) have examined the decay on a usec scale in 10MNaOH ices in the temperature range 80 - 300°K. At 300°K the decay is first order with $t_{\frac{1}{2}}$ = 2 usec. The decay rate decreases on lowering temperature and at 200°K the decay can be separated into a slow first order process and a faster process obeying approximate second order kinetics, both of which however are dose independent. At 180°K the fast portion has $t_{\frac{1}{2}} > 100$ us and a small blue shift in the absorption spectrum is observed in a 15 us interval, accompanying which there is a loss of electrons. The behaviour of the rate constants with temperature is found to obey an amended form of the Arrhenius equation given by

$$k = A\exp\left[-\frac{E_a}{R(T-T_o)}\right]$$

This behaviour is taken to be consistent with the transition of the matrix to a rigid form at the temperature T_o, which was evaluated as 135°K. Activation energies were calculated to be 1.6 k cal/mole. No decay was observed for temperatures between 80°K and the transition point.

Miller (23) has found that in 6MNaOH ice at 77°K, trapped electrons produced by nanosecond pulses are stable over a period of 20 nsec to several minutes. In the presence of $C_rO_4^{-2}$ or NO_3^-

scavengers (10^{-3} - 10^{-1}M), the trapped electrons decay spontaneously over the time range 10^{-8} - 10^{3} sec. This behaviour has been interpreted in terms of a tunneling model.

Methyltetrahydrofuran

Smith and Pieroni (24) have observed the decay of the e.s.r. absorption of trapped electrons produced by gamma irradiation at 77.5°K. At this temperature the electrons are relatively stable having half lives of around 250 hrs. Following a relatively rapid 50 hr portion the decay becomes linear showing no simple kinetics. Between 92 - 95°K a population of electrons (30%) decay rapidly in an interval of 10 min whilst the remainder remain stable up to 101°K when they decay to zero in 5 min. The decay of radical and radical ion e.s.r. intensity corresponds with electron decay.

When the trapped electrons are photobleached the residual radicals remain stable up to 101°K suggesting that the onset of decay for radicals and deeply trapped electrons occurs at this temperature by mechanism (1) above, whilst thermal detrapping of a shallow trap population begins in the 92 - 95°K range (17).. By varying the radiation dose, the spontaneous electron decay at 77.5°K has been found to be independent of initial radical ion concentration, suggesting that the position of initial trapping and final neutralisation locations are situated close together.

Miller (25,26) has observed trapped electrons produced by gamma irradiation at 77°K and 87°K. In the pure solid no decay is observed between 1 min and 1 hr following irradiation. The experiment was repeated with a variety of scavengers present

(napthalene, biphenyl, hexatriene, 9methyl anthracene) in mM concentrations and decay was observed between msec and minutes (with half lives around 8 min). The decay rates were the same at 77°K and 87°K implying an activation energy of less than 0.02 ev. Miller has interpreted this behaviour in terms of a tunneling model. For the pure solid, an activation energy of 0.75 ev for decay has been measured suggesting that only one of the first three decay mechanisms is important at low scavenger concentration.

Trapped electrons can also be produced by photoionisation of tetramethylphenylenediamine (TMPD) (27). Experiments carried out at 77°K (28) have shown that the rate of the ensuing decay depends on the wavelength of photoionising light. For the wavelengths 313 nm and 365 nm the corresponding half lives are 2.4 sec and 1.7 sec. This result is regarded as evidence for a tunneling recombination reaction between the trapped electron and parent $TMPD^+$ ion, the shorter wavelength light producing a more distant population of trapped electrons.

3 Methylpentane

Gallivan and Hamill (29) have found that trapped electrons produced by gamma irradiation at 77°K, in concentrations of 2×10^{-5}M, decay spontaneously over a period of 4 hrs (30). The latter part of this decay follows second order whilst the initial portion (t less than 1 hr) exhibits decay which is independent of dose and is intrinsically first order (31). At the lower temperature of 63°K the overall rate was reduced to 5% of its 77°K value. The presence of 2 mole % 2 methylpentene, which acts as a trap for positive centres, also has the effect of

reducing the overall decay rate. These facts suggest that positive hole migration is responsible for some of the decay (32). The presence of scavengers (10^{-3}M biphenyl or TMPD) reduces the overall half life from 40 min to 20 min, and at biphenyl concentrations greater than 2×10^{-3}M the decay beyond 1 hr follows approximate first order kinetics. This influence of scavengers on the spontaneous decay rate suggests that electron detrapping or tunneling may be important.

Experiments on the conductivity of gamma irradiated samples (33) at 77°K confirm the initial rapid decay portion and slower second order process. The further observation is made that 2 methylpentene has no effect on the initial decay portion. These studies also reveal a second population of trapped electrons which do not apparently decay spontaneously but can be removed by photobleaching or raising the temperature to 85°K and which imply a more deeply trapped species.

Evidence of such a distribution of trap depths comes also from pulse experiments at 76°K (4,34) in which a blue shift in the maximum of the absorption spectrum is observed in the time interval 10^{-4} - 10^{3} sec following irradiation (35,36). Associated with this is an overall decrease in spectral intensity which is consistent with the above findings, suggesting the initial rapid decay of a population of shallow trapped electrons coupled with solvent relaxation .

The importance of parent ion recombination comes from two experiments on trapped electrons produced by photoionisation of TMPD at 77°K. The first of these is identical to that carried out in MTHF (28) the result being again obtained, that the initial

rapid decay over a 10 sec period depends on the photoionisation wavelength. For wavelengths of 313 nm and 365 nm the half lives are respectively 4.3 sec and 2.6 sec. In the second experiment observations were made on the more deeply trapped electron population (37) which decays over a period of hours. Using polarized light for the initial photoionisation it was shown, by observing the polarization of the $TMPD^+$ recombination luminescence, that 95% of electrons recombine with their parent cation.

Observations of pulse produced trapped electrons in 3 methylhexane at 76°K (4) have shown similar blue shift and spectral intensity reduction as with 3MP in the 10^{-4} - 10^{3} sec range (35). Although the scavenger biphenyl increases the decay rate it has little effect on the blue shift rate suggesting that the shift is due to a parent ion recombination effect or medium relaxation.

Possible evidence of electron decay by a tunneling mechanism comes from the observation of the decay of isothermal luminescence in gamma irradiated methylcyclohexane containing 10^{-4} - 10^{-2}M biphenyl (38). The luminescence, thought to be due to recombination with the biphenyl cation, shows a decay rate which is the same between 4.2°K and 77°K.

3 Photobleaching Characteristics

When a trapped electron sample is irradiated with light, whose wavelength lies within the absorption range of the trapped electron, the number of trapped electrons in the sample are seen to decrease. This photobleaching process may be followed by monitoring the change in the trapped electron's optical or e.s.r. absorption intensity with time.

Factors which can influence the photobleaching quantum efficiency Q include:

(a) bleaching wavelength used

(b) fraction of electrons already bleached

(c) temperature

(d) presence of scavengers

(e) mode of trapped electron production.

Presented below is a summary of the photobleaching characteristics for electrons trapped in various solid media:

Crystalline Ice:

The most recent evidence for stimulated decay in pure ice comes from (1). Trapped electrons were produced by gamma irradiation at $77^{o}K$ and electron concentrations were estimated as $5.5 \times 10^{15}/cm^{3}$. Q is zero for bleaching light around the absorption maximum (640nm, 1.9 ev) and reaches 0.22 at 380nm (3.2 ev) being apparently linear for energies above 2.6 ev. The decay rate is approximately first order for the time interval studied (15 min) although non-linearity is observed for the first 3 min. At all bleaching wavelengths the absorption spectrum was found to decay uniformly across the band, a fact which strongly supports the view that only a single species is present in the

medium. The fate of photobleached electrons in pure ice is believed to be in recombination with hydrogen ions and hydroxyl radicals, the latter having a density $5x10^3$ times that of the electrons (6).

Alkaline Ice

The photobleaching characteristics in this medium are complicated by the fact that two species of electrons are apparently present and can be interconverted by the excitation process (3.1(i)) causing a spectral shift. By choosing a suitable monitoring wavelength (590nm) for which interconversion has little effect on the optical density the quantum efficiency at 77^oK has been found to be independent of bleaching wavelength (2) having a value around 0.15. Experiments performed at 4^oK reveal that the process is also temperature independent in this range. Q is also found to be dependent on the fraction of electrons bleached being approximately related to the fraction F by (2).

$$Q=0.15\exp(-3.7F)$$

The initial value of Q is found to increase when acrylamide, acting as an electron scavenger, is present and tends to an apparent plateau of 0.4 when the solute concentration reaches $5x10^{-2}M$.

Smaller values of Q are obtained for electrons produced by photoionisation of potassium ferrocyanide ($5x10^{-3}M$). Since a major part of the electron loss is thought to be due to recombination with O^- ions in gamma irradiated samples the above feature may be due to lower scavenger concentrations since such anions are absent in the former process.

Methyltetrahydrofuran

Experiments at 77°K for gamma radiation produced electrons show the quantum efficiency to be wavelength dependent (9) rising slowly from the optical spectrum threshold (1965nm) to 900nm with a value of 0.005. At higher energies Q increases rapidly to a maximum value of 0.15 at 500nm (3). Q is independent of initial radiation dose but decreases with the fraction of electrons bleached (9), being apparently less dependent on fraction after 50% bleaching. Q increases almost linearly with increasing biphenyl concentration, in the 0.05 mole % range, and this correlates with the increasing formation of the biphenyl anion. The slight temperature dependence (E_{act}=0.001 ev) and light intensity dependence of bleaching in the 900nm range has already been discussed (3.1 (i)) in relation to the proposed energy level structure for the trapped electron.

3 Methylpentane

As with the spontaneous trapped electron decay, the loss of electrons by photobleaching occurs by recombination with positive ions. The quantum efficiency has been measured by following the e.s.r. signal intensity in gamma irradiated samples at 71°K (13). At this temperature spontaneous decay contributions were considered unimportant in the time interval. Q varies from 1.0 around the high energy side of the spectrum (950nm) to zero at the threshold (2300nm), having a value of 0.25 at the maximum (1750nm). Q decreases to zero with the fraction bleached (12) becoming linearly proportional to the optical density of the sample during the later stages, suggesting that non-local scavenging is involved. Initial values of Q, however, are

independent of radiation dose, suggesting the dominance of local scavenging initially. The presence of biphenyl as scavenger (0.02 mole %) maintains Q at its initial value throughout bleaching. The possible importance of scavenging by sites adjacent to trapped electrons in photoionisation produced species has already been mentioned (3.2).

REFERENCES

1 K. Kawabata J. Chem. Phys. 55(8), 3672, (1971)
G. Nilsson, H. Christensen, P. Pagsberg, S. O. Neilsen
J. Phys. Chem. 76(7), 1000, (1972)

2 H. Hase, L. Kevan J. Chem. Phys. 54(3) (1971)

3 L. Kevan J. Phys. Chem. 76(25),3830,(1972)

4 N. V. Kassen, H. A. Gillis, G. G. Teather J. Phys. Chem. 76(25), 3847, (1972)

5 L. Kevan 'Radiation Chemistry of Aqueous Systems', Ed. G. Stein

6 I. A. Taub, K. Eiben J. Chem. Phys 49(6), 2499, (1968)

7 K. Kawabata, S. Okabe, S. Taniguchi J. Chem. Phys. 57(7), 2855, (1972)

8 J. L. Dye, M. G. Debacker, L. F. Dorfman J. Chem. Phys. 52, 6251, (1970)

9 P. J. Dyne, O. A. Miller Can. J. Chem. 43, 2696, (1965)

10 T. Holstein Ann. Phys. (New York) 8, 343, (1959)

11 R. W. Munn, W. Siebrand J. Chem. Phys. 52, 6391, (1970)

12 D. W. Skelly, W. H. Hamill J. Chem. Phys. 44(8), 2891, (1966)

13 J. R. Miller, J. E. Willard J. Phys. Chem. 76(16),2341,(1972)

14 B. D. Michael, E. J. Hart, K. H. Schmidt, J. Phys. Chem. 75(18), 2798, (1971)

15 A. Pikaev Rad. Res. Rev. 5, 177, (1974)

16 R. W. Munn, W. Siebrand J. Chem. Phys. 52, 47, (1970)

17 F. S. Dainton, G. A. Salmon Proc. Roy. Soc. Ser. A.285 319, (1965) T. Shida J. Phys. Chem. 73(12),4311,(1969)

18 V. N. Shubin, S.A. Kabakchi, T.E. Pernikova, Yu.I.Sharanin Proc.Tihany Symp.Rad.Chem. 3rd Budapest, 1151, (1972)

19 T. E. Pernikova, S. A. Kabakchi, V. N. Shubin, P. I. Dolin Radiat. Eff. 5, 133, (1970)

20 K. Kawabata, H. Horii, S. Okabe, Chem. Phys. Lett.14,(2) 223, (1972)

21 K. Kawabata, S. Okabe, H. Horii Chem. Phys. Lett. 20(6) 586, (1973)

22 G. V. Buxton, F. C. R. Cattell, F. S. Dainton Trans. Far. Soc. 67, 687, (1971) V. N. Shubin, V. A. Zhigunov, P. I. Dolin Nature 212, 1002, (1966)

23 J.R. Miller Chem. Phys. Lett. 22(1), 180, (1973)

24 D. R. Smith, J. J. Pieroni Can. J. Chem. 43, 876, (1965)

25 J. R. Miller, J. E. Willard J. Phys. Chem. 76(18), 2641, (1972)

26 J. R. Miller J. Chem. Phys. 56(10), 5173, (1972)

27 J. Moan, H. B. Steen J. Phys. Chem. 75(19), 2893, (1971)

28 H. Moeckel, J. Yuen, L. Kevan J. Phys. Chem. 77(25), 3035, (1973)

29 J. B. Gallivan, W. H. Hamill J. Chem. Phys. 44(3), 1279 (1966)

30 D. Shooter, J. E. Willard J. Phys. Chem. 76(22), 3167, (1972)

31 K. Funabashi, P. J. Herley, M. Burton J. Chem. Phys. 43(11), 3939, (1965)

32 J. B. Gallivan, W. H. Hamill J. Chem. Phys. 44(6), 2378, (1966)

33 B. Wiseall, J. E. Willard J. Chem. Phys. 46(11), 4387, (1967)

34 S. L. Hager, J. E. Willard Chem. Phys. Lett. 24(1),102,(1974)

35 J. T. Richards, J. K. Thomas J. Chem. Phys. 53(1) 218, (1970)

36 J. T.Richards, J. K. Thomas Chem. Phys. Lett. 8(1) 13, (1971)

37 W. M. McClain, A. C. Albrecht J. Chem. Phys. 44(4), 1594, (1966)

38 F. Kieffer, C. Meyer, J. Rigaut Chem. Phys. Lett. 11(3) 359, (1971)

C H A P T E R 4

TRAPPED ELECTRON THEORIES

The theoretical account of localised electrons in liquids and solids has developed along two main lines. These are the continuum and semi-continuum theory and the molecular cluster theory.

1 Dielectric Continuum Theories

(i) Early Developments

The continuum theory has evolved from concepts proposed by Landau (1) and later developed by Pekar (2) to account for excess electron states in ionic crystals. Within this scheme it was proposed that a deformation of the crystal could lead to a localised electron state if the total energy was lower than that of a delocalised one.

The permanent deformation of the crystal was considered to arise from the response of the medium to the presence of the electron itself. For an electron confined to a particular region in the system, the response of the crystal can be described by the instantaneous polarisation $\underline{P}$. This polarisation can be described in terms of optical and inertial components related to the dielectric displacement $\underline{D}$ by the high and low frequency dielectric constants D_{op} and D_s such that

$$\underline{P} = \left(1 - \frac{1}{D_s}\right) \underline{D}$$ is the total polarisation

and $$\underline{P}_{op} = \left(1 - \frac{1}{D_{op}}\right) \underline{D}$$ is that due to optical polarisation alone.

The inertial polarisation is then given by:

$$\underline{P}_i = \beta \underline{D} \quad \text{where } \beta = \frac{1}{D_{op}} - \frac{1}{D_s}$$

Since these two types of polarisation have different response times, corresponding to optical and vibrational frequencies respectively, a localised electron with a period lying between these two extremes is regarded as being able to produce a permanent deformation via inertial polarisation, since the massive nuclei see only the average field due to the electron distribution. This polarisation is regarded as simultaneously providing the potential well which maintains the electron in a state of localisation, the state being termed a polaron. For the evaluation of the polarisation, the medium is regarded as a continuous dielectric, which requires that the change in the displacement $\underline{D}$ within the lattice distance is small. This condition further requires that the polaron radius is greater than the lattice spacing.

The polaron potential in which the electron moves is found by solving Poisson's equation which yields:

$$V(r) = -\beta \int \frac{\Psi^2(r')}{|r-r'|} \partial\tau' \qquad (1)$$

where $\Psi(r')$ is the electron wavefunction.

The states of the electron in such a field are obtained by solving the Schroedinger equation

$$\left\{ \frac{d^2}{dr^2} - 2V(r) - 2E + \frac{\ell(\ell+1)}{r^2} \right\} P_{nl}(r) = 0 \qquad (2)$$

from which the wave function $\Psi(r\,\theta\,\varphi) = Y_{lm}(\theta\,\varphi)\,\frac{P_{nl}(r)}{r}$

where $Y_{\ell m}(\theta\varphi)$ is the spherical harmonic and

$$\int P_{n\ell}^{2}(r)\partial r = 1$$

Pekar (3) obtained an analytical solution to the above equation using a three parameter trial function for the spherical ground state, obtaining for the electronic energy

$$E_{1s} = -0.164\left(\frac{D_s - 1}{D_s}\right)^2 \quad \text{au} \qquad (3)$$

Pekar's choice of the static dielectric constant, although inconsistent with an inertially polarised medium, does not affect the general method of the polaron approach.

To determine the stability of the polaron state, the free energy of the polarised dielectric must be added to eq. (3). This is given by (4, 5).

$$F = \tfrac{1}{2}\int P.D\,\partial\tau = -\tfrac{1}{2}\int V(r)\Psi_{1s}^{2}(r)r^{2}\partial r$$

This yields for the total energy, the value

$$E_T = \tfrac{1}{3}E_{1s}$$

(ii) <u>The Continuum Cavity Model</u>

Some characteristics of the polaron model were present in the scheme proposed by Platzman (6) to account for the ultraviolet absorption by aqueous solutions of halide ions. In this, the absorption was viewed as arising from transitions between the eigenstates of the inertial polarisation associated with the anion. The notion that the additional electron resided partly within a cavity, presented itself naturally through the presence of the ions hydration shell. The experimental results were

remarkably reproduced despite the use of an 'effective hydrogen atom' approximation to evaluate the transition energy.

The concept of a solvent cavity formed the basis of the continuum cavity model proposed by Jortner (7) to account for the properties of solvated electrons in liquid ammonia. The potential is constructed using only inertial polarisation, as required by the adiabatic approximation (4), and on the assumption that the electron resides mainly within the cavity

$$V(r) = -\frac{\beta}{r} \qquad r > R_o$$

$$V(r) = -\frac{\beta}{R_o} \qquad r < R_o$$

Solutions were obtained variationally using single Slater functions for the ground 1s and excited 2p states. The interaction of the electron with the electronic polarisation of the medium was introduced as a correction, taking the form

$$S_i^e = -\tfrac{1}{2}\int_{\bar{r}_i}^{\infty} P_e . D\,\delta\tau = -\tfrac{1}{2}\int_{\bar{r}_i}^{\infty} \frac{P_e}{r^2}\, 4\pi r^2 \partial r$$

in which the electron is regarded as interacting with the induced electronic polarisation of the bulk medium beyond an effective radius, taken as the mean radius $\bar{r}_i$ for state $\underline{i}$. The ground state energy is ammended by the inertial polarisation energy of the medium

$$\Pi = \tfrac{1}{2}\int_{R_o}^{\infty} P . D\,\delta\tau = \tfrac{1}{2}\beta\int_{R_o}^{\infty} \frac{\Psi_{1s}^2(r)}{r}\,\partial r$$

The cavity radius R_o was obtained by fitting the calculated and observed optical transition energy (0.8 ev). A value of 3.2A° was obtained which correlated well with the calculated value of 3.45A° for the ammoniated species, as obtained from liquid expansion measurements. The total ground state energy (1.60 ev) compared favourably with the value estimated from heats of solution (1.7 ev). The temperature variation of β and R_o were used to calculate the thermal coefficient of the absorption maximum ($dh\nu_{max}/dT$) which was calculated as

$$\frac{d(h\nu)}{dT} = 0.88 \left\{\frac{d\beta}{dT}\right\} - 0.277 \left\{\frac{dR_o}{dT}\right\}$$

Based on approximate values of dR_o/dT for anions in solution, this quantity was negative as observed experimentally. This was taken as further justification for attributing a solvent cavity to the ammoniated species, since the non-cavity model used by Pekar predicted a positive coefficient, being dependent only on β.

The polarisation potential within which the electron is considered to move, has been obtained in a different manner by Iguchi (8) who has considered the polarisation in a polar medium to arise from a Boltzmann distribution of non-interacting point dipoles in the field of the excess electron. The polarisation was given as

$$P(r) = \int_o^{\pi} n_\gamma \left[\mu_o \cos\gamma - \frac{eq}{r^2}\right] \sin\gamma \, \partial\gamma$$

where the density of dipoles which make an angle γ with the radius vector is

$$n_\gamma = n_m \exp\left[-\frac{\varepsilon_\gamma}{kT}\right] \Big/ \int_o^\pi \exp\left[-\frac{\varepsilon_\gamma}{kT}\right] \sin\gamma \, \partial\gamma$$

and the interaction energy between the dipole and the orienting field E(r) is

$$\varepsilon_\gamma = -u_o . E(r) - \frac{\alpha E(r)^2}{2}$$

with u_o and α the molecular dipole and polarizability and n_m is the dipole density. When the field $E(r) = -\frac{er}{r^3}$ the potential is given as

$$V(r) = -e \int \frac{P(r') . |r-r'|}{|r-r'|^3} \partial\tau'$$

$$= -4\pi e u_o n_m \int_r^\infty \left[\coth \frac{x}{r^2} - \frac{r^2}{x}\right] \partial r$$

$$x = \frac{eu_o}{kT}$$

The total energy of the calculated levels is obtained by including a contribution due to electronic polarisation in the same manner as above and one due to dipole repulsion. For ethanol, the transition energy (1.69 ev) and temperature coefficient (1.6×10^{-3} ev/deg) are comparable to the experimental values of 1.77 ev and 3.4×10^{-3} ev/deg respectively although the calculated heat of formation seems overestimated (3.61 ev). A subsequent calculation (9) in which a cavity radius (3.2A°) was incorporated, yielded more reasonable heats of formation (2.14 ev) at the expense of agreement with observed transition energies.

Early calculations on organic glasses were made by Fueki (10) who applied Jortner's continuum cavity model within the adiabatic approximation to electrons in solid MTHF. The cavity radius was obtained (1.5A°) by fitting the 1s - 2p transition energy

(1.04 ev). At this radius the value obtained for the photoionisation threshold was 1.69 ev which corresponds with the presently accepted value (1.60 ev) based on photobleaching experiments (cf 3.1 (i)).

(iii) The Inclusion of a Medium Potential

Further developments in the continuum theory were directed toward a better description of the electron-medium interaction beyond the cavity. Based on the observed trends in scattering lengths for the rare gases in the gas phase (11), an adequate description of the scattering process could be obtained in terms of repulsions arising from exclusion effects and attractive polarisation interactions (12, 13). Following on from this, a pseudopotential method was applied to electrons in liquid helium and argon to obtain their ground state energy. The Wigner-Seitz model was applied to the molecules, the potential in which the electron moves being represented by

$$V(r) = v_a + U_p$$

where $v_a = \infty \quad r<r_s$ and $v_a = 0 \; r>r_s$, r_s being the hard core radius and U_p is a constant representing the long range attractive polarisation potential of the medium. The eigenvalue equation to be solved is then

$$\left(-\tfrac{1}{2}\nabla^2 + V(r)\right)\Psi_o = V_o\Psi_o$$

subject to the conditions:

$$\left.\frac{d\Psi_o}{dr}\right|_{r=r_s} = 0$$

Such an analysis was able to account for the positive V_o value in helium and negative value in argon as obtained from adiabatic

electron injection measurements (14). The inclusion of V_o in the potential terms of a calculation for localised electrons was made for liquid helium, in which the most stable state is considered to be that of an electron contained in a large cavity. The eigenvalue equation was represented simply by

$$\left(-\tfrac{1}{2}\nabla^2 - E\right)\Psi(r) = 0 \qquad r < R$$

$$\left(-\tfrac{1}{2}\nabla^2 + V_o - E\right)\Psi(r) = 0 \qquad r > R$$

By incorporating energy terms to account for void formation, this method had considerable success in describing cavity size, mobility and photoionisation threshold for the electron in helium.

The inclusion of a V_o term in the continuum cavity model for polar systems was made by Jortner for the ammoniated electron (15) for which the potential function took the form

$$V(r) = -\frac{\beta}{R} \qquad r < R$$

$$V(r) = -\frac{\beta}{r} + V_o \qquad r > R$$

Since V_o values cannot be easily obtained for polar systems values were chosen around $V_o = 0$. Depending on whether V_o is positive or negative it has the predictable effect of adding or withdrawing electronic charge from the cavity.

(iv) <u>The S.C.F. Approximation</u>

The electronic adiabatic approximation being based on the assumption that the motion of the excess electron can be separated from that of the tightly bound medium electrons, is expected to break down in strongly polar substances, in which the excess electron is bound by several ev (4). In this case the use of inertial polarisation alone becomes invalid and the potential of

eq. (1) becomes

$$V(r) = -\left(1 - \frac{1}{D_s}\right)\int \frac{\Psi^2(r')}{|r-r'|}\,\partial\tau'$$

where D_s is the static dielectric constant.

The self-consistent nature of the polaron problem has been formally acknowledged by the assignment of the term SCF approximation to the above scheme which includes medium electronic and inertial polarisation in a self-consistent manner.

After Pekar, the SCF approximation was first used by Jortner for the hydrated electron (16) using the potential function

$$V(r) = -\left(1 - \frac{1}{D_s}\right) f(R_o) \qquad r < R_o$$

$$V(r) = -\left(1 - \frac{1}{D_s}\right) f(r) \qquad r > R_o$$

where f(r) is the solution of $\mathrm{div}(\mathrm{grad} f(r)) = e|\Psi(r)|^2$.
The medium polarisation energy was calculated for state $\underline{i}$ as

$$\Pi_i = \tfrac{1}{2}\left(1 - \frac{1}{D_s}\right)\int \Psi_i f_i \Psi_i \,\partial\tau$$

Solution was performed using single Slater functions for the ground and excited states. The minimum ground state energy of -1.32 ev was obtained for zero cavity radius compared to the observed value of -1.7 ev. The calculated 1s-2p transition energy was 1.35 ev (ΔE_{expt} = 1.72 ev). Use of a three parameter wave function by Fueki et. al. (17), considerably amended the above results obtained by Jortner and at the same time suggested that results in accord with experiment could be obtained at a finite cavity radius.

(v) The Semi-Continuum Model

The development within the dielectric continuum theory has

been directed toward a more realistic account of the molecular structure of the medium. A refinement of the cavity model, therefore, is the semi-continuum theory which amends the potential terms within the cavity by attributing some molecular structure to the cavity wall. In the usual approximation, the molecules of the first layer are represented by point dipoles and the dipole moment at distance r_d from the centre is expanded in spherical harmonics. If only the first term in the expansion is considered ($\ell=0$), the dipole contribution from N molecules becomes

$$V = -\frac{Nue}{r_d^2}$$

where u is the average radial component of the dipole moment $u = u_o\langle\cos\theta\rangle$ and $\langle\cos\theta\rangle$ is obtained from the Langevin function

$$\langle\cos\theta\rangle = \coth x - \frac{1}{x}$$

where $x = \frac{u_o E}{kT}$ and $E = \frac{eC_i}{r_d^2}$

C_i being the excess electron charge contained within the radius r_d.

Jortner (15) applied the semi-continuum model to the ammoniated electron within the adiabatic approximation using the potential function

$$V(r) = -\frac{Nue}{r_d^2} - \frac{\beta e^2}{r_c} \qquad r < R$$

$$V(r) = -\frac{\beta e^2}{r} + V_o \qquad r > R$$

where the various radii are defined as shown

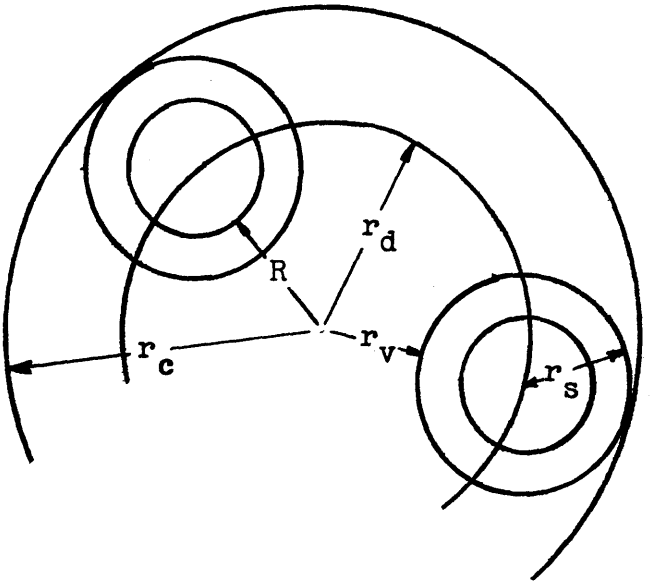

The total energy of the ground 1s state is calculated by incorporating the following additional terms

(a) electron-medium electronic polarisation interaction for state $\underline{i}$

$$S_i = - \frac{N\alpha C_i^2(r_d)}{r_d^4} - \tfrac{1}{2} \gamma_o \int_R^\infty \frac{C_i^2(r)}{r^2} \partial r$$

where α = the molecular polarisability

$$\gamma_o = 1 - \frac{1}{D_{op}}$$

$C_i(r)$ = charge contained within radius $\underline{r}$

The first term represents the interaction with the induced dipole moment of the first layer molecules whilst the second is the interaction with the electronic polarisation of the bulk medium.

(b) energy required to form a cavity in the liquid. This is represented by a surface energy term representing the loss of bonding interactions and a pressure volume term.

$$E = E_{st} + E_{pv} = 4\pi SR^2 + \frac{4}{3}\pi R^3 P$$

where S is the surface tension and P the external pressure

(c) dipole repulsion terms for the first layer molecules given by

$$E_{dd} = \frac{D_N u_T^2}{r_d^3}$$

where D_N is a constant depending on the number of dipoles and u_T is the total dipole moment given by

$$u_T = u_o\langle\cos\theta\rangle + \frac{e\,a\,C_i(r_d)}{r_d^2}$$

(d) the inertial polarisation energy of the medium

$$\Pi = \tfrac{1}{2}\int P.D\,\partial\tau = -\tfrac{1}{2}\int V(r)\psi^2(r)r^2\partial r$$

where V(r) is the inertial polarisation potential. Although the electron wavefunction was calculated using an inertial potential which assumed an electron at the centre of the cavity, the medium energy was evaluated using the strictly correct form for the polarisation

$$V(r) = -\beta\left[\frac{1}{r_c}\int_o^{r_c}\psi_{1s}^2(s)s^2\partial s + \int_{r_c}^{\infty}\frac{\psi_{1s}^2(s)s^2\partial s}{s}\right] \qquad r<R$$

$$V(r) = -\beta\left[\frac{1}{r}\int_o^{r}\psi_{1s}^2(s)s^2\partial s + \int_{r}^{\infty}\frac{\psi_{1s}^2(s)s^2\partial s}{s}\right] \qquad r>R$$

(e) the intermolecular hydrogen-hydrogen repulsion energy. Based on studies of water (18), this term was taken to be of the form

$$E_{H-H} = C_{HH}\exp\left[-4.60(A_N R - B_N)\right]$$

where R is the cavity radius and the constants relate to particular geometries.

For chosen values of the parameter V_o, configuration coordinate diagrams, in terms of the coordinate R, were presented for temperatures of 203°K and 300°K. For V_o values in the range -0.5 - 0.5 ev, the most stable species was found for 4 and 6 first layer molecules.

The calculation of transition energies was performed within the Franck-Condon approximation, the excited states being evaluated within the inertial polarisation field of the ground state.

By allowing for the radius of the first layer molecules, the cavity radius was calculated as 3.1A^{o} compared to the estimated experimental value of 3.2A^{o}. The 1s-2p transition energy was calculated as 1.08 ev (expt. 0.8 ev) whilst the heat of solution was overestimated (2.93 ev, expt. = 1.7 ev). The effective cavity radius was found to decrease with increasing temperature being 2.7A^{o} at 300^{o}K, from which the temperature coefficient of the absorption maximum was found to be -4.7cm^{-1}/^{o}K (expt. = -12cm^{-1}/^{o}K).

Semi-continuum calculations on electrons in water and ice have been carried out by Kevan et. al. (19 - 21) within SCF approximation. For 4 and 6 first layer molecules, and with V_o = -1.0 ev, configurational minima have been found for the ground states in water and ice (77^{o}K) for cavity radii of around 2A^{o}. For N = 6, values for the transition energy, oscillator strength, ionisation threshold and heat of solution agree with the experimental values to within 15%.

Similar calculations have been performed by Nilsson, who has considered the electron in water and ice to be trapped in the naturally existing dodecahedral cavities (22 - 24). Based on the O - O separations which are known as a function of temperature (25) from X ray studies, radii were obtained for the twelve nearest point dipoles which form a double solvation layer. As in previous calculations these dipoles were taken to be in

thermal equilibrium with the excess electron's field. Estimates for the transition energy agreed with experiment to within 5%, over the temperature range 90 - 356°K, although the oscillator strength was consistently high.

Semi-continuum calculations have been performed for various other media, including alcohols and organic glasses. Notable among these, is a study of electrons in MTHF (21) for which good agreement has been found between calculated and observed transition energies, ionisation threshold and oscillator strength. Evaluation of the 2s energy level in this medium has revealed that it lies below the unrelaxed Franck-Condon 2p state which is consistent with the present view of the energy level structure in MTHF.

Use of the semi-continuum model in a less rigorous form, has had some success in accounting for the electron spin density at nitrogen in metal ammonia solutions (26, 27). This was accomplished by applying a Schmidt orthogonalisation procedure to the excess electron wavefunction using the molecular orbitals of the first layer ammonia molecules. The results for the spin density at hydrogen, however, were contrary to experiment.

2 Molecular Cluster Theories

(i) Some Early Models

The molecular cluster theory (30) is based on the notion that the excess electron in liquids and solids can be represented by a compound molecular ion composed of a group of solvent molecules. Since the problem is approached within the context of Molecular Orbital Theory, computational difficulties restrict the number of such molecules which can be considered to 2 - 5, depending on the level of approximation employed.

One of the earliest cluster models was that of Natori and Watanabe (28), who considered a tetrahedral arrangement of water molecules in which an O-H bond from each molecule was directed toward the centre of the tetrahedran. Molecular orbitals were constructed using 1s orbitals from each of the four central hydrogens. The Hamiltonian was constructed within a Hartree approximation, based on empirical charge distributions. Solution of the secular determinant yield energies for the ground state and triply degenerate excited state, which were minimised with respect to the hydrogen orbital exponents. The ground and excited state energies were obtained as -4.38 and -3.58 ev respectively, yielding a transition energy of 0.8 ev. The energy required to form such a tetrahedral arrangement of molecules was considered to be 2.0 ev which gave a total ground state energy of -2.38 ev compared with the experimental value of -1.7 ev. The oscillator strength for the transition was low at 0.26. Later calculations within the above model (29), showed that small changes in the molecular geometry could reproduce the experimental transition energy although the calculated e.s.r.

hyperfine splittings, based on calculated spin densities, were too large by a factor of three.

More rigorous calculations have been performed within the INDO approximation (31) for the hydrated and ammoniated electron, represented by dimer and tetramer structures. For the planar dimer structure in which the hydrogens are opposed, a configurational minimum is obtained for an H--H separation of 1.20A°, at which geometry the transition energy is 1.97 ev. Calculations on a Watanabe type water tetramer have shown stability with respect to dissociated components by an amount equal to 2.22 ev. Similar calculations at the INDO level (32) have confirmed the preferred structure for the $(H_2O)_2^-$ system, a transition energy of 1.33 ev being obtained.

(ii) Inclusion of the Medium

A more recent study of the hydrated electron at the ab initio level (33) has incorporated also the concepts used in the dielectric continuum theory. A tetramer structure was considered, in which the dipole vector of each molecule was directed toward the centre of a tetrahedron and situated a distance R from it. Within the Hartree-Fock formalism, the total energy for such a system is represented in the usual notation by

$$E^{o} = \sum_{i} H_i + \sum_{i,j} (J_{ij} - K_{ij})$$

To this was added the dielectric polarisation energy

$$U = -\tfrac{1}{2}\int P.D\,\partial\tau = -\tfrac{1}{2}\left[1 - \frac{1}{D_s}\right]\int_{o}^{\infty}\rho(r)g(r,r')\rho(r')\,\partial\tau\partial\tau'$$

where $\rho(r)$ is the molecular charge density

$$\rho(r) = \sum_{i}\psi_i^2(r) - \sum_{k} Z_k\delta(r-r_k)$$

and $g(r,r')$ is the operator defined by

$$g(r,r') = -1/\max(r,r',r_c)$$ where r_c is the cavity radius.

Self-consistent solutions were obtained by solving the eigenvalue equation

$$(F_k + f_k)\psi = E_k\psi$$

where F_k is the usual Fock operator

$$F_k = G_k + \sum_\ell (2J_\ell - K_\ell)$$

and f_k is the operator for the polarisation

$$f_k = -\left[1 - \frac{1}{D_s}\right]\left[g(r,r_c)\sum Z_i - \sum_\ell \int g(r,r')\psi_\ell^2(r')\,\partial\tau'\right]$$

A configurational minimum is found for R = 2.68A^{o} which, with the inclusion of a surface tension correction, yields a total ground state energy of -1.1 ev. As with simpler models (32) the correct sign for the electron spin density at hydrogen is predicted as well as a hyperfine splitting constant in good agreement with experiment.

3 The Origin of the Band Width

(i) Cavity Vibration Models

Based on semi-continuum calculations, Jortner has investigated the band width in the ammoniated electron spectrum, on the assumption that the most important contribution comes from the symmetric cavity vibration (15). This vibration is represented by the previously evaluated configuration coordinate diagram in terms of the cavity radius R. A classical approximation is invoked at temperatures in the range 200 - 300°K in which the absorption band is considered to arise from a distribution of vibrational ground states. For a coordinate displacement X from equilibrium, defined by $X = R-R_o$, the vibrational energy is represented by

$$A(X) = E_t(1s) - E_t^o(1s)$$

The classical intensity distribution function F(E) for a transition of energy E is then given by

$$F(E) = \exp\left[-\frac{A(E)}{kT}\right]\left[\frac{dX}{dE}\right]$$

where $\left[\frac{dX}{dE}\right] = \left[B'(X) - A'(X)\right]^{-1}$

and $B(X) = E_t(2p)$

Half widths calculated with the above function are in the range 0.12 - 0.16 ev compared to observed values of 0.46 ev.

In a later study (34, 35)a Boltzmann distribution of first layer cavity dipoles was considered with an improvement of only 0.004 ev in the half width. The possibility that cavities with N = 4 and N = 6 might both contribute to the absorption was also considered statistically yielding a further 0.03 ev to the width. A further source of broadening considered was the deviation of

the medium polarisation field from equilibrium through the medium polaron modes. In terms of the quantity E_s, which represents the non-equilibrium polarisation energy of the excited state, the intensity distribution function due to polaron modes is

$$F(E) = \exp\left[-\frac{(E-E_s-\Delta E)^2}{4kTE_s}\right]$$

where E_s is given by $E_s = \frac{1}{2}\beta\int(P_s-P_p)^2\partial\tau$

where P_s and P_p are the polarisations in the lower and upper states, and ΔE is defined at the equilibrium polarisation configurations X_o by

$$\Delta E = E_t^{2p}(X_o^{2p}) - E_t^{1s}(X_o^{1s})$$

Since the half width due to this factor was 0.09 ev, an upper limit to the theoretical value due to all sources was 0.20 ev.

The possibility that a fluctuation in the medium polarisation may contribute to the half width has also been studied by Tachiya et. al. (36,37) who performed self-consistent continuum calculations on the hydrated electron. The total polarisation energy contained in the dielectric was written as

$U = -\gamma\int P.P\,\partial\tau$ instead of the usual form

$$U = -\frac{D_s}{2(D_s-1)}\int P.P\,\partial\tau$$

The constant γ was chosen such that the total ground state energy fitted the experimental value (-1.7 ev), it being considered that the medium polarisation lay between the saturated dipole limit of Iguchi (8) and the weak field limit. Since the ground state energy is minimum with respect to the polarisation, configuration diagrams were constructed for the ground and excited states in terms of a polarisation coordinate. Using Jortner's

intensity function, the band shape was given as

$$F(E) = \exp\left[-\frac{A(X)}{kT}\right]\left|\frac{dX}{dE}\right| \delta(E-E_{1s}(X)-E_{2p}(X))$$

where X is the polarisation coordinate and

$$A(X) = E_{1s}(X)-E_{1s}(X^{o})$$

For T = 300°K the absorption maximum was at 2.04 ev and the half width was 0.52 ev (expt. = 0.92 ev).

(ii) A Photoionisation Profile Model

An alternative source to spectral broadening was suggested by Kajiwara et. al. (38), who considered the possibility that the absorption spectrum may arise from direct transitions to a continuum state. Using simple spherical wells, defined by depth V_o and radius R, the transition moments for the ground state to the continuum p state were evaluated using exact continuum functions (cf 2.2 (ii)). The three media, ammonia, water and ethanol were considered, and for each at several temperatures, the variables V_o and R were chosen so as to provide photoionisation curves whose maxima coincided on the energy scale with that of the respective absorption spectra. In all cases parameters could be chosen which reproduced the observed spectra for over 90% of the absorption range at various temperatures. The optimum potential radii R chosen, lay in the range 2.0 - 4.0A° and for ammonia (R = 3.61 - 3.88A°) the value was similar to the radius assigned to the species from experiment (7).

REFERENCES

1 L. Landau J. Phys. (USSR) 3, 664, (1933)

2 S. Pekar J. Phys. (USSR) 10, 341, (1946)

3 S. Pekar J. Phys. (USSR) 10, 347, (1946)

4 J. Jortner Mol. Phys. 5, 257, (1962)

5 R. A. Marcus J. Chem. Phys. 24(5), 966, (1956)

6 R. Platzman, J. Franck Z. für. Physik 138, 411, (1954)

7 J. Jortner J. Chem. Phys. 30(3), 839, (1959)

8 K. Iguchi J. Chem. Phys. 48, 1735, (1968)

9 K. Iguchi J. Chem. Phys. 51, 3137, (1969)

10 K. Fueki J. Chem. Phys. 44, 3140, (1966)

11 T. F. O'Malley Phys. Rev. 130, 1020, (1963)
J. Jortner 'Actions Chimiques et Biologiques des Radiations'
Ed. M. Haissinsky

12 N. R. Kestner, J. Jortner, S. A. Rice, M. H. Cohen
Phys. Rev. 140, A56, (1965)

13 D. G. Thomson Proc. Roy. Soc. London A294, 160, (1968)

14 B. E. Springett, J. Jortner, M. Cohen J. Chem. Phys.
48(6) 2720, (1968)

15 D. A. Copeland, N. R. Kestner, J. Jortner J. Chem. Phys.
53, 1189, (1970)

16 J. Jortner Rad. Res. Supp. 4, 24, (1964)

17 K. Fueki, D. F. Feng, L. Kevan Chem. Phys. Lett. 4(5),
313, (1969)

18 D. Eisenberg, W. Kauzmann 'The Structure and Properties of
Water' (O.U.P. New York, 1969)

19 K. Fueki, D. F. Feng, L. Kevan J. Phys. Chem. 74(4),
1976, (1970)

20 K. Fueki, D. Feng, L. Kevan, R. E. Christoffersen
J. Phys. Chem. 75, 2297, (1971)

21 K. Fueki, D. F. Feng, L. Kevan, J. Amer. Chem. Soc.
95(5), 1398, (1973)

22 J. W. Perram Mol. Phys. 20(1), 1077, (1971)

23 G. Nemethy, H. A. Scheraga J. Chem. Phys. 36(12),
3382, (1962)

24 A. T. Hagler, H. A. Scheraga, G. Nemethy J. Phys. Chem.
76(22), 3229, (1972)

25 A. H. Narten, M. D. Danford, H. A. Levy Disc. Farad. Soc.
43, 97 (1967)

26 D. E. O'Reilly J. Chem. Phys. 41(12), 3736, (1964)

27 R. H. Land, D. E. O'Reilly J. Chem. Phys. 46, 4496, (1967)

28 M. Natori, T. Watanabe J. Phys. Soc. Japan 21(8), 1573, (1966)

29 M. Natori J. Phys. Soc. (Japan) 24(4), 913, (1968)

30 L. Raff, H. A. Pohl Adv. Chem. Ser. 50, 173, (1965)

31 G. Howat, B. C. Webster Rad. Res. Rev. 4(2), 259, (1972)

32 S. Ishimaru, H. Tomita, T. Yamabe, K. Fukui, H. Kato
Chem. Phys. Lett. 23, 106, (1973)

33 M. D. Newton J. Chem. Phys. 58(12), 5833, (1973)

34 N. R. Kestner, J. Jortner J. Phys. Chem. 77(8), 1040, (1973)

35 N. R. Kestner, J. Jortner Chem. Phys. Lett. 19(3), 328,(1973)

36 M. Tachiya, Y. Tabata, K. Oshima J. Phys. Chem. 77(2),
263, (1973), J. Phys. Chem. 77(19), 2286, (1973)

37 M. Tachiya, A. Mozumder J. Chem. Phys 60(8), 3037, (1974)

38 T. Kajiwara, K. Funabashi, C. Naleway Phys. Rev. A.6,
808,(1972)

CHAPTER 5

INVESTIGATION OF EXCESS ELECTRON PROPERTIES

1 Hydrogen Bonding and Trapped Electron Theory

(i) Introduction

In the review of trapped electron theories presented in Chapter 4 it was shown that within the most recent semi-continuum and molecular cluster calculations, the total energy of the system involved several terms comprising excess electron energy, medium polarisation, pressure volume work, dipole repulsion, hydrogen-hydrogen repulsion and surface tension energy. From the development of the theory, it is natural to expect that future progress in the description of the total energy, energy surfaces, band shapes and cavity distribution features, will be involved with a more detailed description of the above energy terms.

One such energy contribution which has received little explicit consideration is that which results from a change in the hydrogen bonding interactions in a hydrogen bonded system, when molecular reorientation at the cavity surface takes place. In addition to their role in deciding trapped electron stability criteria, such interactions between first and second layers at a cavity surface can be expected to contribute significantly both to relaxation phenomena accompanying solvation and to the subsequent shape of configuration coordinate curves and hence absorption bands. It is evident that the inclusion of such interactions will require a detailed knowledge of both the magnitude and origin of the hydrogen bond energy as well as their variation with intermolecular geometries.

Whilst the large number of studies which have been carried out on the hydrogen bond interaction have yielded substantial information for various systems on the magnitude of the interaction and its behaviour with intermolecular orientation, few investigations have been made into the origin of the interaction and the extent to which various molecular orbital methods are in agreement as to the relative importance of contributing factors.

Calculations have therefore been performed within a localised molecular orbital framework for some hydrogen bonded dimer systems, in an attempt to reveal the nature of some aspects of the interaction and the associated electron density changes. It is expected that a localised orbital description will be capable of discovering which molecular regions are most affected by the interaction and the manner in which peripheral regions respond.

(ii) Some Earlier Studies Reviewed

A useful description of the term 'hydrogen bond' which has been justified by the many systems exhibiting the phenomenon is that due to Pimentel and McClellan (1) who described it as an interaction between a group A-H and an atom or group of atoms B in the same or a different molecule, when there is evidence of bond formation and when there is evidence that this new bond linking A-H and B specifically involves the hydrogen atom linked to A. Direct evidence of such involvement is often revealed in crystal structures when the H ... B separation is much less than the van der Waals radii of H and B.

Hydrogen bonds can be formed most readily when A-H is a polar molecule or group and B is an electron source such as

N, O, F^-, S or a pi-electron system. The many physical and chemical properties associated with hydrogen bond formation are described in Pimentel and McClellan's book (1).

Interaction energies vary from a few Kcal to around 40Kcal for the FHF^- system and early attempts at their calculation employed electrostatic point charge models (2,3). Such a model applied to the O-H.....O system yielded a value of 6Kcal (3) which is close to the experimental value of 5Kcal/mole for the water dimer (4). Such arguments, however, are incapable of accounting for such effects as charge redistribution, which is implied by the infra red spectral intensity changes, and closed shell repulsion which must be significant at the separations involved.

Progress in the calculations came initially with the development of semi-empirical molecular orbital methods (CNDO (5), CNDO/2 (6), INDO (7)) and latterly with the use of the non-empirical ab initio method (8). Reviews of the development of theoretical approaches to the hydrogen bond have been given by Lin (9) and Bratoz (10).

A much studied system is that of the water dimer some possible structures for which are shown below:

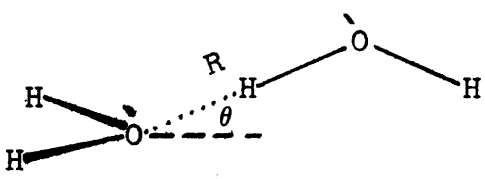

Linear

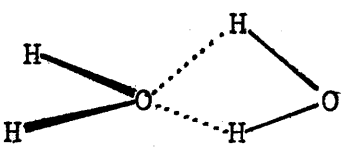

Bifurcated

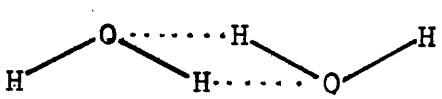

Cyclic

Most of the recent ab initio studies are in agreement that the linear structure is the most stable whilst some differences exist as to the total interaction energy and the value of θ. A summary of the results for the recent ab initio studies on the linear system is presented in Table 5.1.1.

TABLE 5.1.1

Basis Set		Dimerisation Energy (Kcal)	R(O-O)A^{o}	θ deg
(5,3,3) Gaussian	(11)	12.6	2.68	0
Hartree-Fock AO contracted Gaussian	(12)	5.3	3.0	25
Single Slater	(13)	6.55	2.76	57
Gaussian fit to Slaters	(14)	6.1	2.73	57
Extended basis with polarisation functions	(15)	4.7	3.0	40
CNDO (expt'l monomer geometry	(16,17)	5.9	2.53	0
CNDO (optomised geometries)	(17)	8.4	2.53	0

In the above table it can be seen that both ab initio and semi-empirical methods are capable of providing reasonable estimates for interaction energies and separation distances (R (O-O) ice = 2.76A^{o}) although the approximations involved in the latter seems to remove angular sensitivity.

From these and other calculations at different levels of approximation, some general features can be summarised concerning

the change in charge distribution on hydrogen bond formation.

(a) The hydrogen in the hydrogen bond loses electrons

(b) The electronegative atoms gain electrons: more being gained by the atom attached to the donated hydrogen.

(c) The greatest loss of electrons occurs at the atoms attached to the electron donor.

(d) Charge is gained by the peripheral atoms of the proton donor.

These changes have important consequences in the formation of higher polymers for which it is observed that the stabilisation energy per H-bond increases with the number of molecules (15).

(iii) Energy Breakdown Schemes

The first investigations into the individual terms comprising the hydrogen bond energy were those of Tsubomura (18) and Coulson and Danielsson (19). From these valence bond calculations it was concluded that the total energy could be divided into four terms of roughly equal importance represented by electrostatic (E_{es}), exchange repulsion (E_{ex}), delocalisation (E_{ct}) and dispersion interactions (E_d), and for the $(H_2O)_2$ system only the exchange term was destabilising at the distance involved. The concept of a polarisation interaction (E_p) was later introduced by Grahn (20) and found to be weakly stabilising.

Subsequent calculations on various systems at the ab initio level have confirmed these initial observations. However, similar breakdown schemes applied within the semiempirical M.O. method have revealed some basic differences in the way in which such methods account for the hydrogen bond energy (21). These differences can be summarised by the following:-

(a) the use of only valence electrons and the approximations involved in electron-core interactions lead to a repulsive electrostatic contribution.

(b) the selective neglect of certain multi-centre two electron integrals leads to a zero contribution for the exchange term.

A summary of the energy breakdown results for various systems and at different levels of approximation is given in Table 5.1.2.

TABLE 5.1.2

System/Method	E_{es}	E_{ex}	E_{ct}	E_p	E_d
$(H_2O)_2$ ab initio (22)	4.50		3.05		1.54
$(H_2O)_2$ ab initio (21)	8.0	-9.86	8.16	0.25	
$(H_2O)_2$ valence bond (19)	6.0	-8.4	8.0		3.0
$(HF)_2$ ab initio (22)	5.25		1.49		1.53
Formamide dimer ab initio (23)	10	-7	5.0		
H_2CO-H_2O ab initio (21)	4.64	-6.71	5.34	0.18	
H_2CO-H_2O INDO (21)	-4.8	0.0	11.1		

Energies in Kcal/mole, positive terms are stabilising.

The method employed in obtaining these energy contributions has been described in detail by Morokuma (21). For separated molecules A and B the electronic wavefunction is represented by the Hartree product of antisymmetrised molecular functions $\Omega\Psi_A^o\Omega\Psi_B^o$

and the total energy is E_o. At shorter distances, the use of the separated wavefunctions yields an energy E_1 when the coulomb interaction is included. The difference E_1-E_o is the electrostatic interaction energy E_{es}. The effect of mutual polarisation is incorporated by calculating the energy E_2 of the Hartree product $\Omega\Psi_A\Omega\Psi_B$ when each molecular wavefunction is individually optomised in the presence of the other molecule. The difference E_2-E_1 is the polarisation energy E_p. An estimate of the exchange interaction can be made if an antisymmetrised function $\Omega(\Psi_A^o\Psi_B^o)$ is constructed from the separated wavefunctions and the energy E_3 is evaluated. The exchange contribution E_{ex} is then given by E_3-E_1. Since the SCF wavefunction for the whole system is $\Omega\Psi_{AB}$ and the total energy is E_4, the delocalisation or charge transfer energy E_{ct} is given by $E_{ct} = E_4+E_1-E_2-E_3$. The difference in the results of Kollman and Allen (22) from those of (21) stems from their different definitions for the above energy contributions.

Although the approximations involved in the semiempirical theories prevent a proper account by these of the electrostatic and exchange interactions, the evidence of Table 5.1.2 suggests that such methods may be capable of accounting qualitatively for the charge transfer interaction. Since many of the important electronic changes are associated with this stabilising interaction, it is possible that approximate description of these may be obtained within a semiempirical approach.

(iv) Localised Orbital Studies

From the above considerations, the semiempirical INDO molecular method (24) has been employed in the study of three dimer systems. Details of the approximations involved in the method have been reviewed by Pople and Beveridge (25).

To investigate the change in localised orbital structure under different energy breakdown approximations, a localisation program was constructed for use with the above SCF program. In this, the energy localisation technique of Ruedenberg, discussed in Chapter 2.1, was employed. Examples of the localised molecular orbitals produced by this procedure are given in Table 5.1.3 and 5.1.4 for water and methane.

TABLE 5.1.3

Atomic Basis	ℓ_1	ℓ_2	b_1	b_2
O 2s	0.56876	-0.56876	0.33050	-0.33050
O 2px	0.26389	-0.26388	-0.68818	-0.14695
O 2py	-0.70711	-0.70711	-0.00001	0.00000
O 2pz	0.32654	-0.32654	0.00259	0.67231
H 1s	-0.01126	0.01126	-0.00493	-0.64587
H 1s	-0.01126	0.01125	0.64587	0.00493

Localised orbitals for H_2O, ℓ = lone pair, b = bond orbital

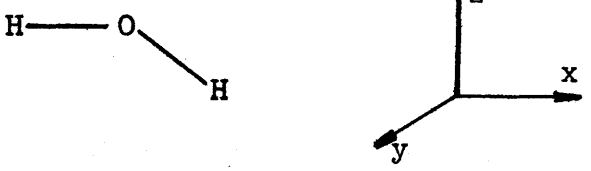

TABLE 5.1.4

Atomic Basis	b_1	b_2	b_3	b_4
C 2s	-0.36715	-0.36715	-0.36715	-0.36715
C 2px	0.34665	0.34665	-0.34665	0.34665
C 2py	0.49031	0.00003	0.00003	-0.49031
C 2pz	0.00003	-0.49031	-0.49031	-0.00003
H 1s	0.01045	-0.01044	-0.71014	0.01045
H 1s	0.01045	0.71014	0.01044	0.01045
H 1s	0.01044	-0.01045	0.01045	-0.71014
H 1s	-0.71014	-0.01045	0.01045	0.01044

Localised orbitals for methane.

The three systems to which the preceding energy breakdown analysis has been applied are $(H_2O)_2$, $(HCN)_2$, and $CH_4.H_2O$. As discussed above, the method neglects the exchange repulsion energy and hence only the terms E_{es}, E_p, and E_{ct} have been evaluated. Experimental monomer geometries have been used throughout and geometries for the dimers are based on the results of recent ab initio studies. The geometry of the methane-water system, for which no energy minimum exists, has been chosen for comparison with the $(H_2O)_2$ system. The dimer geometries are shown in Figure 5.1.1. The monomer separation distances (R), defined by $O_4....H_3$ for $(H_2O)_2$ and $N_3....H_4$ for $(HCN)_2$, were obtained from the energy minima as predicted by INDO. For the $CH_4.H_2O$ system the $O_6....H_4$ distance was taken as 1.50 A^o.

FIGURE 5.1.1

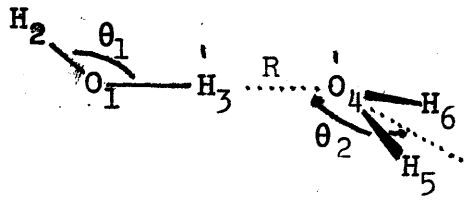

R = 1.55 A°
O-H= 0.96 A°
θ_1 = 102°
θ_2 = 122° (14)

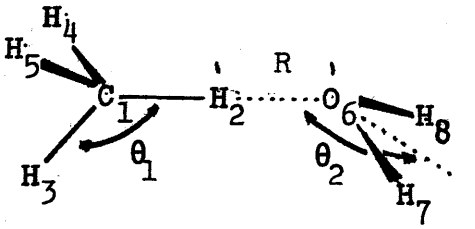

R = 1.50 A°
O-H= 0.96 A°
C-H= 1.09 A°
θ_1 = 109°28'
θ_2 = 122°

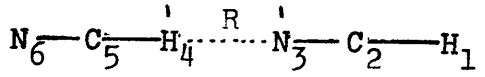

R = 1.75 A°
C-N= 1.153 A°
C-H= 1.07 A°

Geometries used in INDO calculations.

For each energy change E_{es}, E_p or E_{ct}, a further breakdown is possible in terms of a change in electron-electron interactions and electron-core interactions. The former may be represented by a change in charge repulsion ΔJ, and a change in electron-exchange energy ΔK. The change ΔK necessarily represents only the change in intramolecular exchange energy. The change ΔH in electron core energy may be recorded as a change for each localised orbital in the molecule. Furthermore, if the localised orbitals can be assigned to either of the molecules in the dimer then for each orbital the energy change can be represented by an intramolecular electron-core change ΔH_1 and an intermolecular change ΔH_2. This separation is possible in the polarisation

approximation since mixing is prevented. It is found that, with a single exception, the separation can also be applied to the full SCF wavefunction of the dimer. This exception concerns the lone pair orbital of the electron donor molecule which becomes substantially 'contaminated' with the 1s function of the donated hydrogen.

(v) Energy Breakdown Results

The assignment of lone pair and bond pair orbitals in the three dimer systems is shown in Figure 5.1.2.

FIGURE 5.1.2

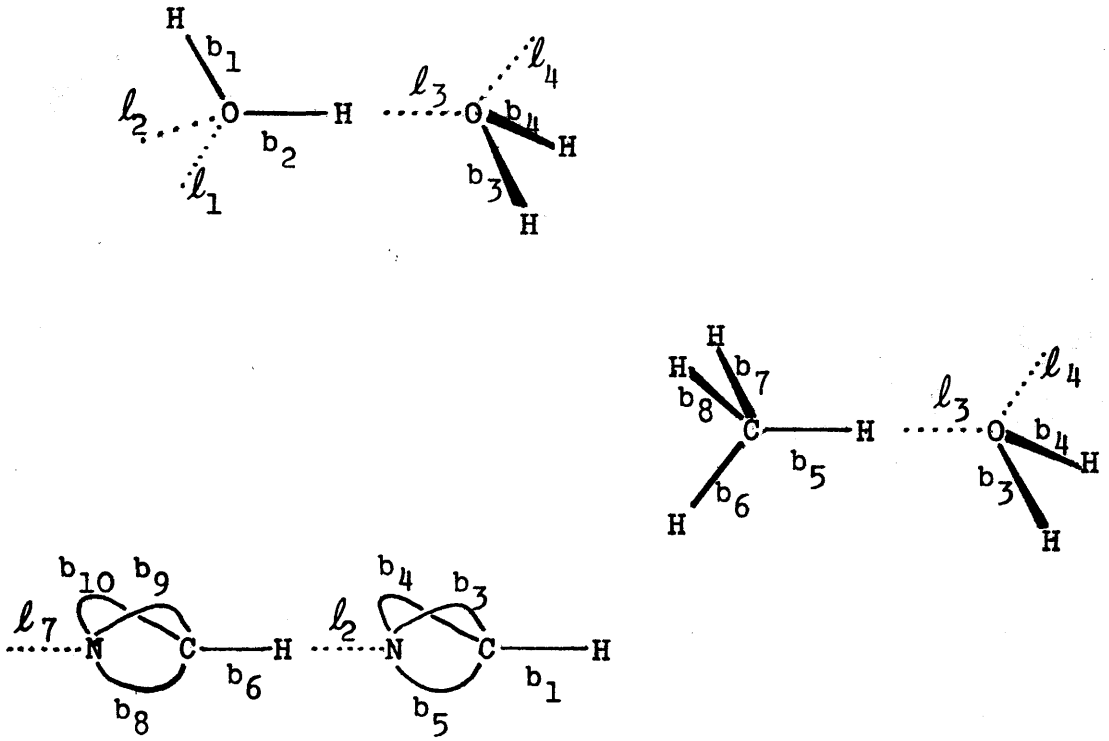

Assignment of localised orbitals.

An example of the localised orbitals for the $(H_2O)_2$ system within the full SCF calculation is given in Table 5.1.5.

TABLE 5.1.5

Localised Orbitals for $(H_2O)_2$

Atomic Basis	ℓ_2	b_1	ℓ_3	ℓ_4	b_2	b_4	ℓ_1	b_3
O_1 2s	0.56562	0.32161	-0.03300	0.00002	0.35106	0.00007	0.56562	0.00007
O_1 2px	-0.27573	-0.14747	-0.06580	0.00007	0.69953	0.00065	-0.27572	0.00065
O_1 2py	-0.70710	-0.00001	0.00000	0.00000	-0.00001	-0.00002	0.70712	0.00002
O_1 2pz	-0.32221	0.67075	-0.00738	-0.00003	-0.00351	-0.00007	-0.32220	-0.00007
H_2 1s	-0.01000	0.65183	0.01176	0.00000	-0.00568	0.00021	-0.00999	0.00021
H_3 1s	-0.01092	-0.00594	0.12191	-0.00123	0.62141	0.00219	-0.01091	0.00219
O_4 2s	0.00092	-0.00041	0.55977	0.56813	-0.01952	-0.33480	0.00092	-0.33480
O_4 2px	0.00124	0.00106	-0.81560	0.36621	0.00788	-0.23206	0.00124	-0.23206
O_4 2py	0.00023	0.00000	0.00000	0.00000	0.00000	0.54141	-0.00023	-0.54141
O_4 2pz	-0.00142	-0.00020	-0.02642	0.73678	0.01266	0.36330	-0.00142	0.36330
H_5 1s	-0.00219	-0.00028	-0.01182	-0.01184	0.01754	0.00376	-0.00176	-0.63947
H_6 1s	-0.00176	-0.00028	-0.01182	-0.01184	0.01754	-0.63947	-0.00218	0.00376

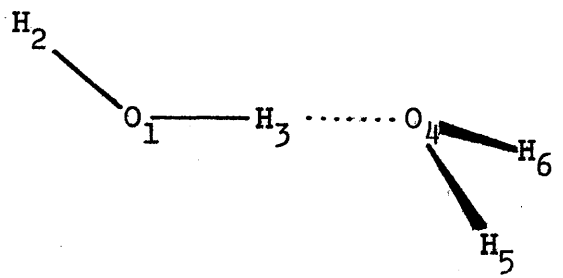

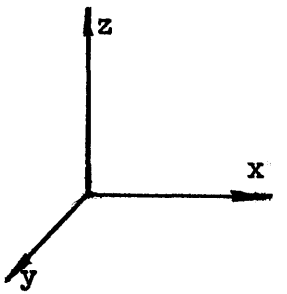

The results for the breakdown of the interaction energy for the three dimers are presented in Tables 5.1.6-5.1.8, along with the change in atomic charges from one approximation to the next.

The following definition of terms applies:

ΔJ = change in total electronic repulsion energy

ΔH = change in total electron-core energy

ΔK = change in total intramolecular exchange energy

H_1 = energy of interaction between specified L.O. and core of its associated molecule

H_2 = energy of interaction between specified L.O. and core of other molecule

ΔH_1 = change in H_1 for specified L.O.

ΔH_2 = change in H_2 for specified L.O.

TABLE 5.1.6.

Breakdown of interaction energy for $(H_2O)_2$

APPROXIMATION

Electrostatic	Polarisation	Charge Transfer
	ΔJ= 0.04220	ΔJ= 0.04174
	ΔH= -0.03780	ΔH= -0.06907
	ΔK= -0.00460	ΔK= -0.00920
E_{es}= 0.02306	E_p= -0.00020	E_{ct}= -0.03653

Localised Orbital	H_1	H_2	ΔH_1	ΔH_2	ΔH_1	ΔH_2
ℓ_1	-5.81387	-1.62117	0.00040	0.00	0.00083	0.00
ℓ_2	-5.81388	-1.62117	0.00040	0.00	0.00083	0.00
b_1	-5.41295	-1.53497	0.00360	0.00030	0.01453	0.00131
b_2	-5.41306	-2.00122	-0.01640	0.00800	-0.03750	0.02234
ℓ_3	-5.81385	-1.78680	0.00050	0.00	-0.02050	
ℓ_4	-5.81386	-1.78680	0.00050	0.00	0.00010	0.00
b_3	-5.41289	-1.65721	-0.00690	-0.00120	-0.00713	-0.00111
b_4	-5.41289	-1.65721	-0.00690	-0.00120	-0.00713	-0.00111

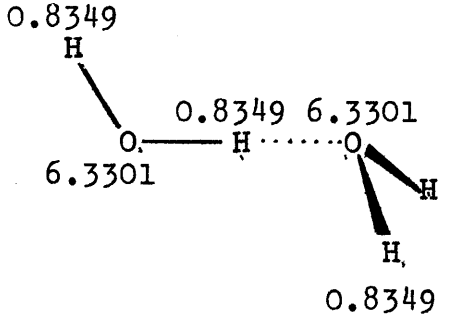

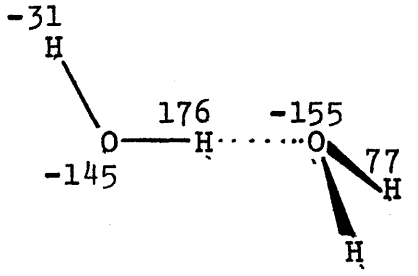

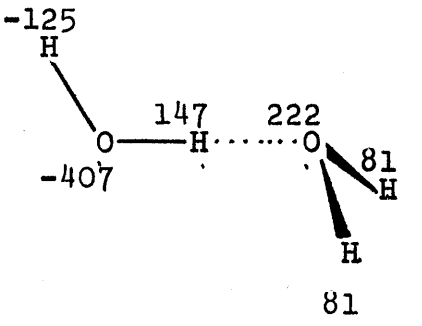

Changes in atomic populations are x10^4; energy in au.; localised orbital energies and energy changes are for each electron.

TABLE 5.1.7

Breakdown of interaction energy for $(HCN)_2$

APPROXIMATION

	Electrostatic	Polarisation	Charge Transfer
		ΔJ= 0.01359	ΔJ= 0.02894
		ΔH= -0.01902	ΔH= -0.04122
		ΔK= 0.00532	ΔK= -0.00566
	E_{es}= 0.01249	E_p= -0.00011	E_{ct}= -0.01794

Localised Orbital	H_1	H_2	ΔH_1	ΔH_2	ΔH_1	ΔH_2
b_1	-4.65103	-1.11565	-0.00145	-0.00024	-0.00125	-0.00038
ℓ_2	-5.37284	-1.70219	0.00045	-0.00001	-0.00758	
b_3	-5.45207	-1.49082	-0.00116	-0.00098	-0.00097	-0.00090
b_4	-5.45207	-1.49082	-0.00116	-0.00098	-0.00097	-0.00090
b_5	-5.45207	-1.49082	-0.00116	-0.00098	-0.00096	-0.00090
b_6	-4.65103	-1.94629	-0.00652	0.00404	-0.01799	0.01125
ℓ_7	-5.37284	-1.18122	0.00020	0.00018	0.00013	0.00034
b_8	-5.45207	-1.35836	-0.00054	0.00045	0.00016	0.00
b_9	-5.45207	-1.35836	-0.00054	0.00045	0.00016	0.00
b_{10}	-5.45207	-1.35836	-0.00054	0.00045	0.00016	0.00

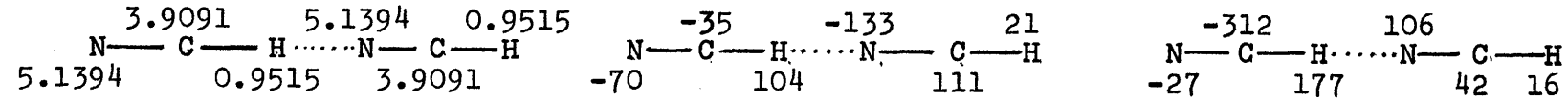

Changes in atomic populations under polarisation and charge transfer are $x10^4$; energies in au.; localised orbital energies and energy changes are for each electron.

TABLE 5.1.8

Breakdown of interaction energy for $CH_4.H_2O$

	APPROXIMATION					
	Electrostatic		Polarisation		Charge Transfer	
			ΔJ= -0.01137		ΔJ= -0.02622	
			ΔH= 0.01416		ΔH= 0.00729	
			ΔK= -0.00299		ΔK= -0.00616	
	E_{es}= 0.03279		E_p= -0.00020		E_{ct}= -0.02509	
Localised Orbital	H_1	H_2	ΔH_1	ΔH_2	ΔH_1	ΔH_2
b_5	-3.99008	-2.09367	-0.00823	0.01026	-0.01644	0.02657
b_6	-3.99011	-1.44888	0.00260	0.00072	0.00160	0.00025
b_7	-3.98928	-1.43962	0.00127	0.00036	0.00158	0.00026
b_8	-3.98928	-1.43962	0.00127	0.00036	0.00158	0.00026
ℓ_3	-5.81385	-1.67252	0.00005	0.00	-0.00272	
ℓ_4	-5.81386	-1.67252	0.00006	0.00	-0.00013	0.00004
b_3	-5.41289	-1.56004	-0.00082	-0.00012	-0.00373	-0.00087
b_4	-5.41289	-1.56004	-0.00082	-0.00012	-0.00373	-0.00087

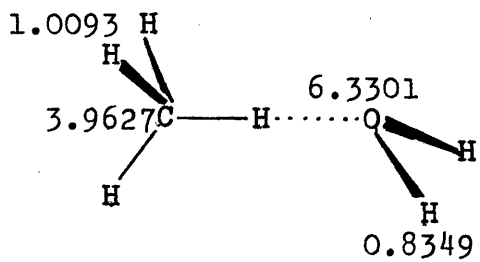

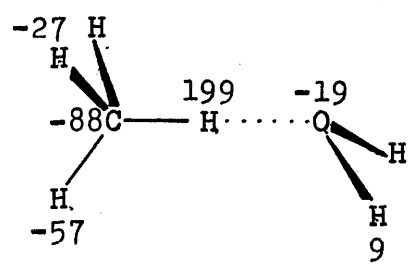

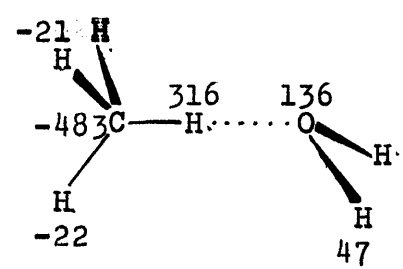

Changes in atomic populations under polarisation and charge transfer are $x10^4$; energy in au.; localised orbital energies and energy changes are for each electron.

An examination of the results shows that, as with ab initio calculations, the polarisation and charge transfer energies are stabilising, and that the former has a comparable magnitude, being of the order 0.1 Kcal/mole in each system. The values of E_{ct} however, are overestimated and vary between 10-23 Kcal/mole.

Concerning the energy changes and charge shifts, several similarities can be seen in each of the dimer systems.

(a) There is a redistribution of charge in the polarisation calculation equivalent to a movement of charge toward the lone pair donating centre from the peripheral parts of the lone pair donor molecule. This is accompanied by a movement of charge away from the donated hydrogen toward the periphery of the proton donor molecule. The lone pairs experience little change in their orbital structure and only small changes in ΔH_1 and ΔH_2 result.

In the bond pairs the relative contributions of basis functions change, consistent with the above charge movement, with ΔH_1 and ΔH_2 being negative for peripheral bonds in the lone pair donor, while for peripheral bonds in the proton donor ΔH_1 and ΔH_2 are positive. The bond involving the donated hydrogen has ΔH_1 negative and ΔH_2 positive, consistent with a movement of charge in this orbital away from the lone pair donor towards the more 'electronegative' parts of the proton donor molecule- oxygen in the case of $(H_2O)_2$ and carbon in $CH_4.H_2O$.

This redistribution of charge yields very little energy as the E_p values show, since the change in electronic repulsion energy almost matches that in electron-core energy.

(b) As previously stated, the localised orbitals of the systems retain their local nature in the charge transfer calculation

with the exception of the donated lone pair which becomes 'contaminated' with 1s function from the donated hydrogen and to a smaller extent, basis functions of the atom to which this atom is bound - carbon in the case of $CH_4.H_2O$. It is clear that no charge transfer from the lone pair donor molecule to the acceptor will occur unless the localised orbitals of the donor become 'contaminated' with basis functions of the acceptor molecule, and in the systems studied all of this charge is accounted for by the mixing in the lone pair orbital, with the inclusion of H_{1s} accounting for 75% in $(H_2O)_2$, 73% in $(HCN)_2$, and 66% in $CH_4.H_2O$.

(c) The redistribution of charge in the C.T. calculation has the same form in each of the systems and will be described for $(H_2O)_2$.

The transfer of charge occurs directly from the donated lone pair ℓ_3 principally to the donated hydrogen (H_3) with a loss of charge from O_4. There is a loss of charge from H_3 toward O_1 by a change in the relative contributions of oxygen and hydrogen in the bond pair b_2. This is accompanied by a movement of charge to H_2 by an opposite change in the bond pair b_1. The hydrogens H_5 and H_6 lose charge by a change in the oxygen and hydrogen contributions in b_3 and b_4 thereby compensating somewhat for the loss of charge at O_4 due to the changes in ℓ_3.

The above changes can be understood by analysing the energy changes which accompany them. The transfer of charge might be expected to bring about the following energy changes in the system:

(a) a decrease in the intramolecular electron repulsion in the donor due to delocalisation over the donated hydrogen.

(b) an increase in the intermolecular electron repulsion due to the fact that the donated lone pair contains some Hls making

the repulsion between ℓ_3 and b_2 severe.

Because of further changes in charge distribution within the acceptor, some of this repulsive energy would be expected to appear as intra-acceptor electron repulsion and also intra-acceptor electron-core changes.

(c) a decrease in the electron-core interaction in the donor due to a loss of oxygen functions from the lone pair.

The expected changes in electron repulsion energy are confirmed for each of the systems in Table 5.1.9 where the change in electronic repulsion has been separated into the above three components.

TABLE 5.1.9

	$(H_2O)_2$	$(HCN)_2$	$CH_4.H_2O$
Intra-donor	-0.09798	-0.04337	-0.08232
Intra-acceptor	0.04793	0.02984	0.03061
Intermolecular	0.08859	0.04376	0.02549

Change in electronic repulsion in charge transfer; energies in a.u.

As can be seen from Table 5.1.9, the increase in intermolecular and intra-acceptor repulsion outweighs the decrease in intradonor repulsion in $(H_2O)_2$ and $(HCN)_2$. However, since the movement of charge which gives rise to these changes also produces intra-acceptor electron-core changes described by ΔH_1 and ΔH_2, the net effect of such movement can only be seen by including these latter values. When this is done the energy change for

each system is repulsive, which shows that the stabilising energy in E_{ct} does not arise from overall electron repulsion changes coupled with electron-core changes in the acceptor molecule.

It was previously stated that, due to the loss of oxygen function arising from the incorporation of some H_{1s} in ℓ_3, a repulsive change in the overall electron-core energy might be expected in the lone pair donor molecule. An examination of the results shows that this is not the case and that much of the E_{ct} energy derives from stabilising electron-core changes. In addition, the lone pair orbital itself undergoes a stabilising change rather than a destabilising one. This can be traced to the additional stabilising effect arising from a resonance or overlap interaction between the hydrogen and lone pair donor orbitals with the atomic cores. This interaction only becomes possible with the mixing of hydrogen function into the lone pair orbital. It may be represented by β where

$$\beta = 2C_u \sum_{\nu} C_\nu H_{u\nu}$$

and

$$H_{u\nu} = \int \Phi_u H_{core} \Phi_\nu \, d\tau$$

C_u is the coefficient of hydrogen 1s in the lone pair orbital and the C_ν are the donor atom orbital coefficients. In the INDO method $H_{u\nu}$ is evaluated semiempirically. In the three dimer systems β has the following values

	$(H_2O)_2$	$(HCN)_2$	$CH_4.H_2O$
β(au)	-0.0455	-0.0234	-0.0357

The presence of the above energy contribution shows the transfer of charge to be an implicit feature of the interaction since it

results from the inclusion of H_{1s} orbital in the lone pair orbital. For $(H_2O)_2$ as an example, the ensuing charge rearrangement can be accounted for in terms of the following:

(a) the severe interorbital repulsion between the lone pair ℓ_3 and the bond orbital b_2, due largely to the repulsive terms at the donated hydrogen, favours a movement of charge in b_2 toward the oxygen O_1.

(b) the increased electron repulsion at O_1 due to the above favours movement of charge in the other bond orbital b_1 toward the peripheral hydrogen.

(c) the decreased electron repulsion at the electron donor atom O_4 favours a movement of charge in the peripheral bond orbitals b_3 and b_4 toward this oxygen.

The changes in electron distribution for $CH_4.H_2O$ in the C.T. calculation show the same features as the other systems. Differences exist however in the individual components of the stabilising E_{ct} energy which reflect the non-polar nature of the methane molecule. These differences concern the decrease in overall electron repulsion and a net destabilising change in electron core interactions. The initial electron repulsion between the donated hydrogen and donor oxygen is high due to the large electron density at the hydrogens in CH_4. The inclusion of H_2 1s function in the lone pair ℓ_3 on charge transfer is therefore expensive due to interorbital repulsion between b_5 and ℓ_3. This repulsion is relieved in going from the polarisation to C.T. calculation by a large movement of electrons in b_5 toward the carbon, resulting in a decrease in total electron repulsion energy. This change takes place at the expense of electron-core interactions

since the loss of such interaction between the H_2 electrons and the O_6 core is not compensated for by the gain in that with the less 'electronegative' carbon core.

The above results suggest that the donated hydrogen plays a central role in both the transfer of charge from the lone pair donor to acceptor and the associated stabilisation which results. This has been considered further for the case of $(H_2O)_2$ by observing the variation in E_{ct} as the acceptor molecule is rotated in the dimer symmetry plane about its oxygen. This variation is shown in Figure 5.1.3 along with that of E_{es} and E_T, the total hydrogen bonding energy. The relationship between the total charge transferred and the coefficient of the acceptor hydrogen functions (H_2 and H_3) in ℓ_3 has also been calculated for the above angular variation and is shown in Figure 5.1.4.

In these it can be seen that maximum transfer of charge and maximum E_{ct} results when either H_3 or H_2 lie on the line joining O_1 and O_4 (θ = 0 or 260°). Furthermore, the variation of these with θ correlates exactly with the 'contamination' of ℓ_3 by either H_3 or H_2, confirming the intimate relationship between these factors as suggested by the energy breakdown analysis.

To discover the extent to which the above relationships are a property of the INDO method, ab initio calculations were performed on the $(H_2O)_2$ system using a version of the ATMOL program. The same geometry type was taken as before and for bond lengths and molecular separation, the results of Pople et al (14) were used (H.....O = 1.737A°). A minimal basis set of Slater atomic orbitals was employed with exponents taken from (14). These were represented by a four gaussian expansion (STO-4G).

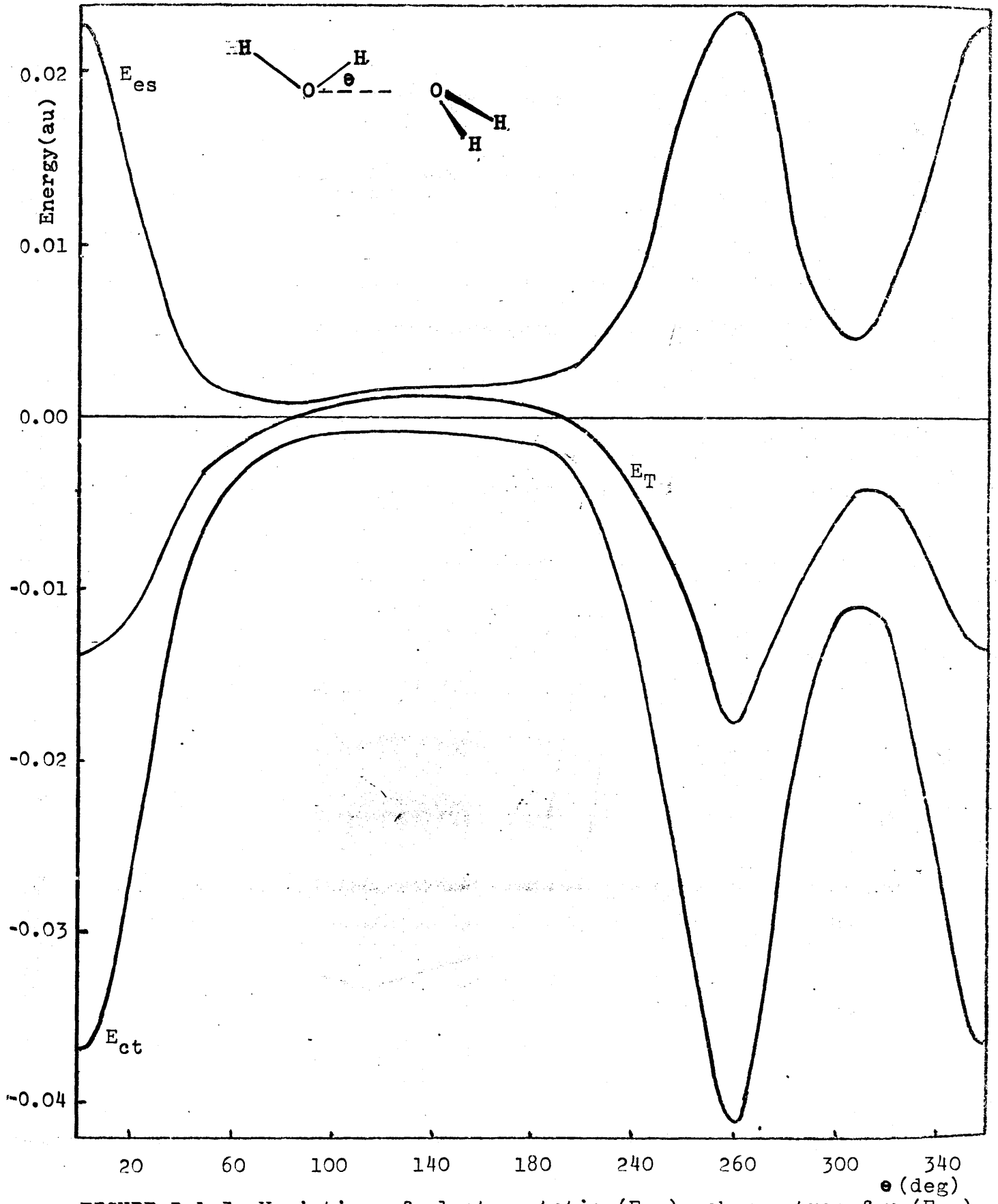

FIGURE 5.1.3 Variation of electro-static (E_{es}), charge transfer (E_{ct}) and total hydrogen bond energy (E_T) with acceptor molecule rotation for INDO approximation.

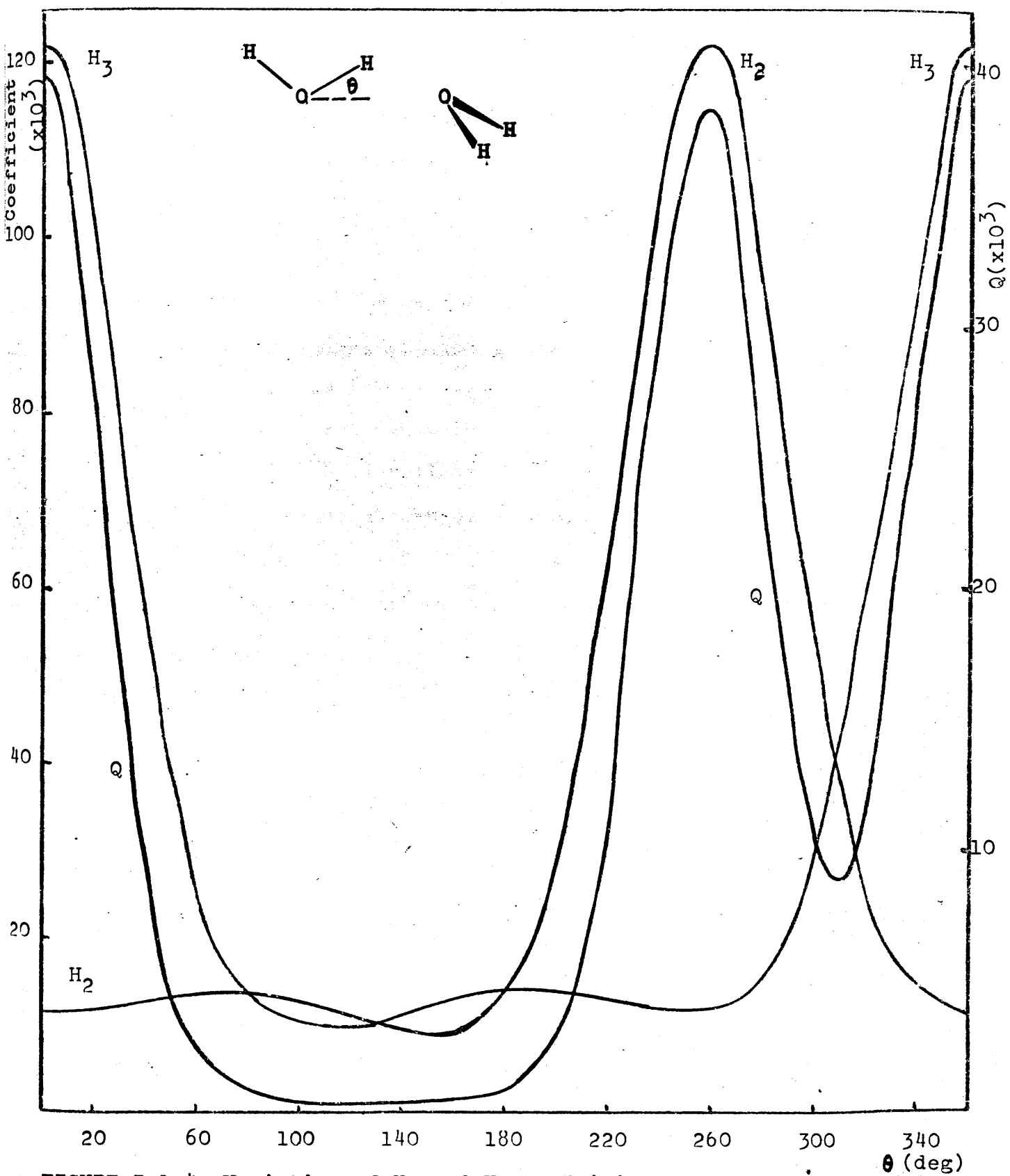

FIGURE 5.1.4 Variation of H_3 and H_2 coefficients in ℓ_3 and total charge transferred (Q) with acceptor rotation for INDO approximation.

The variation of the total dimerisation energy with rotation of the lone acceptor molecule as before is shown in Figure 5.1.5. As expected the minimum energy occurs when either of the hydrogens lie between O_1 and O_4.

To investigate the previous lone pair contamination effect a localisation program was developed for use with the above program. An example of the localised orbitals for the $(H_2O)_2$ system is given in Table 5.1.10. The variation with θ of the coefficients of H_3 and H_2 1s functions in the lone pair ℓ_3 is shown in Figure 5.1.6 as well as the total charge transferred.

From these it can be seen that substantial agreement exists between ab initio and INDO methods in their description of the localised orbital structure, lending support to the conclusions drawn from the INDO study regarding the forces involved in charge redistribution. In terms of the parameter β for the donated lone pair orbital, the ab initio results give a value of -0.0474 au for the $\theta=0^{\circ}$ geometry, which is close to the value of -0.0455 au obtained from INDO.

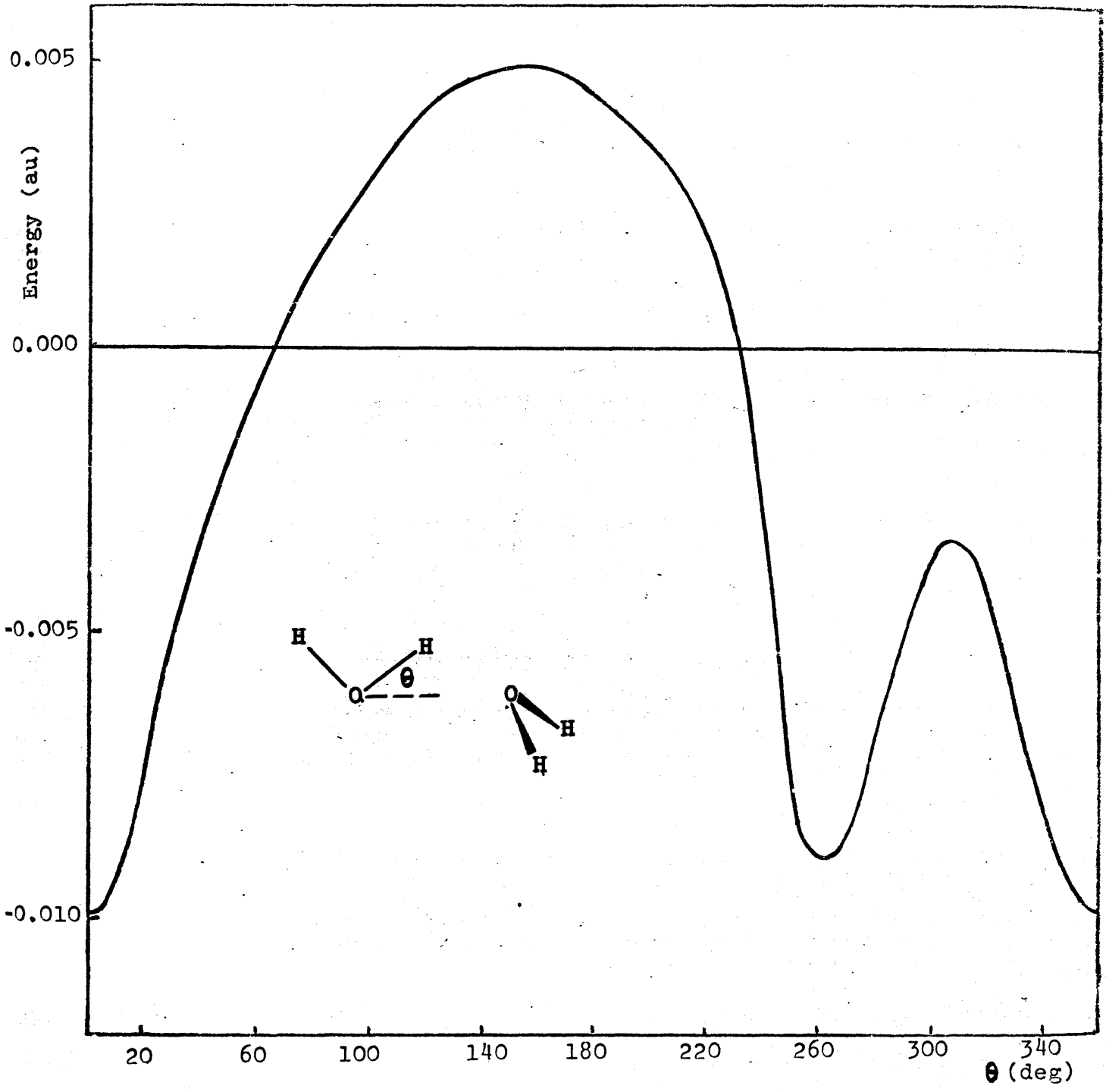

FIGURE 5.1.5 Variation of total hydrogen bond energy with acceptor rotation for ab initio level.

TABLE 5.1.10

Localised ab initio wavefunctions for $(H_2O)_2$

Atomic Basis	ℓ_1	ℓ_2	ℓ_3	ℓ_4	b_2	b_4	b_1	b_3	c_1	c_4
O_1 1s	-0.05935	0.05935	0.00666	0.00079	0.04127	-0.00120	-0.04145	0.00120	1.01949	0.00048
O_1 2s	0.64836	-0.64836	-0.06705	-0.01281	-0.26394	0.01557	0.26993	-0.01557	-0.11720	-0.00326
H_2 1s	-0.12462	0.12462	0.00250	-0.00741	0.06713	-0.00047	0.52955	0.00047	-0.00391	0.00108
H_3 1s	-0.07932	0.07932	0.07878	0.03725	-0.48923	-0.02794	-0.14001	0.02795	-0.00656	0.00160
O_4 1s	-0.00128	0.00128	-0.06464	0.05849	-0.00332	-0.03785	-0.00113	0.03785	-0.00031	-1.01951
O_4 2s	0.01456	-0.01456	0.69114	-0.63109	0.04299	0.23403	0.01399	-0.23403	0.00189	0.11733
H_5 1s	-0.00380	0.00279	-0.10158	0.08145	0.00012	-0.09984	-0.00194	-0.51274	-0.00014	0.00513
H_6 1s	-0.00279	0.00380	-0.10158	0.08144	0.00012	0.51274	-0.00194	0.09984	-0.00014	0.00513
O_1 2px	-0.23488	0.23488	-0.09165	-0.00978	-0.61369	0.01698	-0.14716	-0.01698	0.02009	0.00848
O_1 2py	0.70711	0.70711	0.00000	0.00000	0.00000	-0.00058	0.00000	-0.00058	0.00000	0.00000
O_1 2pz	-0.30496	0.30496	-0.01339	-0.00811	-0.07348	0.00236	0.55176	-0.00236	0.02600	-0.00064
O_4 2px	-0.00696	0.00696	-0.75408	-0.44792	-0.04288	0.20991	-0.02735	-0.20993	-0.00461	-0.01537
O_4 2py	-0.00198	-0.00198	0.00000	0.00001	0.00000	-0.44628	0.00000	-0.44628	0.00000	0.00000
O_4 2pz	-0.00073	0.00073	-0.02952	-0.68102	-0.02291	-0.35609	-0.01240	0.35608	-0.00008	0.02757

c_1 and c_4 refer to the core orbitals of O_1 and O_4.

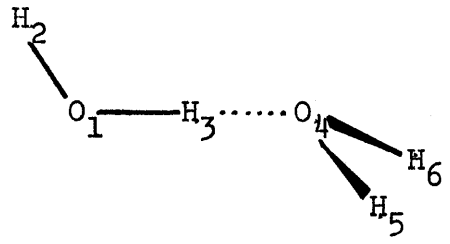

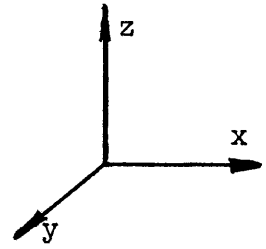

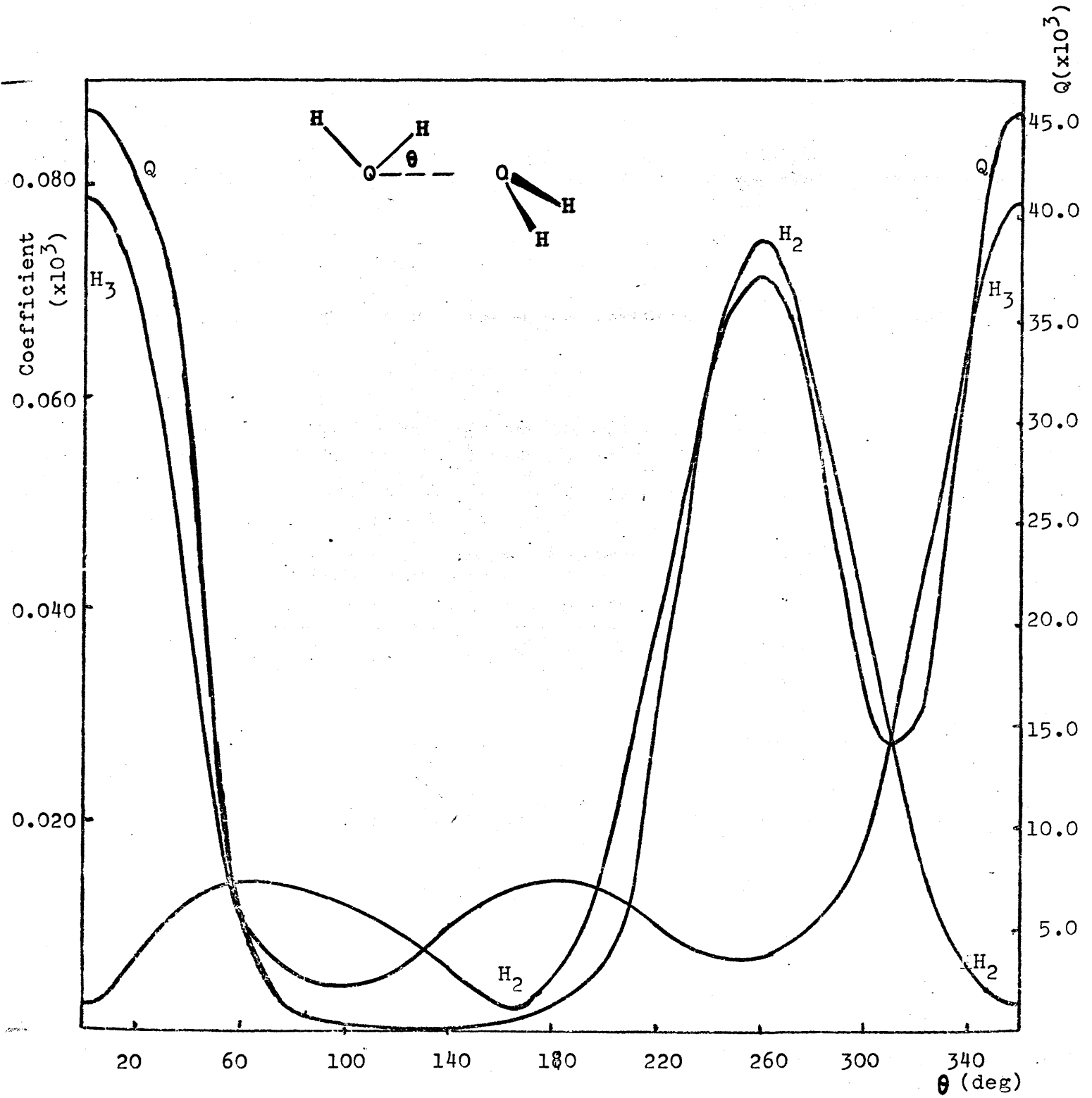

FIGURE 5.1.6 Variation of H_3 and H_2 coefficients in ℓ_3 and total charge transferred with acceptor rotation within ab initio level.

Discussion

The manner in which present semi-continuum studies of trapped electrons consider the short range medium rearrangement energy has been described in Chapter 4.(iii) where it was shown to take the form of surface tension and dipole repulsion energy. The former is chosen to represent the loss of attractive intermolecular interactions when a medium cavity is formed and is approximated by the bulk surface tension of the medium which yields an energy term close to 0.1 ev (26). Since hydrogen bond energies are typically of the order 0.25 ev, and several may be broken on cavity formation and reorientation, the assignment of structure to the cavity in a hydrogen bonded system may substantially increase the above energy term.

Dipole repulsion energies,for which quoted values range from 0.2-1.6 ev (26,27,28), and electron dipole interactions are evaluated on the assumption that the dipoles are free rotate in the field of the excess electron. It is evident however,that the directional nature of the hydrogen bond may significantly restrict the angular space available for such equilibration leading to a marked change in the contribution of first layer molecules to the potential well parameters.

A natural extension to the approximation of first layer dipoles would be to assign point charges to the individual atoms. Such an approach has already been used within early molecular cluster studies (29). The charge transfer results indicate however that for hydrogen bonded systems the assignment of such charges is strongly dependent on first and second layer interactions. A further quantity which contributes to the excess electron energy

is the induced dipole moment of the first layer molecules, which is represented by an average polarisability obtained from gas phase experiments. The localised orbital studies indicate that the transfer of charge from lone pair donor to acceptor is influenced by the relative orientation of the two molecules. Since such a transfer of charge would be expected to be influenced by the field of the excess electron, the polarisability of first layer molecules in a hydrogen bonded system may be strongly dependent on their orientation.

This likely effect of the excess electron in modifying the intermolecular interaction may have important consequences in the description of solvent relaxation processes. It has been recognised for some time that "microscopic" solvent relaxation times as indicated by solvated electron formation times (30-33) are significantly shorter than those obtained from macroscopic studies (34, 35). Since the relaxation time is a function of the potential barrier opposing the coordinate change any rapid modification of the barrier, which may result from electronic changes, would be expected to alter such times.

Although the potential function describing angular changes in a hydrogen bonded system is the result of several contributing factors, ab initio studies have shown that the electrostatic and exchange repulsion terms approximately cancel one another. In addition, the polarisation interaction has been shown to be small whilst the dispersion energy might be expected to have only a slight angular dependence. Of the remaining charge transfer term it has been shown that stabilisation requires a movement of charge to the periphery of the lone pair acceptor molecule.

The possibility exists, however, that in the field of an excess electron, such a charge movement may be unfavourable leading to a weakening of the intermolecular attraction and decrease in relaxation time.

2 Photoionisation Spectra for Ice

A considerable number of calculations have been performed within the semi-continuum and molecular cluster theories in an attempt to account for the spectral characteristics of electrons in various media (cf 4i1, 4.2). In many of these studies, the notion that a bound excited state is involved in the optical transition has had a measure of success in accounting for a range of spectral and other properties. The possibility that direct photoionisation may contribute to the absorption band, however, has been considered in only a few cases (28,36,37).

Based on the success of Kajiwara et. al (36) in accounting for the optical absorption of electrons in alcohols, photoionisation calculations have been performed using simple model potentials, in an attempt to discover the importance of such a process in pure and alkaline ices.

The features of the spectra in these two media has already been discussed (cf 3.1(i)). Both display thresholds around 1.3 ev and maxima near 2.0 ev, at which point the photoexcitation cross sections are $7.2\times10^{-17}cm^2$ and $8.0\times10^{-17}cm^2$ for pure and alkaline ice respectively (38,39). The principal difference in the absorption bands lies in the half width, which for alkaline ice, is 1.03 ev whilst for pure ice is only 0.55 ev.

(i) Model Potentials

Two potential types were considered, the spherical square well (I) and one which behaved exponentially at large distances and had a radial cut off near the origin (II). These are described by

$$\text{I} \qquad V(r) = -V_o \qquad r < R_o$$
$$V(r) = 0 \qquad r > R_o$$

$$\text{II} \qquad V(r) = -V_o \exp(-kR_o) \qquad r < R_o$$
$$V(r) = -V_o \exp(-kr) \qquad r > R_o$$

Ionisation cross sections were evaluated using the analysis of Chapter 2.2. Ground state (1s) and continuum p functions were obtained by numerical solution using the Numerov method (40) and transition moments were calculated by performing integrations over 60 au, by which point the ground state function was effectively zero. Phase shifts were fixed absolutely by monitoring their dependence on wave vector as the energy was decreased from an initially high value.

A useful alternative to the numerical or graphical method of obtaining solutions to the spherical square well, in the case where $\ell = 0$, was devised and is described in 5.2(ii) below.

The photoionisation profiles derived from the above potentials have features which are similar to trapped electron spectra and can be characterised by a threshold energy, an energy at which the intensity is maximum, a maximum cross section and a half width. In the two types of potentials considered the parameters have been chosen such that the resultant cross section curves have a maximum at 2.0 ev in accord with the observed spectra in pure and alkaline ice at low temperature. For potential I, the infinite set of such parameters is defined by a locus in the space of V_o and R_o, whilst for potential II, the locus is represented in three dimensions defined by V_o, R_o and k.

To determine the sensitivity of the photoionisation curves to the well parameters, the locus of the 2.0 ev maximum cross section curves have been determined for potential I over a range of parameters whilst for potential II the locus has been found in terms of V_o and R_o for selected values of k.

The curve for the square well is shown in figure 5.2.1. For each of the points in figure 5.2.1 there corresponds the set of properties previously mentioned - ionisation threshold E_T, cross section maximum X_{max} and half width $W_{\frac{1}{2}}$. Figures 5.2.2 and 5.2.3 show the variation of these properties with well radius.

For potential II, three values of the exponential factor k were considered, these being 0.50, 0.75 and 1.00 au^{-1}. Figure 5.2.4 shows the locus of the 2.0 ev maximum cross section as a function of V_o and R_o for each of these values of k. The corresponding quantities E_T, X_{max} and $W_{\frac{1}{2}}$ are shown as a function of R_o for the different k values in Figures 5.2.5 - 5.2.7.

Examination of Figures 5.2.2 and 5.2.3 shows that the experimental threshold and maximum cross section can be adequately represented in both media for square well radii around 4.5 au. However, at such radii the half width is around 1.0 ev, corresponding more closely with that of alkaline ice.

For the exponential potential, and for k values of 0.75 and 1.0, Figures 5.2.5 and 5.2.6 show that appropriate values of E_T and X_{max} can be obtained at cut off radii around 3.0 au. In this case also, however, the half width is around 1.0 ev.

An important quantity in the description of delocalised states in solids is the effective mass of the electron (41)

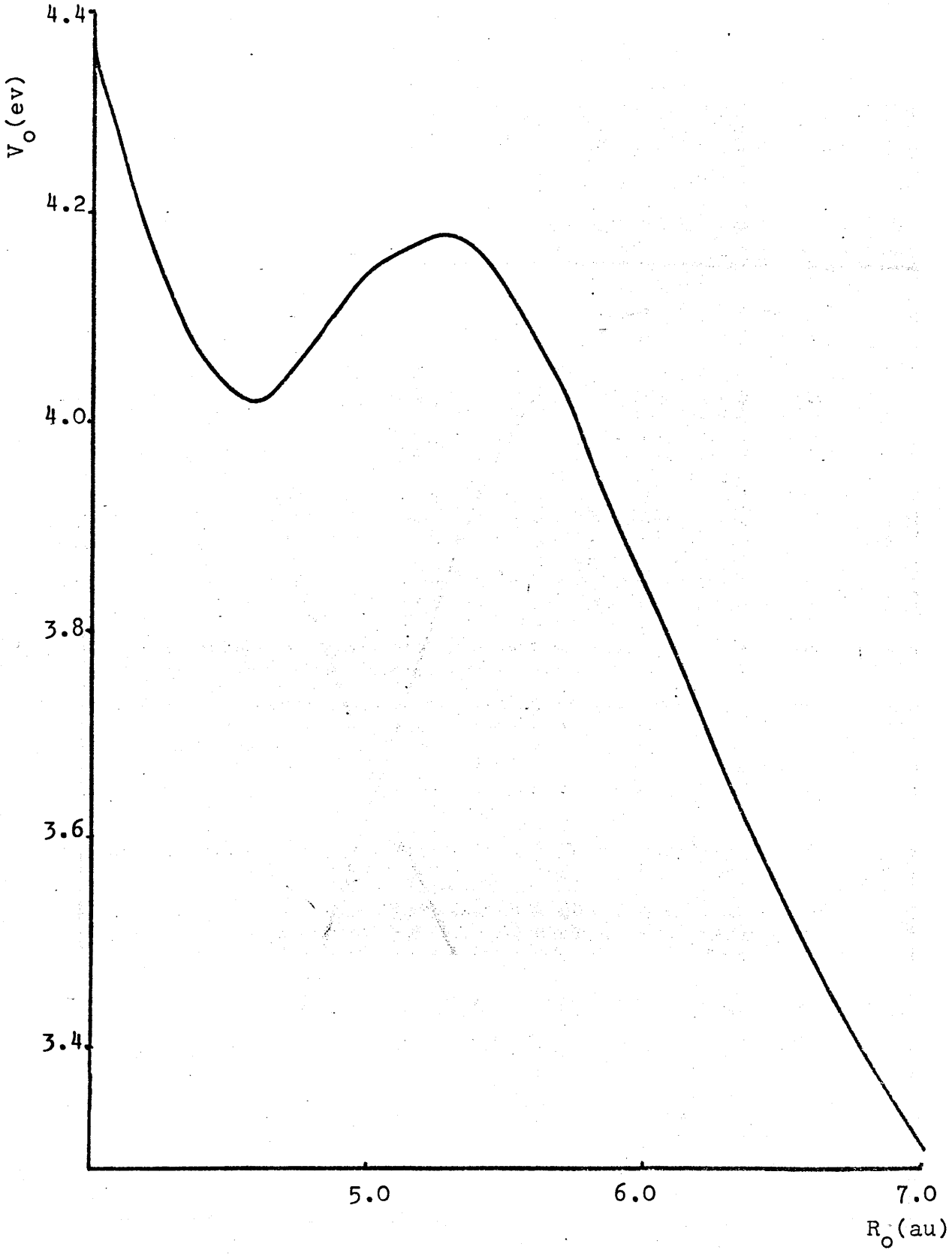

Figure 5.2.1 Locus of 2.0 ev maximum ionisation cross section for square well.

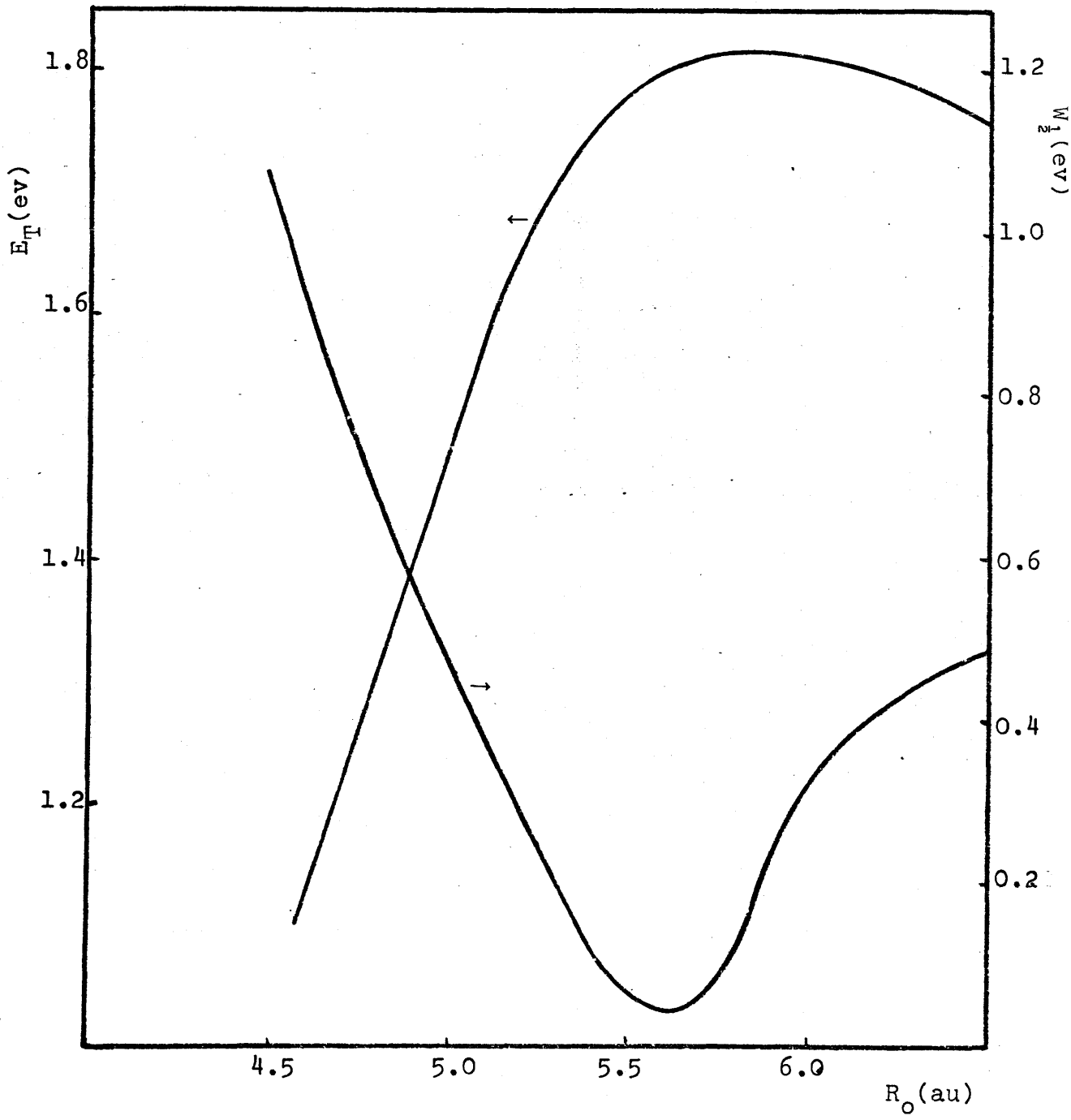

Figure 5.2.2 Variation of energy threshold (E_T) and half width ($W_{\frac{1}{2}}$) with square well radius for ionisation spectra.

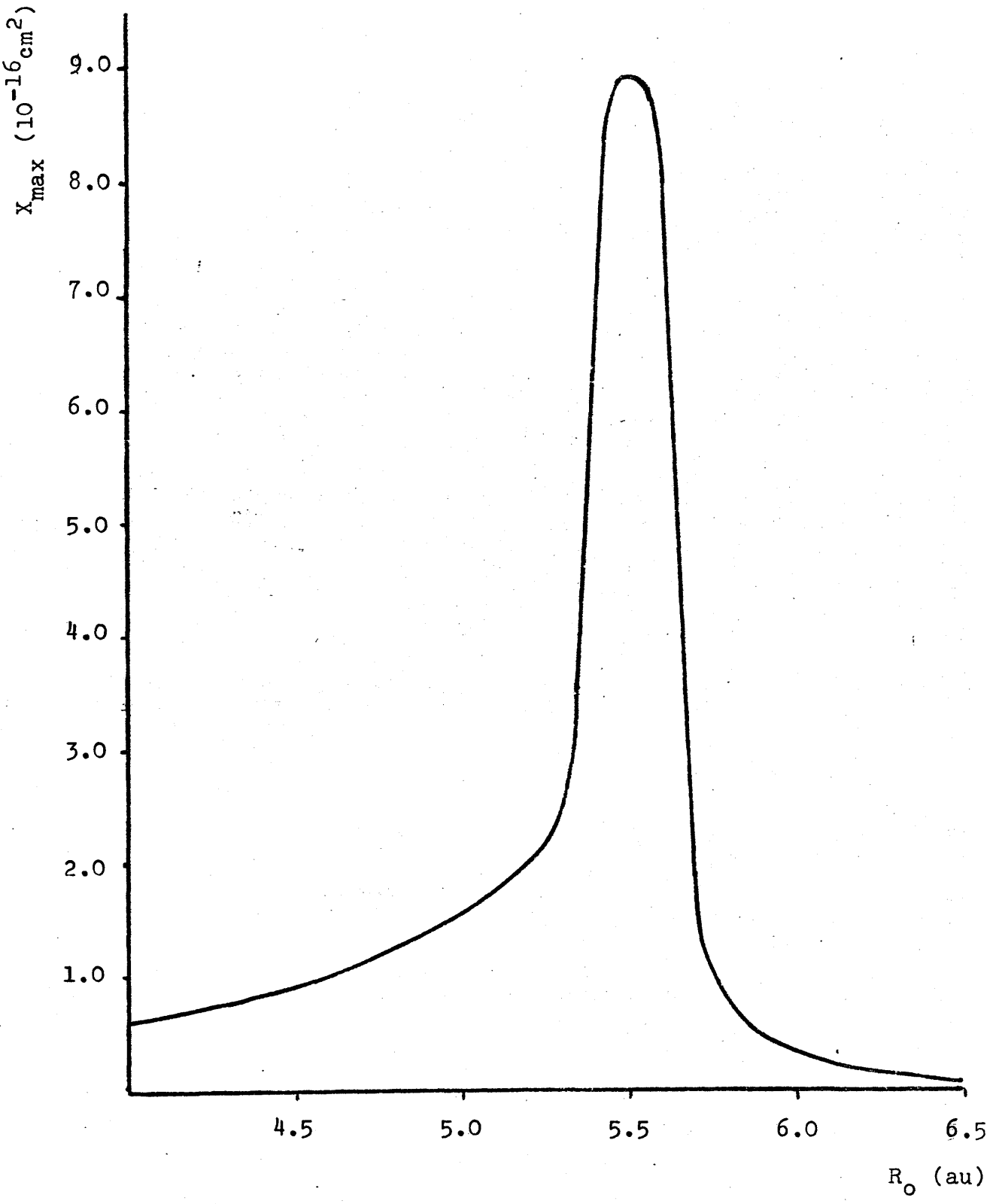

Figure 5.2.3 Variation of maximum ionisation cross section with square well radius.

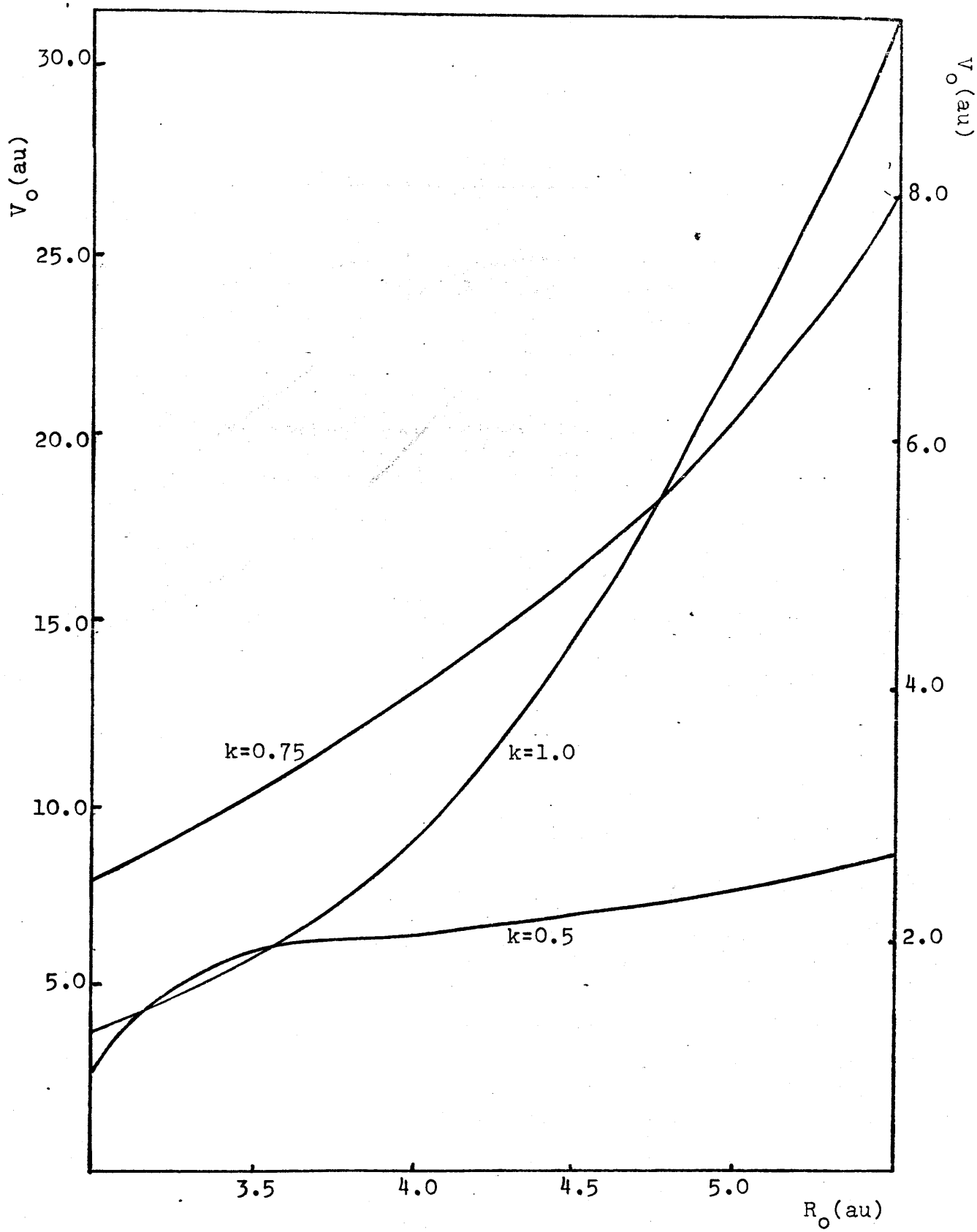

Figure 5.2.4 Locus of 2.0 ev maximum ionisation cross section with V_o and cut off radius R_o for exponential potential at different k values.

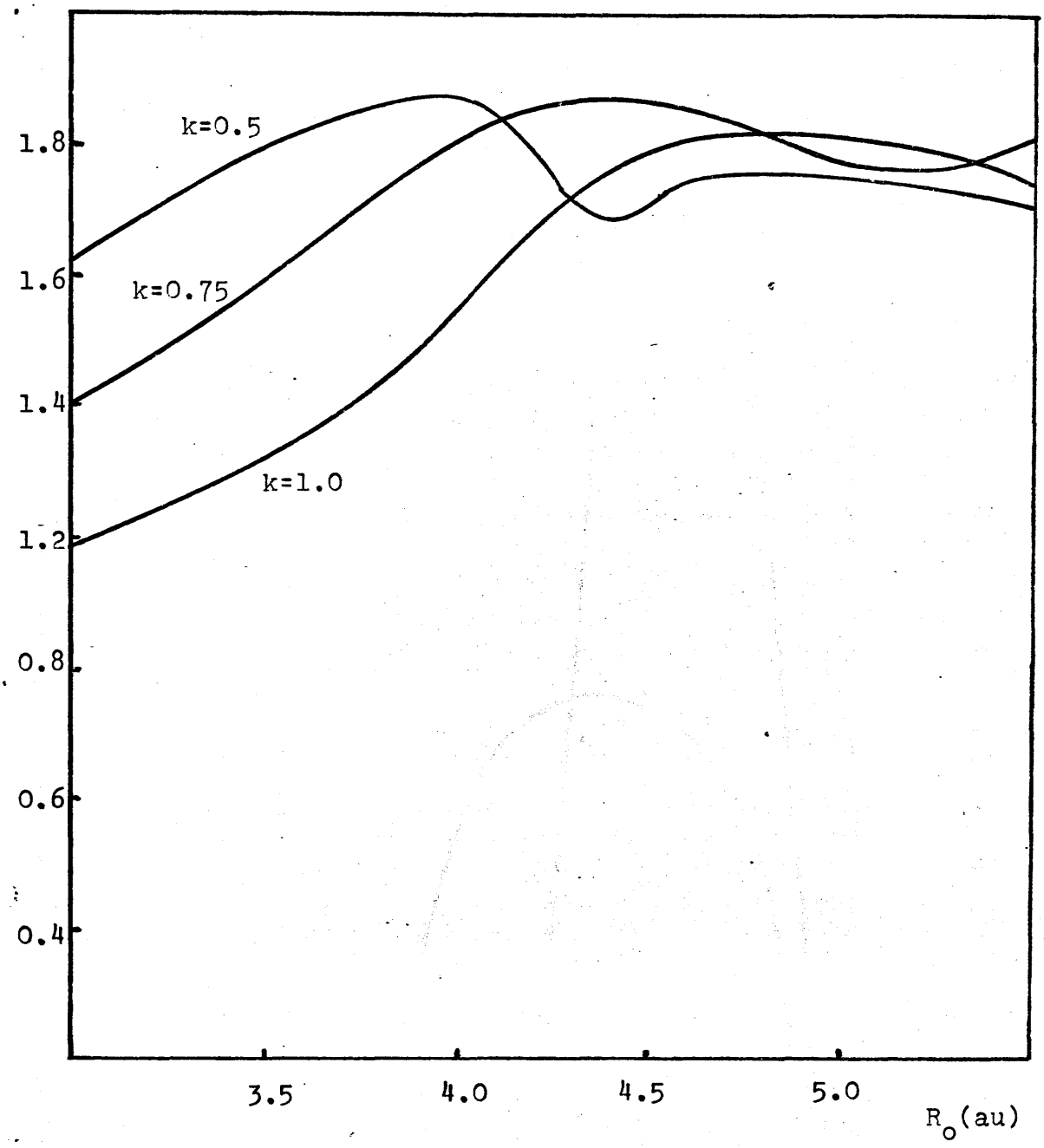

Figure 5.2.5 Variation of energy threshold (E_T) of ionisation spectra with cut off radius for exponential potential at different k values.

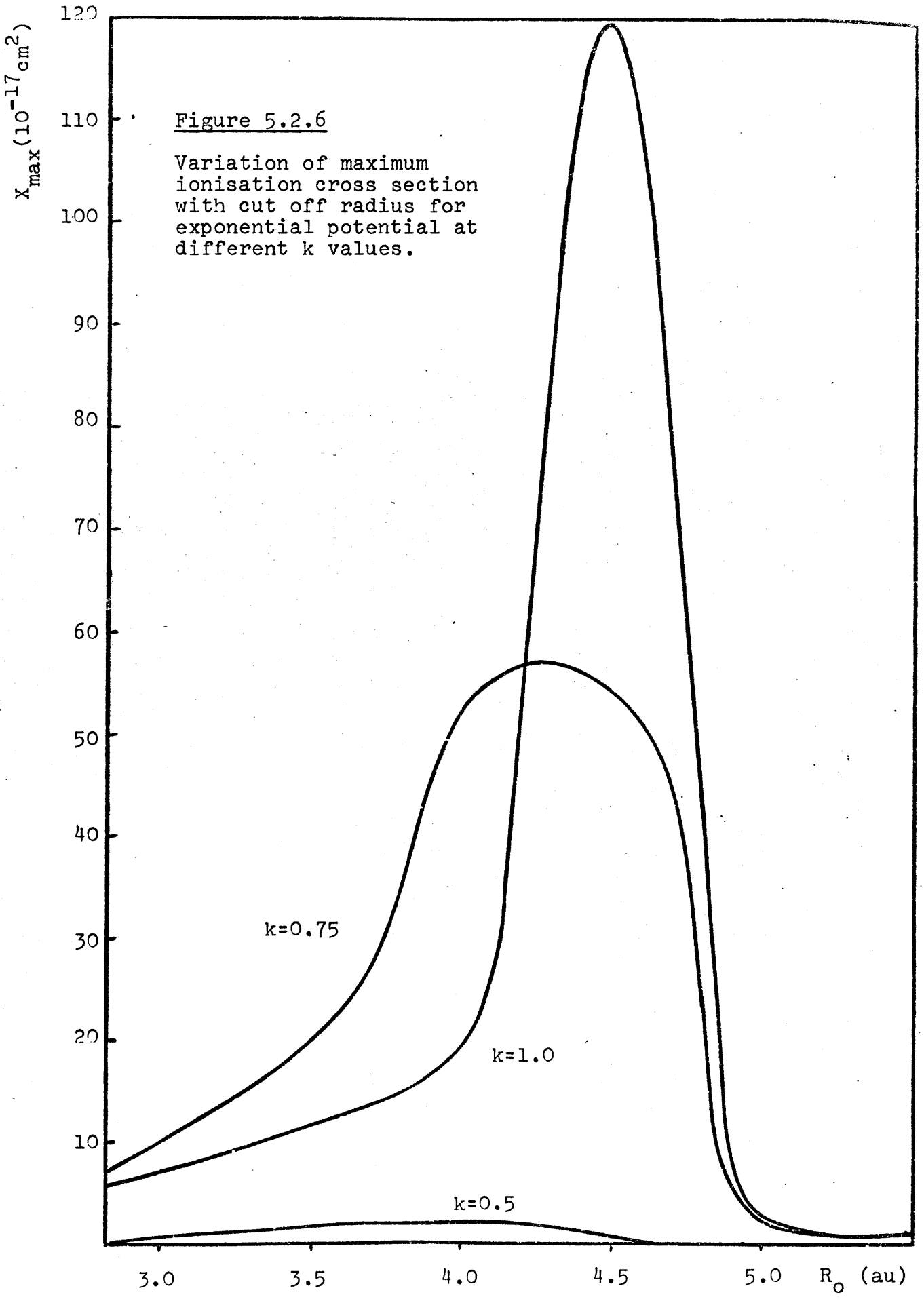

Figure 5.2.6

Variation of maximum ionisation cross section with cut off radius for exponential potential at different k values.

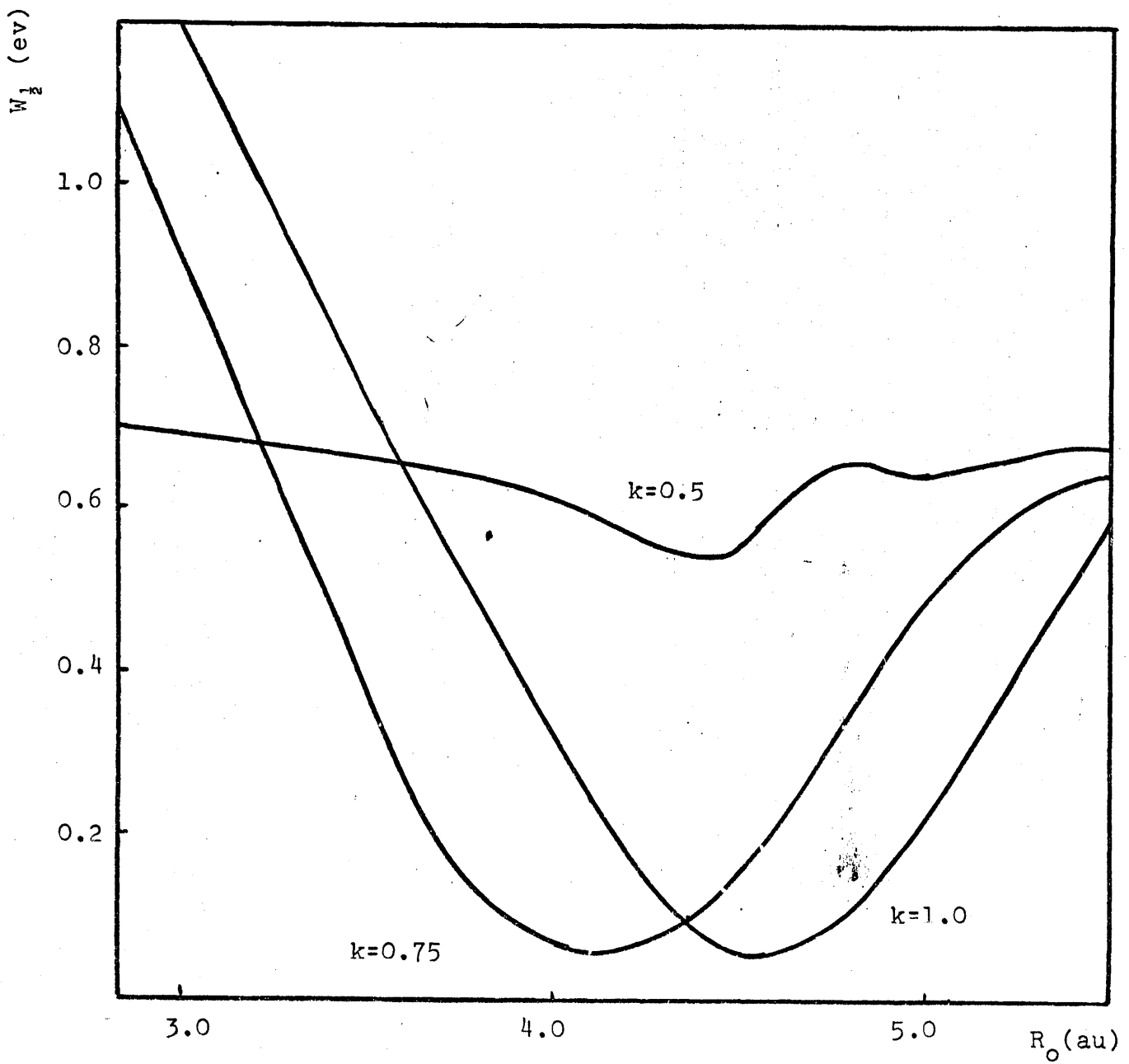

Figure 5.2.7

Variation of half width $W_{\frac{1}{2}}$ of ionisation spectra with cut off radius for exponential potential at different k values.

which is dependent on electron energy. However, since no such detailed knowledge exists about the dynamics of mobile electrons in the media considered, the use of a gas phase photoionisation analysis assumes that the free electron mass may be used. If such an assumption is valid and the principal features of a gas phase photoionisation analysis can be applied to polar solids, then the above observations are consistent with the present evidence that the absorption band in alkaline ice involves photoionisation.

The optimum well parameters for the two potentials considered have been used to calculate photoionisation spectra. These potentials (in au) are represented by

$$\text{(I)} \qquad V(r) = -0.148 \qquad r < 4.5$$
$$V(r) = 0 \qquad r > 4.5$$

$$\text{(II)} \qquad V(r) = -0.188 \qquad r < 3.14$$
$$V(r) = -4.35\exp(-1.0r) \qquad r > 3.14$$

The calculated spectra are compared with the experimental absorption band for alkaline ice in Figure 5.2.8.

In this it can be seen that, in addition to threshold maximum intensity and half width, the general shape of the observed spectrum is closely reproduced, suggesting that, at least in disordered systems such as alkaline ice, the above approximation may have some use in the description of ionisation in solids.

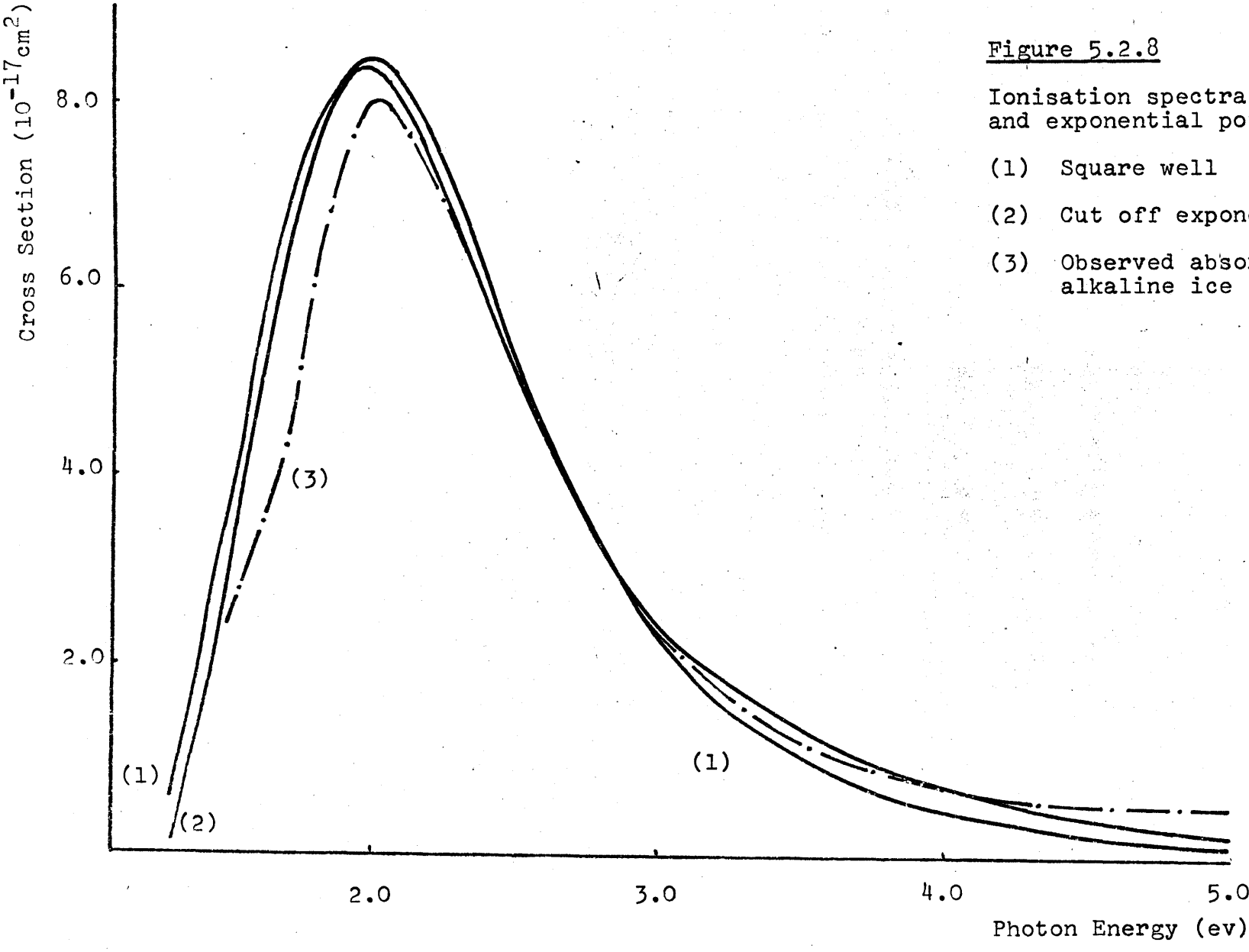

Figure 5.2.8

Ionisation spectra for square well and exponential potentials.

(1) Square well

(2) Cut off exponential

(3) Observed absorption spectrum for alkaline ice

(ii) Iterative Analytical Technique for the Square Well

The Schrödinger equation for a square well of depth V_o and radius a in the case of $\ell = 0$ is

$$-\tfrac{1}{2}\frac{d^2G(r)}{dr^2} - V_oG(r) = EG(r) \qquad r < a$$

$$-\tfrac{1}{2}\frac{d^2G(r)}{dr^2} = EG(r) \qquad r > a$$

with the wave function in the well given by $L(r) = \frac{1}{r}G(r)$

G(r) is given by $G(r) = A\sin\alpha r \quad \alpha = \left[2(V_o - |E|)\right]^{\frac{1}{2}} \quad r < a$

$$G(r) = Be^{-\beta r} \quad \beta = (2|E|)^{\frac{1}{2}} \qquad r > a$$

where $B = \frac{\sin\alpha a}{e^{-\beta a}} A$ and A is a normalising factor.

The energy levels are found from matching the gradients of the inner and outer solutions at the boundary and are obtained from solutions of the equation:

$$-\cot\eta = \frac{(\xi^2-\eta^2)^{\frac{1}{2}}}{\eta} \qquad \eta = \alpha a \qquad \xi = (2V_o)^{\frac{1}{2}}a$$

A method of solving this equation other than by graphical means has been devised and depends on an iterative technique which converges rapidly.

Since $\cot\eta$ is negative then $\frac{n\pi}{2} < \eta < (\frac{n+1}{2})\pi$

where n = 1,3,5, ...,

and the number of radial nodes = $\frac{n-1}{2}$

Due to the orthogonality of radial solutions each angular quadrant contains only a single solution.

If an arbitrary choice η_1 is made in the appropriate quadrant then $\eta_1 = \eta_T + \Delta\eta$ where η_T is the true solution.

For this arbitrary η_1 a difference is defined by

$$\varepsilon = \cot^2 \eta_1 - \left(\frac{\xi^2-\eta_1^2}{\eta_1^2}\right)$$

Substituting for η_1 in terms of the true solution and making the approximations $\tan\Delta\eta\approx\Delta\eta$, $\Delta\eta^2\approx 0$ yields:

$$\Delta\eta = \frac{\eta_T^2}{2\eta_T\cot^2\eta_T - 2\xi^2\cot\eta_T - 2\varepsilon\eta_T^2\cot\eta_T + 2\eta_T(1-\varepsilon)}$$

Making the final assumption that η_1 is sufficiently close to η_T to allow its use in the above yields a value of $\Delta\eta$ from which a new value of η_1 may be obtained by $\eta_1 \longrightarrow \eta_1 - \Delta\eta$.

It has been found that the above approximations do not prevent good accuracy being obtained within six cycles even starting with values of η_1 a few degrees above the limiting $n\pi/2$ level.

3 A Study of Electron Decay by Tunneling

From the evidence on trapped electron decay presented in Chapter 3.2, the frequent temperature independence and time behaviour of the decay suggests that long range tunneling may be important in the overall loss of trapped electrons in solid media.

One of the consequences of a tunneling decay scheme is that electron loss is spread over several orders of magnitude of time (10^{-9} - 10^{6} sec), and since no observations covering such a time range have been made for a single medium, any statement concerning the eventual stability of electrons becomes relevant only to the interval of time or fraction of the decay curve studied. In low temperature ice , for example, half the population is lost between 0.5usec and 2msec at which point an apparent levelling off is observed, whilst in MTHF, for which no short term studies exist, long term observations reveal a half life of ten days.

The possibility that at higher temperatures, electrons may react by a tunneling mechanism has recently been considered, in order to explain the unusually high rate constants of electrons in diffusion controlled reactions (42). A tunneling model was used with some success by Miller (43,44), to account for the variation of electron yields with added scavengers and their subsequent decay characteristics. The sensitivity of the tunnelling rate constant to tunnelling distance, however, suggests that the distribution of electron-scavenger distances will play an important part in both the long and short term decay behaviour, particularly in the case of non-random electron-cation distributions, which are thought to be an important feature of the radiation effects in liquids and solids (45,46).

Using an analysis similar to that presented by Miller (43),

calculations have therefore been performed for a tunneling decay scheme with the inclusion of electron scavenger distribution features. The two distribution types described bellow are chosen to represent both random electron-scavenger arrays and non-random electron-parent ion systems.

(i) An Approximate Tunneling Rate Constant

In the discussion of Chapter 2.4, the approximate method of Robinson and Frosch was presented for the calculation of electron tunneling rates. It was also shown there that the use of a rectangular barrier approximation in the calculation of the β parameter may partly cancel the error introduced by a one dimensional analysis. In the calculations presented below therefore, the tunneling rate constant $\lambda(R)$ has been taken to be of the form suggested by Brocklehurst, giving

$$\lambda(R) = \frac{I^2\sigma}{\hbar d} \exp\left[-2\left(\frac{2mI}{\hbar^2}\right)^{\frac{1}{2}}R\right] \qquad (1)$$

where I is the ionisation potential, σ the Franck-Condon factor and $\underline{d}$ is related to the vibrational relaxation time t_{vib} by $t_{vib} = \hbar/d$. For relaxation times of 10^{-11}sec, equation (1) becomes

$$\lambda(R) = 5.9\times10^{17}\sigma I^2 \exp(-1.0202\, I^{\frac{1}{2}}R) \qquad (2)$$

where I is in $\underline{ev}$ and R in A^{o}.

Since no information exists on the factor σ, which can be widely varying, and since the main dependence of $\lambda(R)$ on the ionisation potential derives from its presence in the exponent, a lower limit of 10^{15} has been chosen for the pre-exponential factor in all the calculations performed. Equation (2) then takes the form

$$\lambda(R) = k \exp(-cR) \qquad (3)$$

where $k = 10^{15}$ and $c = 1.0202\times I^{\frac{1}{2}}$.

(ii) Kinetics of Electron Decay

The analysis presented by Miller (43) to account for the yields and subsequent long term decay of trapped electrons in solids by long range tunneling is developed to incorporate distribution characteristics of electrons with respect to scavengers. By this means the uncertainty in effective tunneling radii can be removed.

If the volume of a system containing trapped electrons and N scavengers is $\underline{V}$, and the two species are distributed randomly with respect to one another, then the probability that an electron is outside the range $\underline{R}$ of all scavengers but one is given by $(1-a/V)^{N-1}$, where $a = 4\pi R^3/3$. The probability that such an electron is within $\underline{R}$ and $\underline{R}+d\underline{R}$ of a particular scavenger, and at the same time outside the range $\underline{R}$ of all others can be represented by

$$\frac{4\pi N R^2 dR}{V} (1-a/V)^{N-1}$$

If this probability is represented by P(R)dR, then

$$P(R) = \frac{4\pi N R^2}{V} (1-a/V)^{N-1} \qquad (1)$$

This function is chosen to represent the distribution of electrons with respect to scavengers and assumes that electrons can tunnel only to their nearest scavenger.

If the number electrons in $\underline{V}$ before any tunneling has taken place is N_e^o, then the electron distribution is given by

$$\frac{dN_e^o}{dR} = N_e^o P(R) \qquad (2)$$

It is easily shown that this is a normalised function since,

$$\int_0^{R_V} P(R)\partial R = \frac{N}{V}\int_0^{V}(1 - a/V)^{N-1}\partial a \quad = \frac{N}{V}\left[-\frac{V}{N}(1 - a/V)\right]_0^{V} = 1$$

When electrons are allowed to tunnel to their nearest scavenger, the distribution (2) will decay by first order. If the rate constant for tunneling of an electron to a scavenger at distance R is $\lambda(R)$ then the distribution decays according to:

$$\frac{d}{dt}\left(\frac{dN_e}{dR}\right) = \frac{dN_e}{dR}.\lambda(R)$$

$$\therefore \quad \frac{dN_e}{dR} = \frac{dN_e^o}{dR}\, e^{-\lambda(R)t}$$

$$\therefore \quad N_e(t) = N_e^o\int_o^{\infty} P(R)e^{-\lambda(R)t}\partial R \qquad (3)$$

This gives the variation with time of the total concentration of electrons $N_e(t)$ based on the initial distribution.

Since the number of scavengers is usually very large ($10^{19}/cm^3$), the expression for P(R) can be simplified to

$$P(R) = \frac{4\pi NR^2}{V}\exp\left[-\frac{4\pi NR^3}{3V}\right] \qquad (4)$$

From the previous discussion (cf 5.3(i)) the tunneling rate constant $\lambda(R)$ is taken to have the simple form

$$\lambda(R) = ke^{-cR}$$

where $k = 10^{15}$, $c = 1.0202I^{\frac{1}{2}}$, and I is the trap ionisation potential in ev.

Equation (3) then becomes

$$\frac{N_e}{N_e^o} = \frac{4\pi N}{V}\int_o^{R_V} R^2\exp\left[-\frac{4\pi NR^3}{3V}\right].\exp\left[-kte^{-cR}\right]\partial R \qquad (5)$$

Integrating by parts:

$$\frac{N_e}{N_e^o} = -\left[\exp\left\{-kte^{-cR}\right\}\exp\left\{-\frac{4\pi NR^3}{3V}\right\}\right]_o^{R_V} + \int_a^b \exp\left\{\frac{4\pi N}{3Vc^3}\left[\ell n(-\ell nx)-\ell nkt\right]^3\right\}\partial x \qquad (6)$$

where $x = \exp\left[-kte^{-cR}\right]$, and for the integration limits

$a = e^{-kt}$ and $b = \exp\left[-kt\exp(-cR_v)\right]$

For times which are accessible, the first term on the RHS is zero effectively at both limits due to the large value of k ($\approx 10^{15}\,sec^{-1}$) and N/V ($\approx 10^{19}/cm^3$).

Since $R_v \approx 10^8 (A^o)$ the integral limits a and b are effectively 0 and 1 respectively.

The fraction of electrons remaining after time t is then given by:

$$\frac{N_e}{N_e^o} = \int_o^1 \exp\left\{\frac{4\pi N}{3Vc^3}\left[\ell n(-\ell n(x)) - \ell nkt\right]^3\right\}\partial x \qquad (7)$$

The time dependence of the integral derives from the strong influence which the ℓnkt term has in determining the distribution of the integrand in x space as is shown qualitatively in Figure 1

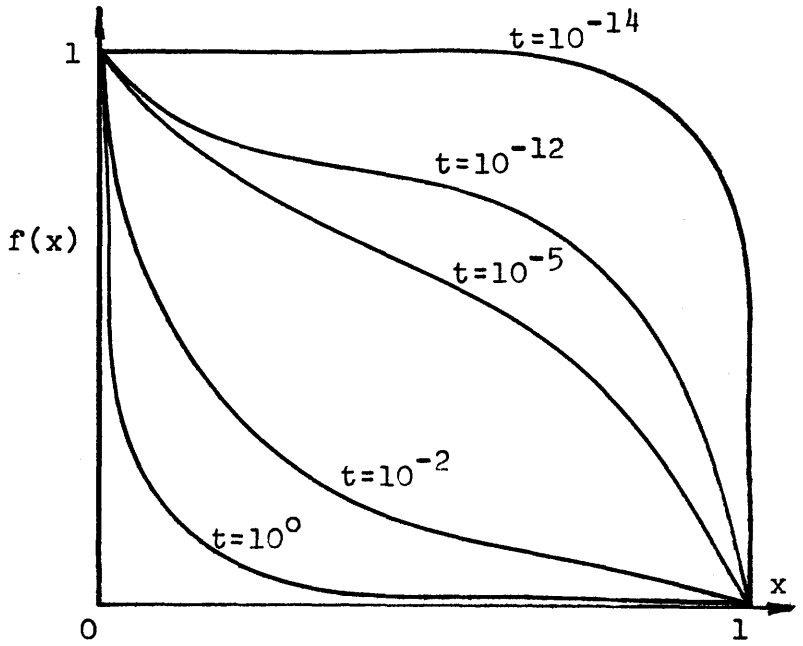

Figure 1

(iii) Non-Random Decay

The possibility that the distribution of trapped electrons with respect to scavengers may be of a non-random nature depending on the method of trapped electron production has already been discussed (3.2). It is envisaged that trapped electrons produced for example by photoionisation, may be trapped within a relatively close distance to the positive ion, depending on the average trapping distance. Such a situation may give rise to a non-random electron-scavenger distribution, depending on the concentration of scavengers and other positive ions.

The following analysis simulates the decay of trapped electrons by tunneling in such a non-random situation by treating the tunneling to the parent ion or radical separately. The initial distribution of trapped electrons with respect their parent ions or radicals can be considered to derive from an energy loss process in which the decay of a population of free electrons takes place with effective rate constant k such that the fraction f remaining after time t is

$$f = e^{-kt} = \exp(-t/t_{\frac{1}{2}})$$

If an average velocity $v_{\frac{1}{2}}$ is assigned to the pulse of electrons and $v_{\frac{1}{2}}t_{\frac{1}{2}} = R_{\frac{1}{2}}$ is taken to represent an average distance travelled, then the fraction f can be represented by

$$f = \exp(-R/R_{\frac{1}{2}})$$

where $R=v_{\frac{1}{2}}t$, and represents approximately the average distance travelled by the pulse in time t. According to this scheme, the probability of a trapped electron being found between R and R+dR of the parent species is P(R)dR where

$$P(R) = -\frac{df}{dR} = \frac{1}{R_{\frac{1}{2}}} \exp(-R/R_{\frac{1}{2}}) \qquad (1)$$

The use of such a distribution function has recently had some success in accounting for the yield of scavenged electrons resulting from ion pair recombination (47).

For each electron in this distribution the possibility of tunneling to other species is also permitted. Since the relative distribution of parent species and scavengers is taken to be of a random nature, the distribution of each trapped electron is considered to be random with respect to the other scavenging species in the system, to which the previous random analysis will be applied.

There is thus a distribution of electrons relative to the parent species given by

$$\frac{dN_e}{dR} = N_e P(R)$$

and this distribution is further distributed with respect to other scavengers such that

$$\frac{d}{dr}\left(\frac{dN_e}{dR}\right) = N_e P(R) P(r) \qquad (2)$$

where $$P(r) = \frac{4\pi N_V r^2}{V}(1-a/V)^{N_V-1}$$ as before.

This distribution decays with a composite rate constant $[\lambda(r)+\lambda(R)]$ according to

$$\frac{d}{dt}\left(\frac{d^2N_e}{dRdr}\right) = \frac{d^2N_e}{dRdr}[\lambda(R)+\lambda(r)]$$

$$\therefore \quad \frac{d^2N_e}{dRdr} = \left(\frac{d^2N_e}{dRdr}\right)^{o} \exp\left\{-[\lambda(R)+\lambda(r)]t\right\}$$

$$\therefore \quad \frac{d^2N_e}{dRdr} = N_e^o P(R)P(r)\ \exp\left\{-[\lambda(R)+\lambda(r)]\,t\right\} \qquad (3)$$

Representing the tunneling mechanism as before with square well parameters and assigning these same parameters to all scavenger types in the system gives

$$\frac{N_e}{N_e^o} = \frac{4\pi N_V}{R_{\frac{1}{2}}V}\int_o^{R_V}\int_o^{\infty}\exp(-R/R_{\frac{1}{2}})\exp\left[-kte^{-cR}\right]r^2(1-a/V)^{N_V-1} \times \exp\left[-kte^{-cr}\right]\partial R\partial r \qquad (4)$$

If $R_{\frac{1}{2}}$ is large then that region of R for which $\exp\left[-kte^{-cR}\right]$ is around unity will coincide with most of range of $\exp(-R/R_{\frac{1}{2}})$ and the integral over R will be close to unity. In that situation, decay to the parent species will be insignificant and the equation (4) reduces to that for decay of the random distribution (ii)5.

From equation (4) it can be seen that the total remaining fraction of electrons at time $\underline{t}$ is given by the product of fractions for each of the decay modes and may be represented by

$$\frac{N_e}{N_e^o} = P(t).S(t)$$

where P(t) and S(t) represent the fractions due to parent and bulk scavenger respectively.

(iv) Application in Solids

The preceding analysis has been used in an attempt to discover the extent to which a tunneling decay scheme is consistent with some of the observed decay characteristics of electrons in various solid media. The low temperature decay behaviour in crystalline ice, 3 methyl pentane and methyltetrahydrofuran has been investigated, and the choice of parameters in each of the systems is discussed below.

Crystalline Ice

Although a comprehensive study of the initial decay in pure ice at $77^{o}K$ has not been made, it is known from the work of Kawabata (32), that in the interval 0.5 usec-2 msec, half the electron population is lost and of this 50%, only 15% is lost between 0.4 msec and 2 msec. In this study the decay could only be followed for 10 msec, at which point stability had been almost apparently reached. From earlier studies (48), the electron concentration is known to be around $10^{-5}M$, whilst $OH^{\bullet}$ radical, which, aside from possible parent cations, is considered to be the main scavenging species, has a concentration around $10^{-2}M$ (49).

Application of equation (iii)4 to the decay, requires a knowledge of the bulk scavenger concentration, the average trapping distance from the parent ion $R_{\frac{1}{2}}$, and the trap ionisation potential. The scavenger concentration has been taken to be $10^{-2}M$ and from the evidence of Chapter 3.2, an ionisation potential of 1.9 ev has been used. Results are presented for three values of $R_{\frac{1}{2}}$, equal to 15,20 and 30 A^{o}.

From equation (iii)4, the overall decay is given by the product of the fractional decays from parent and bulk scavenger

recombination. The results presented in Figures 5.3.1 - 5.3.3, therefore, show the fractional decay due to each mode as well as the total decay for the combination, at each value of $R_{\frac{1}{2}}$.

3 Methyl pentane

Studies on the decay of electrons in this medium at $77^{o}K$ in the range 10^{-4} - 10^{3} sec have been performed by Klassen et. al. (50) at several absorption wavelengths. From this it was apparent that a spectral shift occurs simultaneously with decay. Since the decay at 800 nm, however, is little affected by the spectral shift, the intensity change at this wavelength has been taken as representative of the overall electron loss. Earlier studies (51) revealed that the bulk scavenger concentration is around 10^{-4}M. From the results of photobleaching studies (52), the ionisation potential has been taken as 0.53 ev.

Decay curves were calculated for several values of $R_{\frac{1}{2}}$ and the best agreement with experiment at 10^{3} sec was obtained for $R_{\frac{1}{2}} = 30A^{o}$. Figure 5.3.4 shows the component and total fractional decay for this value compared with the observed decay curve.

Methyltetrahydrofuran

Studies on the low temperature spontaneous decay in this medium have been performed only for the long term decay (53) in which a half life of 250 hrs is observed. Such a slow decay, however, may be used to test the extent to which a tunneling model is capable of simulating near stability. In the above study, an e.s.r. analysis revealed that the average spin separation corresponded to a local radical and electron concentration

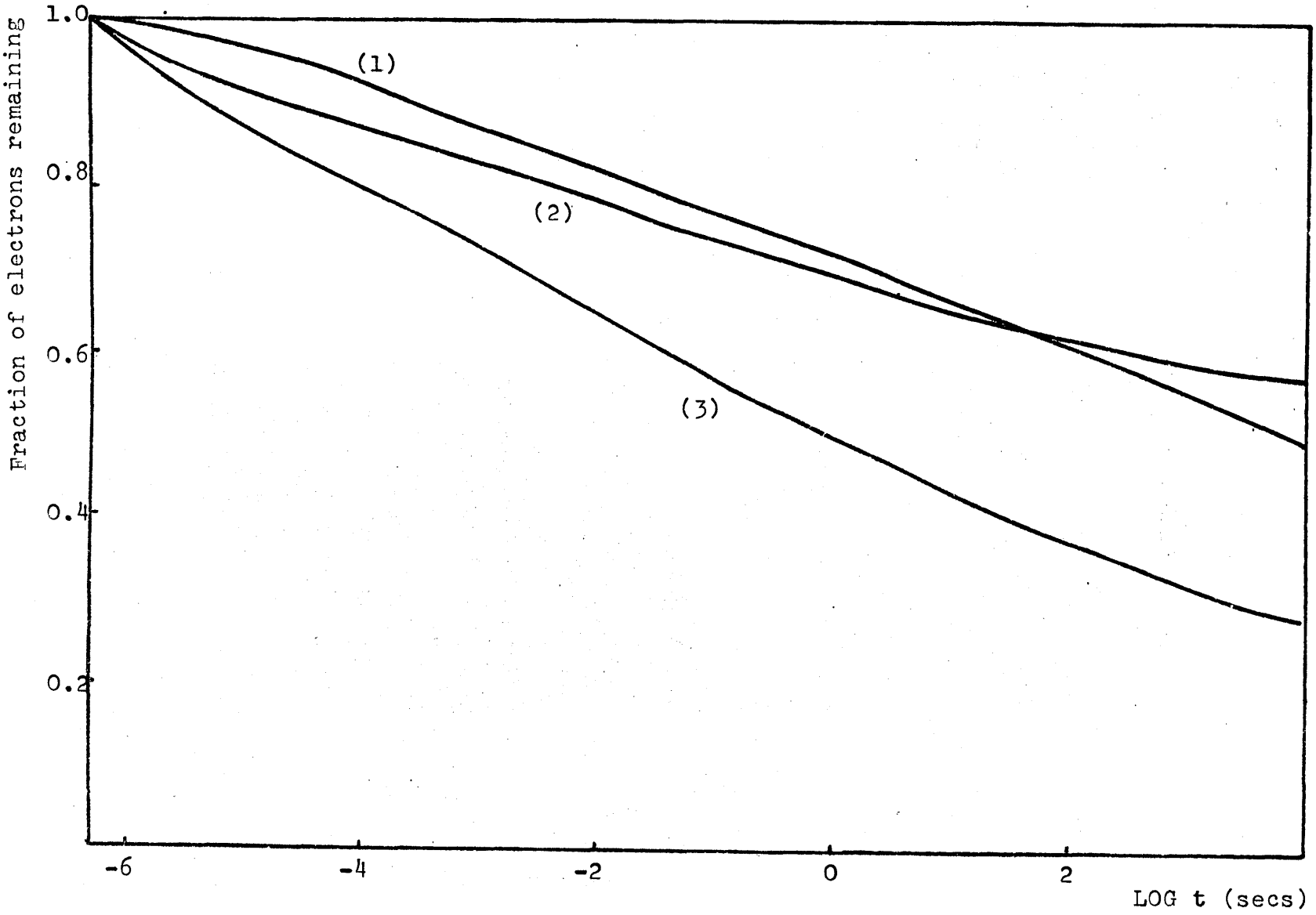

Figure 5.3.1

Calculated decay curves for electron in ice.

(1) Decay to bulk scavengers (10^{-2}M)

(2) Decay to parent ion with $R_{\frac{1}{2}}=30A^{\circ}$

(3) Total fractional decay

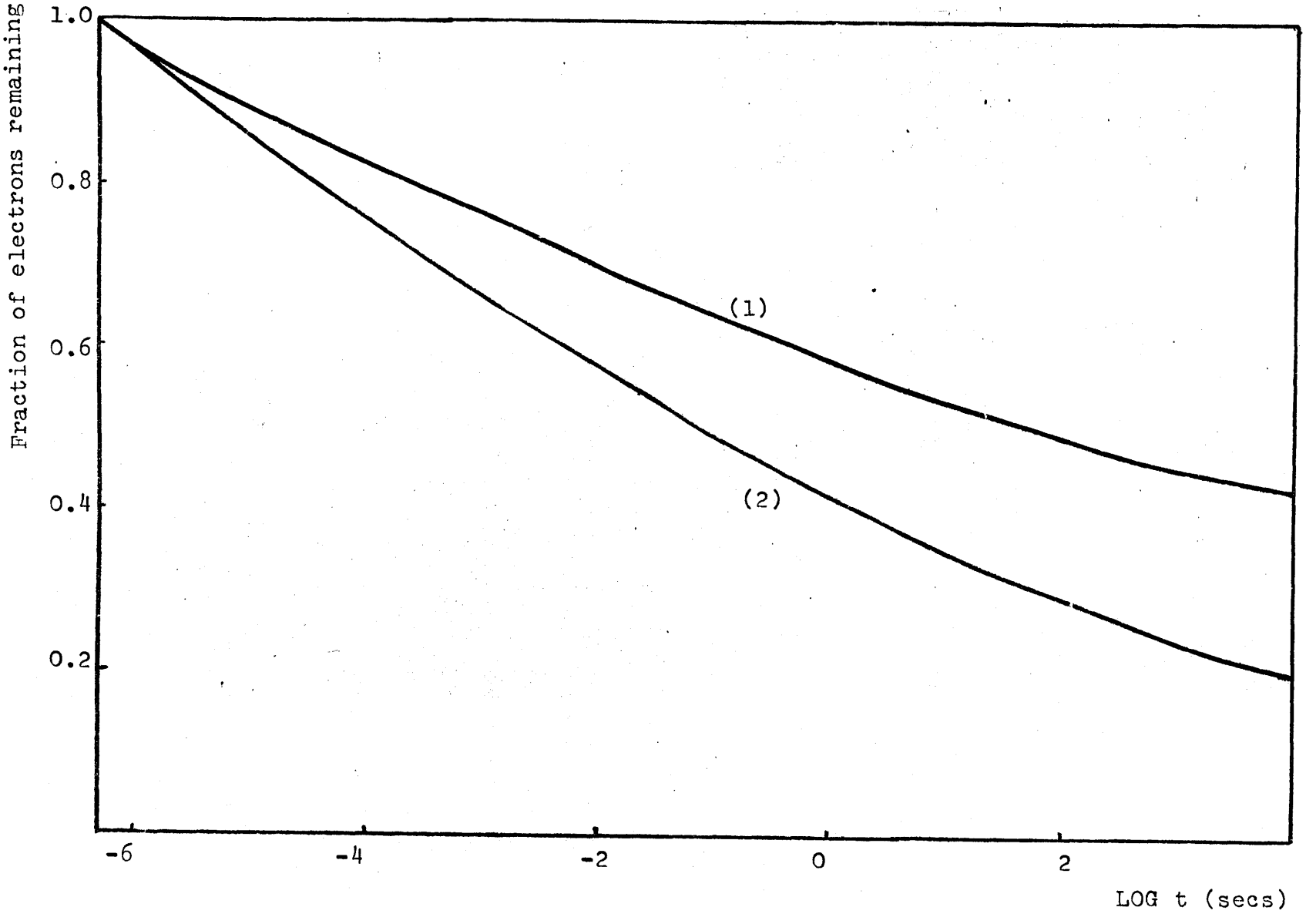

Figure 5.3.2

Calculated decay curve for electron in ice.

(1) Decay to parent ion with $R_{\frac{1}{2}}=20A^{\circ}$

(2) Total fractional decay due to parent and bulk scavengers ($10^{-2}M$)

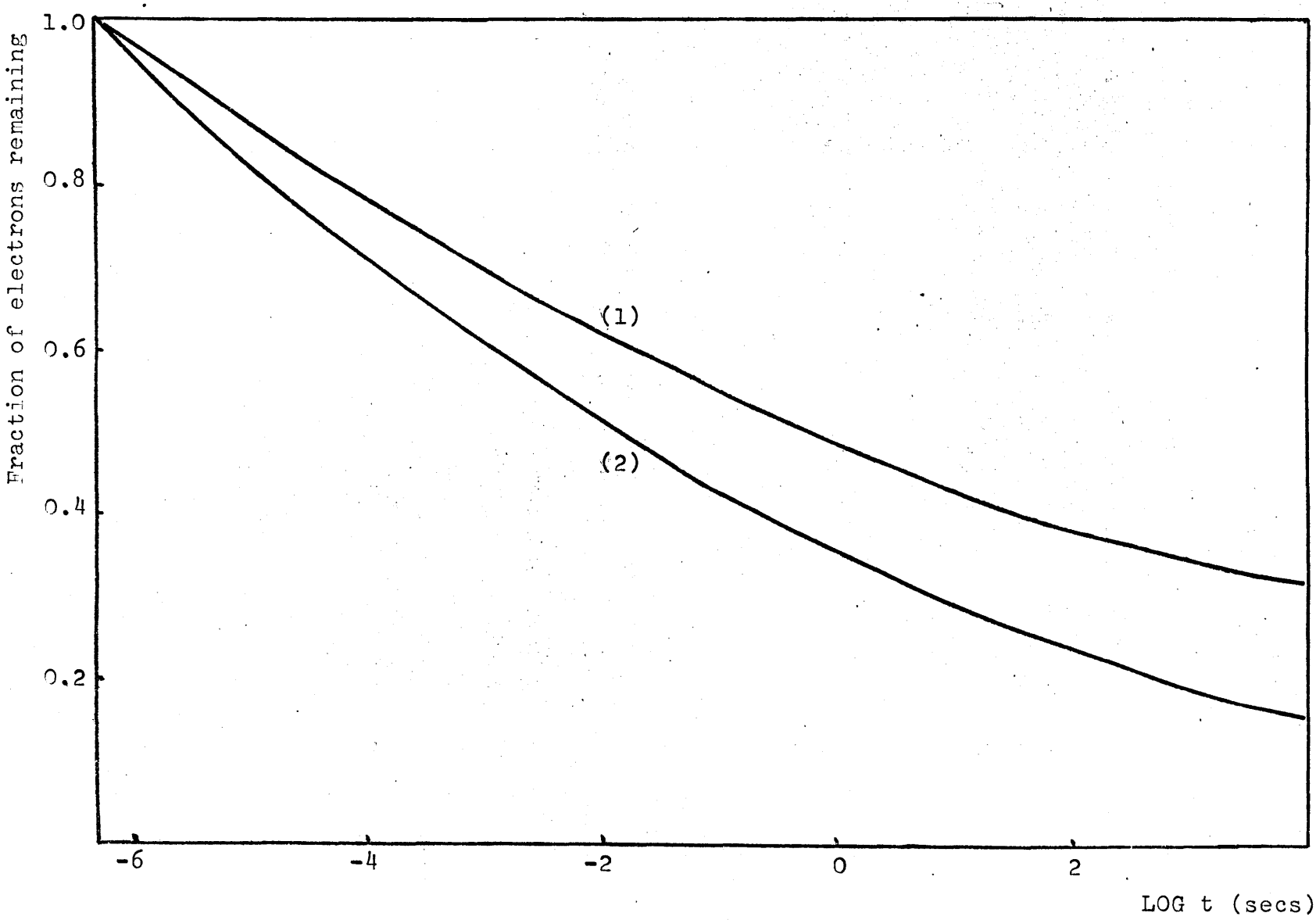

Figure 5.3.3

Calculated decay curve for electron in ice.

(1) Decay to parent ion with $R_{\frac{1}{2}}=15A^{o}$

(2) Total fractional decay due to parent and bulk scavengers ($10^{-2}M$)

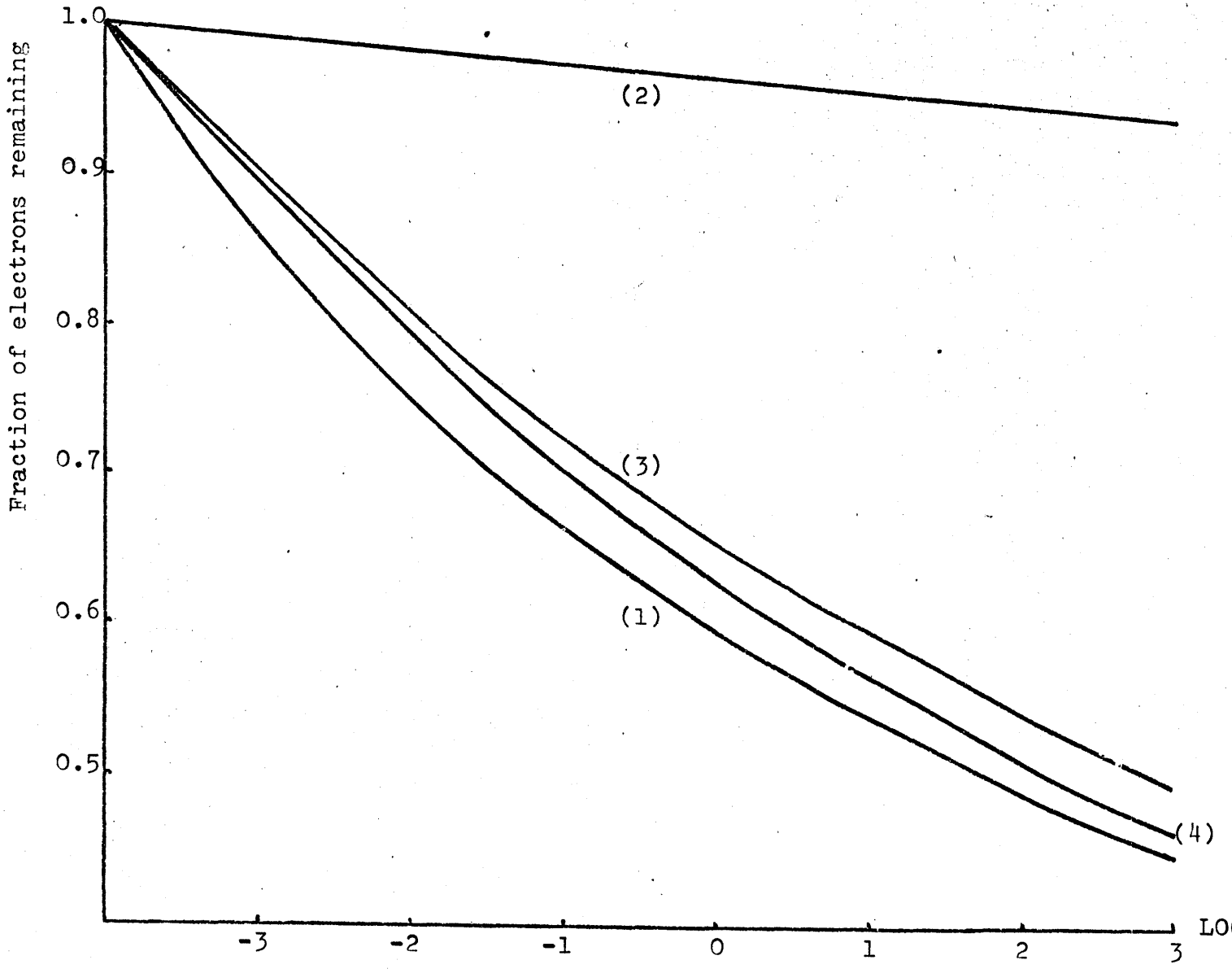

Figure 5.3.4

Calculated decay curve for electron in 3MP.

(1) observed decay in 3MP

(2) decay to bulk scavengers (10^{-4}M)

(3) decay to parent ion with $R_{\frac{1}{2}} = 30A^{\circ}$

(4) total fractional decay

of 10^{-2}M. It was found however, that the total concentration of spins was 1.8×10^{-3}M. From this it was concluded that electrons were associated with radical ions, having an average separation of $44 \pm 7 A^{o}$.

The above data has been used to calculate the long term decay curve for MTHF. The value of $R_{\frac{1}{2}}$ was taken as $40 A^{o}$ and the bulk scavenger concentration as 10^{-3}M. Figure 5.2.5 shows the component and total decay curves, normalised to unity at 1 sec, compared with the experimental curve.

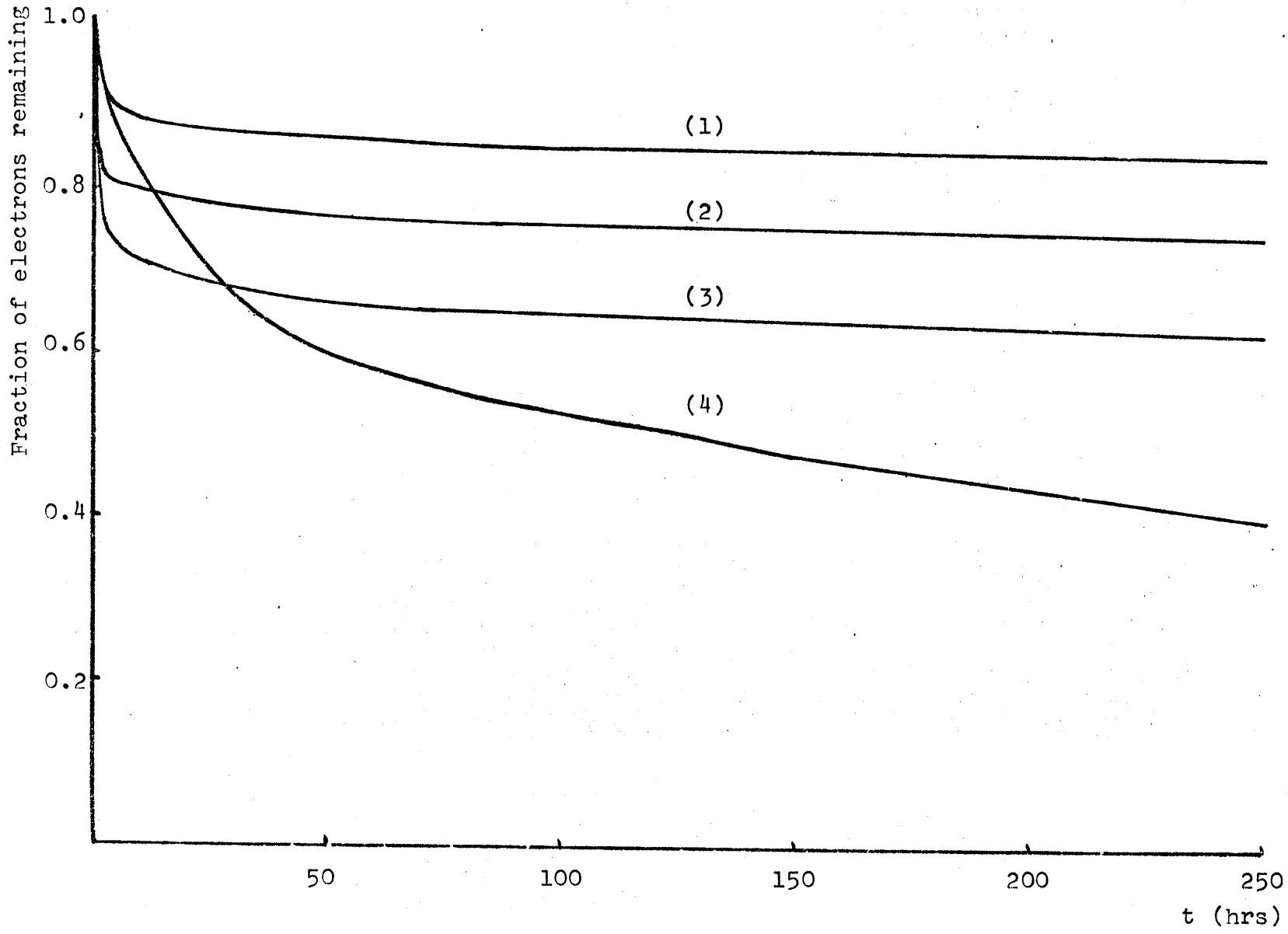

Figure 5.3.5

Long term decay of electron in MTHF.

1 Decay to bulk scavengers (10^{-3}M)

2 Decay to parent ion with $R_{\frac{1}{2}}=40A^{o}$

3 Total fractional decay

4 Observed long term decay

Discussion

An examination of Figures 5.3.1 - 5.3.3 for pure ice shows that the usec - msec decay can be accounted for by an average parent ion separation of 15A°. At this distance the total fractional decay to 2 msec is 44%, and of this, around 32% is due to recombination with parent, the remainder being due to bulk scavengers. The rapidly decreasing nature of the decay rate found experimentally is also shown within this decay scheme by the fact that 34% of the total decay takes place within 0.4 msec. Figure 5.3.3 also shows that a further significant fraction decays in the msec - hrs time range, indicating that the applicability of the model may be tested by future observations covering such a time scale.

The above results indicate that, within the tunneling model employed, short term decay in ice can only be explained by the use of non-random electron scavenger distributions. This is consistent with the long held view that trapped electrons exist within local ionisation regions or spurs (45,46).

Among the several calculations which have been performed within the spur model, in an attempt to account for the yields of various substances following the passage of radiation (45,46, 48,49), that of Schwarz (46) is of particular relevance to the above results. In this study, the initial electron-parent ion distribution was estimated from the final yield of hydrogen. For a gaussian distribution P(r) of the form

$$P(r) = \frac{2}{b\sqrt{\pi}} \exp\left[-r^2/b^2\right],$$

best agreement with experiment was obtained for $b = 23\sqrt{2}A^{\circ}$.

The mean radius for this distribution is 18A° which corresponds well with the mean radius of 15A° for the exponential distribution found from the tunneling analysis.

The results of Figure 5.3.4 for 3MP show that at the chosen value of $R_{\frac{1}{2}}$ (30A°), the form of the observed decay curve is well reproduced over a wide time range. In this case most of the decay is due to parent recombination, the low concentration of bulk scavengers contributing only 3%. The calculated curve also stresses the unusual kinetics which a tunneling mechanism, employing a distribution function, produces, where around 10% decay takes place for each order of magnitude of time.

Very little quantitative information exists about electron-parent ion separations in this medium, making the relevance of the average separation distance of 30A° uncertain. The importance of electron-parent reactions is implied however, from initial decay rates which are found to be almost independent of radiation dose (54), and from the photoinduced recombination luminescence studies of McClain and Albrecht (55), which showed that 95% of electrons were scavenged by their parent ion. For the exponential distribution used above, it is found that 95% of electrons are initially contained within a radius of 90A° from the parent. It was initially suggested that the 5% of photoexcited electrons which escape recombination with their parent ions should be situated sufficiently distant for the coulombic attraction to be less than thermal energies. From this, a radius of 500A° was deduced for this population. For a population situated beyond 90A°, the coulombic attraction, for a dielectric constant of 2.3, is around 0.07 ev, which is considerably greater than

thermal energies at 77°K. Such a short radius cannot be ruled out on these grounds however, since the stimulating light used in the experiment had an energy of around 0.2 ev above the presumed ionisation threshold.

The calculated curve of Figure 5.3.5 for MTHF shows only approximate agreement with experiment, the initial decay within 3 hrs being overestimated, whilst the latter part becomes insignificant at too early a stage. In view of the significant decay which the observed curve exhibits at long times however, it is possible that an additional mechanism, such as positive ion migration, operates in MTHF with a half life around 150 hrs. If this was the case, then the rapid 3 hr portion observed could be contributed by a tunneling mechanism. The overall contribution by such a mechanism in the 250 hr period would be less however, than the 37% calculated with $R_{\frac{1}{2}} = 40A^{\circ}$. This could be accommodated by a larger $R_{\frac{1}{2}}$, which the results of Smith and Pieroni (53) would still permit.

A general feature of the above tunneling model is revealed by the use of a linear time scale in Figure 5.3.5, and concerns the fact that most of the decay is compressed into the initial fraction of the linear scale, which has the effect of concealing the long term nature of the decay.

4 Calculation of Photobleaching Properties in Solids

(i) Introduction

Evidence for the spontaneous decay of electrons by recombination with scavengers in solid media has already been presented in Chapter 3.2. In this it was shown that in many systems the decay rate becomes so low that the term stability can eventually be applied to the remaining population, and the calculations of 5.3.(iv) suggest that decay by tunneling can account for such general features. The photobleaching evidence of 3.3, however, has shown that such a state of stability can be removed by exciting electrons with light lying within their normal absorption range.

The nature of such excited states, discussed in 3.1, therefore becomes important in a description of the photo-induced recombination process. Whilst in some systems only a delocalised state would seem to exist (39) and in others the existence of a high energy threshold for bleaching suggests the importance of only a delocalised state (48), in some media long lived excited states are thought to be accessible (56), introducing the possibility of loss from these by a tunneling mechanism.

The fact that quantum efficiencies are less than unity at all wavelengths of the absorption band indicates that excited electrons can return to the ground state without being scavenged, and the effect of scavengers in increasing the efficiency reveals the competitive nature of these two processes. Whether the excited state involved is of a delocalised or localised nature, such a scavenger effect is consistent with the effect of scavengers on both the initial yield and subsequent decay of electrons.

In the following calculations, a simple photobleaching model is constructed and applied to the case of ice, 3 methylhexane and methyltetrahydrofuran. In the former case a mobile electron capture model is considered, while for the organic media, bleaching efficiencies are obtained by considering decay from a localised excited state by a tunneling mechanism.

(ii) A Photobleaching Model

On the basis of the above considerations a general scheme is presented to account for the behaviour of systems undergoing photobleaching.

A trapped electron is regarded as having three states accessible to it:

a) a ground state which may be excited by light, leading to

b) an excited state - the nature of which remains unspecified

c) a 'lost' state representing a scavenged electron

The possibility of induced emission is included in the model although in some systems, depending on the nature of the excited state, this process would be unimportant. It is assumed that the scavenged state is accessible only from the excited state and that the process of scavenging is irreversible. The process may be represented by;

$$N_1 \underset{k_1+k_2}{\overset{k_1}{\rightleftharpoons}} N_2 \xrightarrow{k_3} S$$

N_1 = ground state particle concentration

N_2 = excited state particle concentration

S = concentration of scavenged electrons

k_1 = excitation rate constant

k_2 = rate constant for retrapping or returning to the ground state

k_3 = scavenging rate constant

Solving for N_1 is carried as follows

$$\frac{dN_1}{dt} = N_2(k_2+k_1) - k_1N_1 \equiv (D+k_1)N_1 = (k_2+k_1)N_2 \qquad (1)$$

$$\frac{dN_2}{dt} = k_1N_1 - (k_1+k_2+k_3)N_2 \equiv (D+k_1+k_2+k_3)N_2 = k_1N_1 \qquad (2)$$

This leads to $\left\{D^2+(2k_1+k_2+k_3)D+k_1k_3\right\}N_2 = 0$

Putting $N_2 = Ae^{bt} + Be^{ct}$

gives $b = \frac{-Z+(Z^2-4Y)^{\frac{1}{2}}}{2}$, $c = \frac{-Z-(Z^2-4Y)^{\frac{1}{2}}}{2}$

where $Z = 2k_1+k_2+k_3$, $Y = k_1k_3$

At $t = 0$, $N_2 = 0$. Hence $B = -A$. Using (2) this leads to

$$N_1 = \frac{A}{k_1}\left[e^{bt}(b+Z-k_1) - e^{ct}(c+Z-k_1)\right]$$

Since $N_1 = N_1^o$ at $t = 0$, this gives

$$N_1 = \frac{N_1^o}{(b-c)}\left[e^{bt}(b+k_2+k_3) - e^{ct}(c+k_2+k_3)\right] \qquad (3)$$

This equation takes a simpler form when $c \ll b$ in which case the second decays rapidly to zero. This is the situation which prevails when the excitation and scavenging rate constants k_1 and k_3 are much less than the retrapping rate constant k_2.

Under these conditions $b = -\frac{Y}{Z} = -\frac{k_1k_3}{(2k_1+k_2+k_3)}$

and the ground state population decays by first order following the equation

$$N_1 = N_1^o e^{-Kt} \qquad (4)$$

in which $K = \frac{k_1 k_3}{(2k_1+k_2+k_3)}$ and $'N_1^o = \frac{(b+k_2+k_3)}{(2k_1+k_2+k_3)} N_1^o$

$'N_1^o$ being the ground state concentration when the steady state is reached. This steady state relation can also be derived directly from equations (1) and (2) by setting dN_2/dt to zero.

The quantum efficiency for photobleaching is the ratio of the rate at which ground state electrons are lost and the rate of photon absorption. The latter quantity is the resulting rate when induced emission is included. The quantum efficiency is then given by

$$Q = -\frac{dN_1/dt}{k_1 N_1} = \frac{K}{k_1} = \frac{k_3}{(2k_1+k_2+k_3)}$$

(iii) A Mobile Electron Capture Model for Photobleaching

Using the photobleaching kinetics of 5.3(i) a mobile electron capture model is considered in which the excited state, ie the state from scavenging occurs, is a conduction state. The electron is envisaged as being ejected into this state where it loses its energy to vibrations in the system and eventually becomes scavenged or retrapped at some different site. In this respect it is considered identical with pre-thermal electrons from an external pulse.

Since the electron traps are regarded as evolving in time following trapping, there is justification in ignoring spontaneous and induced emission at the exciting wavelength in the previous expression for the quantum efficiency.

(a) An Approach to Electron Trapping

The trapping or retrapping of electrons is identified with a transformation from a free state from which scavenging may occur to a spatially localised state. The problem of finding a reasonable estimate for the retrapping rate constant k_2 must be solved by constructing a retrapping model based on experimental observations. The possibility of scavenging is assumed to exist during the entire lifetime of the electron in the free state and hence the mechanism of retrapping is taken to begin at the instant of excitation. Within this framework there may be several steps involved in the overall retrapping, and only the rate determining step will play a significant part in deciding the value of k_2.

Evidence on the nature and magnitude of k_2 might be expected to be available from experiments on the formation time of solvated electrons in various media. Following earlier studies (57,58), present time resolution techniques reveal that for water ($300^{\circ}K$), the solvated electron spectrum appears in the infra red region in a time of 2psec and develops to its long time position by shifting to the blue in a further 2psec (30). Similar short formation times have been reported for liquid alcohols (31).

The above spectral shift is taken to be the result of medium relaxation around the trapped species, despite the fact that observed dielectric relaxation times at this temperature are somewhat higher (59). Further possible evidence of a rapid relaxation mechanism in water comes from the observation of the solvated electron excited state lifetime (60), which is found to be less than 4psec.

Studies on the formation time in H_2O and D_2O ice ($77^{\circ}K$)

provide an upper limit of 0.5 usec, at which time a visible and an infra red portion can be seen (32,33). This formation time is again short compared with that of the observed relaxation modes in ice (34,35). Various models based on strong field effects, have been invoked to account for these short relaxation times associated with electron solvation in liquids and solids (35,61).

The above formation times certainly provide an upper limit to the localisation time of the mobile electron, but an uncertainty exists as to whether localisation occurs simultaneously with orientational relaxation or whether the latter occurs in response to the presence of the localised electron. If the former is the case then k_2 would seem to be governed by such relaxation varying by a factor of 10^6 between 77-300°K. Such behaviour would be expected to impose a strong temperature dependence on the bleaching quantum efficiency Q. For alkaline ice no such dependence has been observed (39).

In the model considered, therefore, it is assumed that electron localisation occurs immediately after thermalisation and that the process of thermalisation represents the rate determining step for electron retrapping.

Pursuing this assumption that the rate determining step for retrapping is the rate at which electrons can become thermalised, an energy transfer mechanism must be devised in which an electron can give up its energy to the vibrational modes of the system. Within this framework the electron is viewed as losing its energy in discrete amounts as it passes through the system following photoejection.

The following analysis, which requires a knowledge of the

vibrational excitation cross section by electron impact as a function of electron velocity calculates the average rate at which an electron loses its energy when only a single vibrational mode is available for excitation.

Rate at which electron loses first quantum = $v_1\sigma_1 N_V$

v_1 = incident electron velocity (cm sec^{-1})

σ_1 = vibrational excitation cross section by electron impact at incident velocity v_1 (cm^2)

N_V = number of molecules/cm^3

Rate at which second quantum is lost = $v_2\sigma_2 N_V$

where $v_2 = \left[\frac{sv_1^2-\varepsilon}{s}\right]^{\frac{1}{2}}$

sv_1^2 = initial electron energy, ε = energy of vibrational mode

Average time for loss of energy = $\bar{t} = \sum_i \frac{1}{v_i\sigma_i N_V}$

where $n = \frac{sv_1^2}{\varepsilon}$

The energy loss rate constant becomes

$$k_2 = \frac{1}{\bar{t}} = N_V\left[\sum_i \frac{1}{v_i\sigma_i}\right]^{-1}$$

When an electron can lose its energy to several different vibrational modes the analysis becomes more complicated since at each molecular encounter several possibilities exist. As the electron passes through the system it will interact with molecules and give up some of its energy. The probability that a certain vibrational mode is excited can be taken as being equal to the relative cross section of that vibration at the incident electron energy. This situation prevails at each encounter of which there are several. The set of vibrational excitations

which an electron leaves behind it after thermalisation constitutes a single path and the number of possible paths through the system is very large. The probability of a particular path being followed is the product of all the individual probabilities which constitute the path. For simple molecular systems and low initial electron energies the number of paths can be large.

(b) Thermalisation in Ice

The preceding analysis has been used to calculate the thermalisation rate constant k_2 for ice. To obtain an estimate of the variation of the above vibrational excitation cross sections with electron energy, the theory of Takayanagi, presented in Chapter 2.3 (ii) has been employed. The range of validity of theory in the gas phase has already been discussed. It is hoped that at least the variation of σ with $\underline{v}$ is sufficiently well represented to justify its application to solids.

The infra red active vibrational modes were taken from absorption spectra (62-65), which exhibit four main peaks corresponding to inter and intramolecular vibrations. Vibrational energies were taken from the respective band maxima. Table 4.1 summarises the relevant energies and transition moments taken from reference (64).

$\nu_i(cm^{-1})$	$\nu_i(ev)$	$10^{-6}\int K(\nu)\partial\nu$	$10^{19} \times \lvert u_{01}\rvert^2$ (cm^2)
3200	0.3968	6.86	6.673
1730	0.2145	1.14	2.051
840	0.1042	0.85	3.575
240	0.0298	0.24	3.087

TABLE 4.1 Properties of the infra red vibrations of ice.

For a particular initial electron energy, a maximum of twenty energy loss paths, as defined in 5.4 (iiia), were considered, these being chosen to range from the most to the least probable. The average rate constant for a particular initial energy was obtained by taking the weighted average of the rate constants for each of the possible paths. The weight factor for each path was calculated as the product of the relative cross sections for the set of vibrational excitations comprising the path, the relative cross section for vibration $\underline{i}$ at each encounter being that fraction of the total excitation area which the $\underline{i}^{th}$ vibration presents at the incident electron energy.

If the mean electron velocity $\bar{v}$ is defined in terms of the initial energy E_i by

$\bar{v} = \left(\frac{E_i}{2s}\right)^{\frac{1}{2}}$ where s is a conversion factor

then an average thermalisation distance $\bar{R}$ can be defined in terms of the rate constant k_2 by

$\bar{R} = \frac{\bar{v}}{k_2}$ since $\frac{1}{k_2}$ is the average half life for energy loss.

Figure 5.4.1 shows the variation of $\bar{R}$ and $1/k_2$ for initial electron energies in the range 0 - 2 ev. Although the half life curve lies within the correct time range (10^{-14} - 10^{-13} sec), comparison with experiment can only be made indirectly through the range parameter $\bar{R}$. Very little information exists, however, on the range of low energy electrons in liquids and solids, most observations having been made for high energy particles (54). Although classical calculations have been performed for electron ranges in water (66) and qualitative agreement exists with those

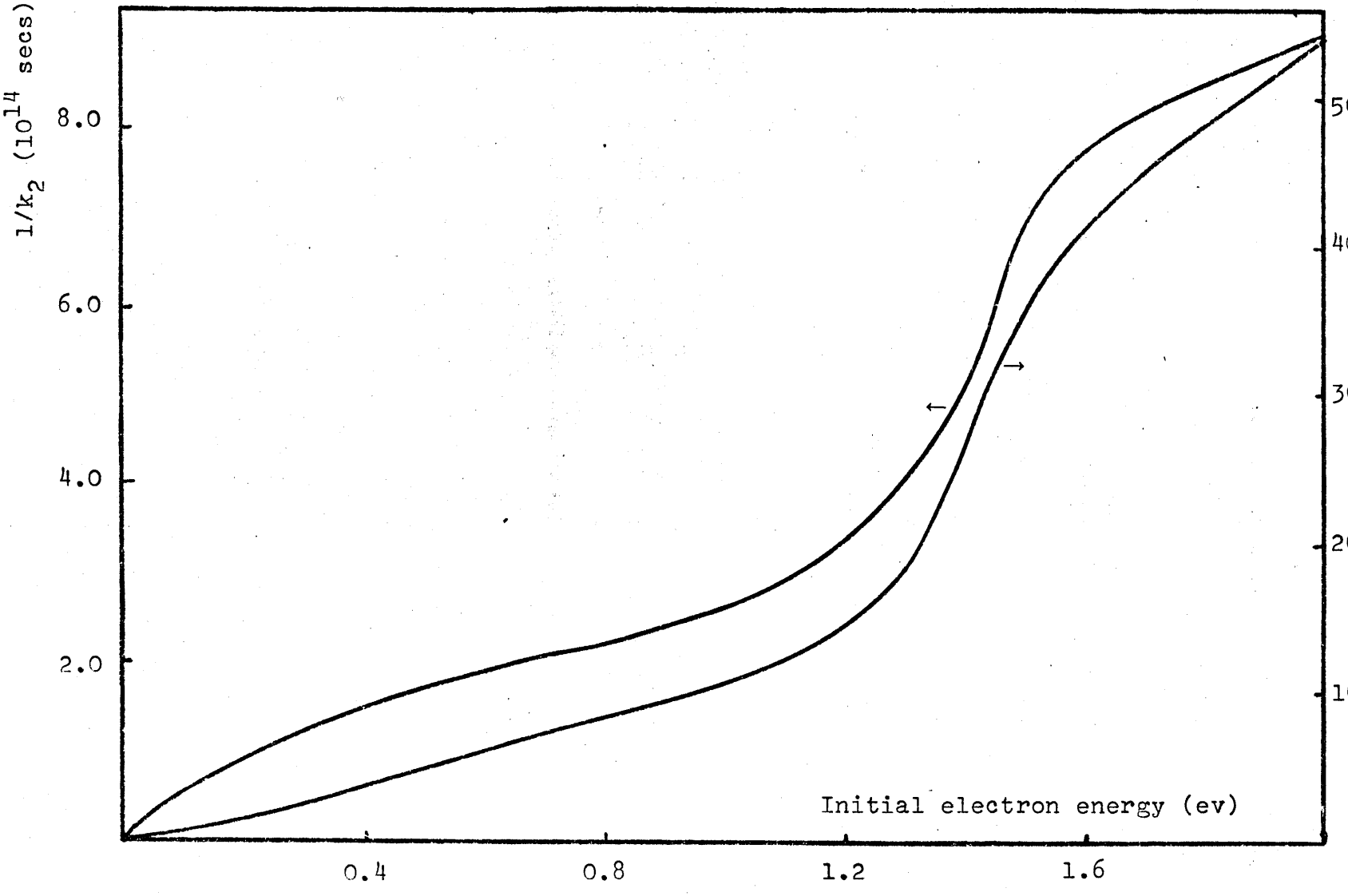

Figure 5.4.1

Variation of energy loss half life ($\frac{1}{k_2}$) and average thermalisation distance ($\bar{R}$) with initial electron energy.

of Figure 5.4.1, direct comparison is complicated since such calculations were concerned with electron escape from positive ions.

Recent experimental observations, however, on low energy electron ranges in liquid hydrocarbons confirm the magnitude of $\bar{R}$ and its general sensitivity to electron energy in this region (67). An approximate check on the relative magnitudes and variation of the calculated excitation cross sections can be made by comparing calculated values of the mean fractional energy loss for an electron molecule collision (68,69) with observed values for several molecules in the gas phase. In terms of the calculated cross sections, this quantity η is defined as

$$\eta(E) = \frac{\sum_i \sigma_i \varepsilon_i}{E \sum_i \sigma_i}$$

where σ_i and ε_i are the vibrational excitation cross section and excitation energy at electron energy $\underline{E}$.

Although values for $\eta(E)$ are not available for water in the range 0 - 2 ev, the comparison with CH_4 and N_2O (70) in Figure 5.4.2 show that calculated values of $\eta(E)$ for water have the expected magnitude and variation.

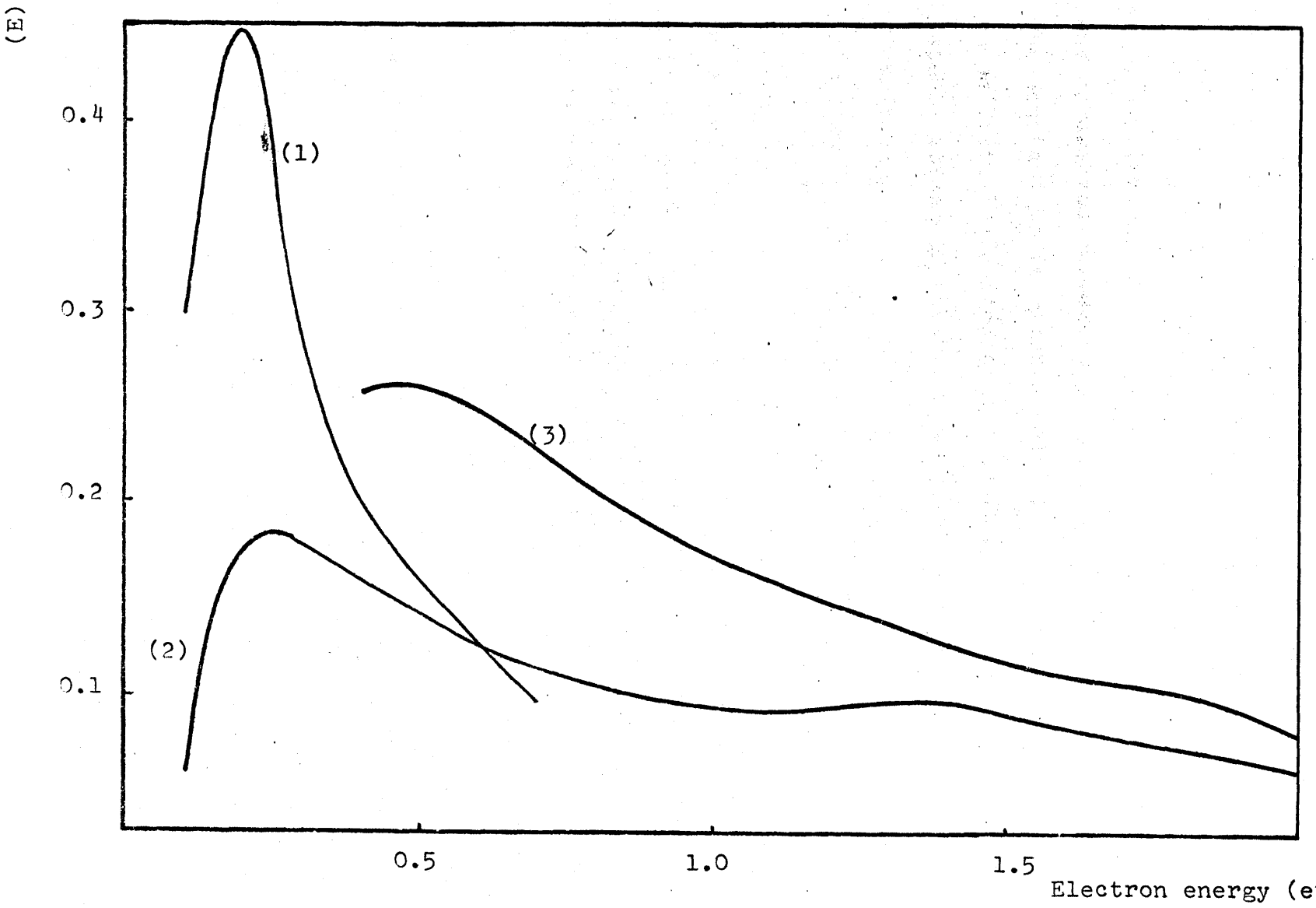

Figure 5.4.2

Mean fractional energy loss for electron-molecule collisions.

1 Observed for CH_4

2 Observed for N_2O

3 Calculated for ice

(iv) Photobleaching Quantum Efficiency in Ice

From the analysis of 5.4(ii), the photobleaching quantum efficiency, neglecting induced and spontaneous emission, is given by

$$Q(E) = \frac{k_3}{k_1+k_2+k_3}$$

with k_1 the rate constant for excitation from the ground state, k_3 the scavenging rate constant and k_2 the thermalisation rate constant calculated above.

The constant k_1 is given simply as $k_1 = \sigma_{ex}\Omega$, where σ_{ex} is the ground state ionisation cross section and Ω is the light flux. For a steady stream of electrons of velocity $\underline{v}$, being captured by a distribution of scavengers (N_s/cm^3) with capture cross section σ_s, the constant k_3 can be represented by (68)

$$k_3 = N_s v \sigma_s$$

The above analysis has been applied in the calculation of Q as a function of energy for ice, using the data of Kawabata (48). Based on the spectral evidence presented in Chapter 3.1 (i), it has been assumed that the photoionisation threshold lies at 1.9 ev.

The above formula for Q must then be amended to take into account the transition to a bound state in the range 1.9-2.3 ev

$$Q(E) = Q'(E).\ \frac{k_3}{k_1+k_2+k_3}$$

where Q'(E) is the fraction of light absorbed by the photoionisation process. The function Q'(E) has been calculated from the separated spectral components of Figure 3.1 on the assumption that the higher energy curve represents the ionisation spectrum. From the absorption spectrum the maximum cross section is found

to be 3.6×10^{-17} cm^2. Since the light intensities (48) are typically $5 \times 10^{15}/cm^2 sec$, the value of k_1 is calculated as 0.18 sec^{-1} and can be ignored in comparison with k_2 ($10^{13} sec^{-1}$). Hence

$$Q(E) = Q'(E). \frac{k_3}{k_3 + k_2}$$

The scavenging species in ice is believed to be the OH• radical (48,49) whose concentration at 77°K can be fixed at $2.7 \times 10^{19}/cm^3$. However, a proper calculation of the constant k_3 also requires a knowledge of the capture cross section of electrons by OH• radicals as a function of energy and no such information presently exists. To proceed further, it was therefore assumed that σ_s was only a slowly varying function of E in the 0 - 2 ev range considered and the calculated and the observed Q values were equated at a photon energy of 2.5 ev. In this it was assumed that the electron flux could be represented by the average electron velocity $\bar{v}$, giving

$$k_3 = \bar{v} N_s \sigma_s$$

with $\bar{v} = \left(\frac{E}{2s}\right)^{\frac{1}{2}}$ where E is the initial energy and s a conversion factor.

A final requirement of the model is a knowledge of the threshold energy of electrons in the conduction state. The energy of electrons at the threshold of ionisation will only be zero if the minimum in the configuration coordinate diagram of the conduction state lies vertically above that of the ground state. Semi-continuum calculations on water and ice (71,26) show that this is not the case and the most recent calculations (26) reveal that a threshold energy of 0.4 ev should be taken.

At the threshold of ionisation therefore ($h\nu$ = 1.9 ev), electrons are taken to have an initial energy of 0.4 ev.

The process of equating the curves at $h\nu$ = 2.5 ev yields $N_s\sigma_s = 6.01 \times 10^{4} cm^{-1}$. If OH· radicals are indeed the scavengers, then a value of $2.18 \times 10^{-15} cm^{2}$ is indicated for σ_s. This value is quite consistent with capture cross sections observed for many other electron scavengers (72).

The calculated and observed quantum efficiency curves are shown in Figure 5.4.3.

Discussion

The process of equating the calculated and observed curves at 2.5 ev makes the absolute agreement of the calculated quantum efficiency insignificant. In addition, the inclusion of the function Q'(E) causes the calculated curve to follow the observed one between 1.9 and 2.3 ev where Q'(E) becomes unity. It can be seen however, that the general shape above 2.5 ev is reproduced quite well despite the several assumptions implicit in the model.

The general increase in Q with photon energy is accomplished within the model by the ability of electrons to contact a greater number of scavengers as their ejection energy increases. This is facilitated by an energy loss mechanism which allows a greater electron range as initial energy increases, and hence the correctness of the details of the loss mechanism may not be a crucial factor in determining the properties of the resultant curve.

Implicit within the model is the assumption that capture by scavengers may occur with electrons which are above thermal energies. This is expected for most molecules in the gas phase,

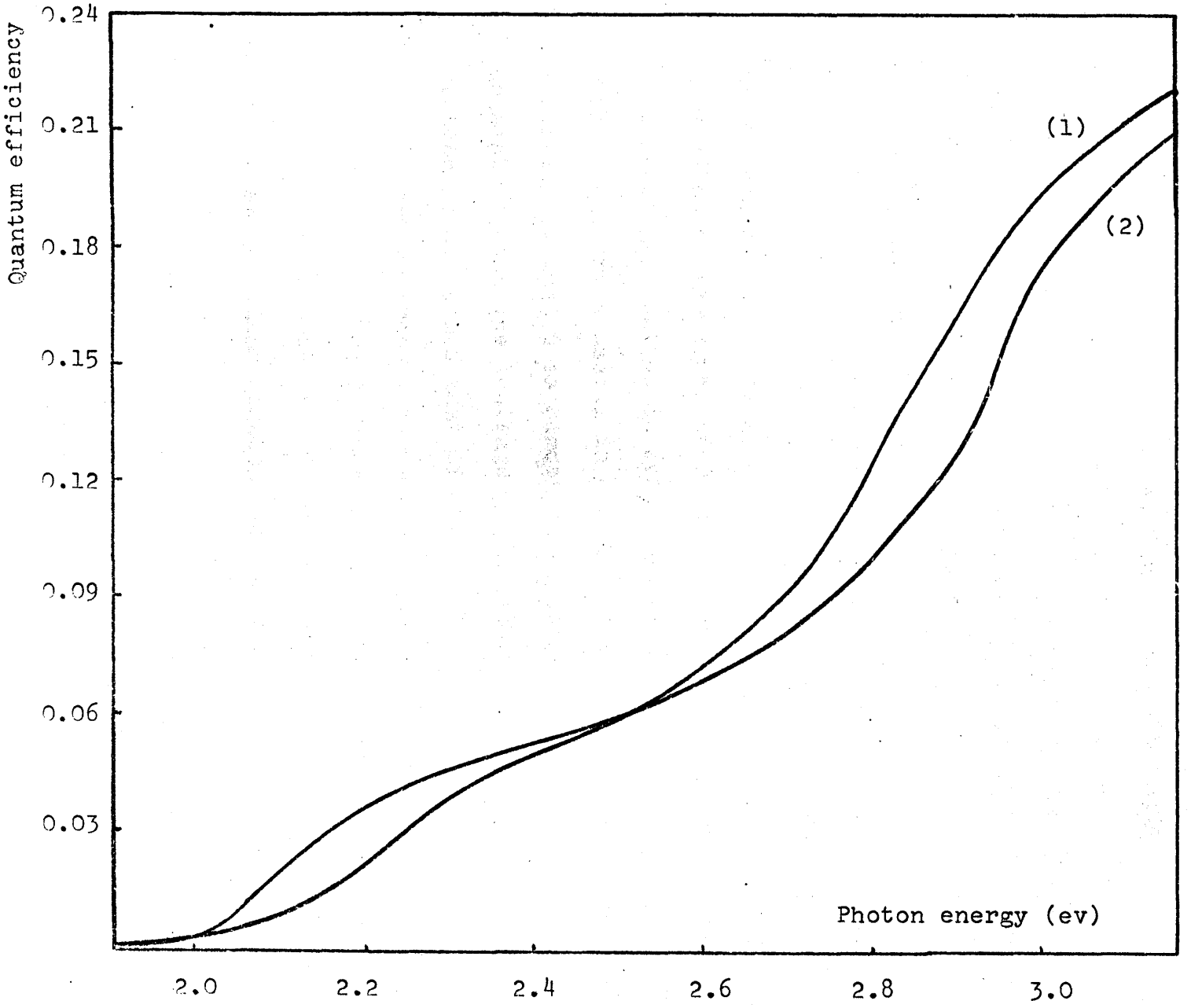

Figure 5.4.3

Variation of photobleaching quantum efficiency in ice with photon energy

1 Observed

2 Calculated

depending on the separation of the configuration curves for molecule and ion (54), and its operation in solids also is suggested by recent studies on methylcyclohexane (73), where the product of certain anions by electron capture was found to be dependent on the energy of light used to eject the electrons.

Some other properties of the photobleaching process have a possible explanation within the model presented. These are the dependence of Q on added scavengers and the tendency in some systems for Q to decrease with the fraction of electrons bleached. Since the rate constant k_3 depends on the scavenger density N_s, addition of scavengers would be expected to increase Q. The evidence presented in Chapter 3.3 shows that this is observed in many systems.

In systems in which the scavenger concentration is comparable with that of the trapped electrons, a significant decrease in scavengers and hence k_3 might be expected during bleaching, leading to a dependence of Q on the fraction bleached. This dependence is observed in some systems and not in others, a fact which might prove useful in deciding the nature of the scavenging species. In ice, Q is almost independent of fraction which is consistent with the scavenger being OH' radical, whose concentration is 10^3 times that of the electron.

A further property which may find a qualitative explanation within the model concerns the recent observation (74) that in some systems the efficiency curve has a high energy maximum. When additional mechanisms exist for electrons to lose their energy, the application of the simple dipole excitation analysis will cease to be valid. It is known for example, that

for vibrational excitation of N_2, resonance phenomena involving negative ion states operate at electron energies around 2 ev (69). Such resonance effects might be expected in other systems also, and their inclusion in the energy loss mechanism could have the effect of increasing k_2, and hence decreasing the bleaching efficiency, for electron energies above a certain value.

(v) A Tunneling Model for Photobleaching

In the discussion of Chapter 3.3 it was indicated that for some excess electron systems there is evidence to suggest that relatively long lived excited states are indirectly accessible by some interconversion process from an initial bound excited state, the latter being produced by light absorption. From the discussion and analysis of 5.3 it was shown that, within the model presented, substantial rates of electron scavenger recombination could be achieved by a tunneling mechanism from the ground state of the trapped electron. These two facts suggest that an additional mechanism for electron decay is one which involves tunneling from an excited state of the trapped species, and when this state is reached by a light absorption process, the mechanism formally becomes one of photo-induced decay or photobleaching.

The ground state decay analysis has shown that the spontaneous decay rate eventually becomes so small that effective stability is reached, and within the distribution model used, such behaviour is influenced by the scavenger concentration, electron parent ion separation and the barrier through which the electron must tunnel. Since the decreasing decay rate results from the preferential loss of short range species, the distribution function describing the population of electrons when effective stability is reached will be one which is deficient in the shorter electron scavenger distances.

It is expected however that the decay rate of such a population may be increased if the barrier through which they must tunnel is reduced. Such a situation results when excited states of the excess electron are produced since, within the tunneling model,

these are described by a different ionisation potential from that of the ground state.

Such induced decay may be described by the previous photobleaching kinetics. The excitation rate constant k_1 retains its previous form whilst the scavenging rate constant k_3 is now replaced by a tunneling constant and the retrapping constant k_2 now relates to a relaxation rate constant from the long lived state.

Using the electron distribution function previously employed for ground state decay gives for the ground state N_1

$$\frac{d}{dr}\left(\frac{dN_1}{dR}\right) = N_1 P(R)P(r)$$

where r refers to parent ion separation and R to bulk scavengers.

By means of the excitation process a population of excited states N_2 are produced whose distribution function derives from that of the ground state. Using the kinetics of 5.4.(ii) the process of excitation, relaxation and decay is represented by

$$\frac{d}{dr}\left(\frac{dN_1}{dR}\right) \underset{k_2}{\overset{k_1}{\rightleftharpoons}} \frac{d}{dr}\left(\frac{dN_2}{dR}\right) \xrightarrow{\lambda(R)+\lambda(r)} S$$

Assuming a steady state relation for the excited yields

$$\frac{d}{dr}\left(\frac{dN_2}{dR}\right) = \frac{k_1}{k_2+\lambda(r)+\lambda(R)} \cdot \frac{d}{dr}\left(\frac{dN_1}{dR}\right) \qquad (1)$$

Since the ground state decay is given by

$$\frac{d}{dt}\left[\frac{d}{dr}\left(\frac{dN_1}{dR}\right)\right] = k_2 \cdot \frac{d}{dr}\left(\frac{dN_2}{dR}\right) - k_1 \cdot \frac{d}{dr}\left(\frac{dN_1}{dR}\right) \qquad (2)$$

then

$$\frac{d}{dt}\left[\frac{d}{dr}\left(\frac{dN_1}{dR}\right)\right] = \frac{d}{dr}\left(\frac{dN_1}{dR}\right)\left[-\frac{k_1(\lambda(R)+\lambda(r))}{k_2+\lambda(R)+\lambda(r)}\right] \qquad (3)$$

This gives

$$\frac{d}{dr}\left(\frac{dN_1}{dR}\right) = \left[\frac{d}{dr}\left(\frac{dN_1}{dR}\right)\right]^{o} \exp\left\{-\frac{k_1(\lambda(R)+\lambda(r))t}{k_2+\lambda(R)+\lambda(r)}\right\} \qquad (4)$$

The initial distribution to which the pre-exponential factor refers is that which exists when photobleaching begins. Since this takes place at some time t^{o} after the formation of the trapped electron population then

$$\left[\frac{d}{dr}\left(\frac{dN_1}{dR}\right)\right]^{o} = N_1' P(R)P(r)\exp\left[-(\lambda'(R)+\lambda'(r))t^{o}\right]$$

where $\lambda'(R)$ and $\lambda'(r)$ refer to the ground state tunneling rate constant and N_1' is the initial electron concentration. Substituting in (4) yields

$$\frac{d}{dr}\left(\frac{dN_1}{dR}\right) = N_1' P(R)P(r)\exp\left\{-\frac{k_1(\lambda(R)+\lambda(r))t}{k_2+\lambda(R)+\lambda(r)} - (\lambda'(R)+\lambda'(r))t^{o}\right\} \qquad (5)$$

When the effective range of integration of (5) is such that $k_2 \gg \lambda(R), \lambda(r)$ then (5) becomes

$$\frac{d}{dr}\left(\frac{dN_1}{dR}\right) = N_1' P(R)\exp\left[-\frac{k_1}{k_2}\lambda(R)t - \lambda'(R)t^{o}\right]P(r)\exp\left[-\frac{k_1}{k_2}\lambda(r) - \lambda'(r)t^{o}\right] \qquad (6)$$

The quantum efficiency for photobleaching is given as before by the ratio of the rate of loss of ground state electorns and the rate excitation

$$Q = -\frac{dN_1/dt}{k_1 N_1} = -\frac{dR/dt}{k_1 R}$$

where $R = \frac{N_1}{N_1'}$

In the above it is assumed that the interconversion process is rapid compared with the rate of any relaxation process occurring from the initial excited state, allowing the former to be represented by k_1.

Very little information exists as to the value of the relaxation rate constant k_2 in the media for which long lived excited states are thought to exist. In ionic solids however relaxation times for the excited states between 10^{-6}-10^{-5} sec have been observed (75). Calculations on the radiative lifetimes of p states in these media have yielded values of the correct order, the long lifetimes being partly due to the smaller transition moment for emission resulting from lattice relaxation (76).

For low temperature non-radiative processes from presumed s type states of non-ionic media it might be expected that lifetimes of the same order or longer would be applicable.

(a) Sample Estimates for MTHF and 3MH

Using the preceding analysis, sample calculations have been carried out using the well parameters for methyltetrahydrofuran and 3 methyl hexane, the two media for which long lived excited states are thought to exist. For the parameters used, the approximation involved in equation (6) has been found to be valid, and since only recombination with scavengers in the bulk of the medium has been considered, the parent contribution to equation (6) can be neglected giving

$$\frac{dN_1}{dR} = N_1' P(R) \exp\left[-\frac{k_1}{k_2}\lambda(R)t - \lambda'(R)t^o\right] \qquad (7)$$

The delay time t^o has been taken as 2min in all cases and the tunneling rate constant $\lambda(R)$ has been assigned the same form

as before

$$\lambda(R) = k\, e^{-cR} \qquad k = 10^{15}$$
$$c = 1.0202\, I^{\frac{1}{2}}$$

The constant k_1 has been described in 5.4(iv) where it was taken as $k_1 = \sigma\Omega$ where σ is the excitation cross section and Ω the light flux. Since σ is typically $3\times10^{-17}cm^2$ and the light flux usually around $5\times10^{15}/cm^2sec$, a value of 10^{-1} has been used for k_1 throughout. Summarised below are the ionisation potentials for the ground and excited states of the two media, consistent with the current spectral evidence as presented in 3.1 and 3.3.

	MTHF		3MH	
	$\lambda(R)$	$\lambda'(R)$	$\lambda(R)$	$\lambda'(R)$
I (ev)	1.08	1.60	1.00	0.70

Values for the relaxation constant k_2 have been chosen from 10^3-10^5 sec^{-1} and for scavenger concentrations, values of 10^{-1} and 10^{-2}M have been used . Tables 4.2 and 4.3 show the calculated quantum efficiencies Q, evaluated 400 sec after the start of bleaching.

TABLE 4.2

scavenger molarity(M)	k_2 (sec^{-1})	Q ($\times10^3$)
0.01	10^3	0.563
	10^4	0.0638
	10^5	0.00647
0.10	10^3	4.614
	10^4	0.719
	10^5	0.0518

Bleaching efficiency for 3 methyl hexane

TABLE 4.3

scavenger molarity(M)	k_2 (sec^{-1})	Q ($x10^3$)
0.01	10^3	0.473
	10^4	0.0583
	10^5	0.00597
0.10	10^3	4.122
	10^4	0.497
	10^5	0.0508

Bleaching efficiency for methyltetrahydrofuran.

The results show that except for excited state lifetimes in the msec range, the quantum efficiencies are small. It can also be seen that Q is almost inversely proportional to k_2. As a result of the manner in which k_1 and k_2 appear in equation (7), this dependence also makes Q almost independent of k_1 and hence no wavelength dependence is expected for this bleaching mechanism.

Increasing the scavenger concentration has the expected effect of increasing Q. However, for concentrations in the range for which Q is measurable (10^{-1}M), it might be expected that bleaching efficiencies resulting from two photon ionisation would mask the tunneling effect (77). This could be avoided however by the use of light in the low energy part of the spectrum ie. below the second absorption threshold.

Systems for which such a method of bleaching could be important are those which have (i) a long lived excited state, (ii) a large ground state well depth and (iii) an excited state which is close to the conduction state. The second factor is needed

since it preserves the short electron-scavenger distances which would then provide high decay rates from the excited state, particularly when the latter experienced only a small tunneling barrier.

REFERENCES

1 G. C. Pimentel, A. D. McClellan "The Hydrogenbond" W. A. Freeman & Co. (1960)

2 L. Pauling Proc. Nat. Acad. Sci. 14,359,(1928)

3 J. Lennard-Jones, J. A. Pople Proc. Roy. Soc. A205,155,(1951)

4 J. A. Rowlinson Trans. Far. Soc. 47,120,(1951)

5 J. A. Pople, D. P. Santry, G. A. Segal J. Chem. Phys. 43,5129,(1965)

6 J. A. Pople, D. L. Beveridge, P. A. Dobosh J. Chem. Phys. 47,2027,(1967)

7 J. A. Pople, G. A. Segal J. Chem. Phys. 44,3289,(1966)

8 J. L. Whitten J. Chem. Phys. 44,359,(1966)

9 H. F. Schaefer 'The Electronic Structure of Atoms and Molecules' Addison-Wesley (1972)

9 S. H. Lin 'Physical Chemistry - An Advanced Treatise' H. Eyring, D. Henderson, W. Jost, Acad. Press New York (1970)

10 S. Bratoz Adv. Quantum Chem. 3,209,(1967)

11 K. Morokuma, L. Pederson J. Chem. Phys. 48,3275,(1968)

12 P. A. Kollman, L. C. Allen J. Chem. Phys. 51,3286,(1969)

13 K. Morokuma, J. Winick J. Chem. Phys. 52,1301,(1970)

14 J. Del Bene, J. A. Pople J. Chem. Phys. 52(a),4858,(1970)

15 D. Hankins, J. W. Moskowitz, F. H. Stillinger J. Chem. Phys. 53,(12), 4544,(1970)

16 J. R. Hoyland, L. B. Kier Theor. Chim. Acta. 15,1,(1969)

17 P. A. Kollman, L. C. Allen J. Amer. Chem. Soc. 92,753,(1970)

18 H. Tsubomura Bull. Chem. Soc. Jap. 27,445,(1954)

19 C. A. Coulson, V. Danielsson Arkiv. fur Fys. 8,245,(1954)

C. A. Coulson Research 10,149,(1957)

20 R. Grahn Arkiv. Fys. 15,257,(1959)

21 K. Morokuma J. Chem. Phys. 55(3),1236(1971)

22 P. A. Kollman, L. C. Allen Theor. Chim. Acta. 18,399(1970)

23 M. Dreyfus, A. Pullman Theor. Chim. Acta. 19,20,(1970)

24 P. A. Dobosh Quantum Chemistry Program Exchange No. 141

25 J. A. Pople, D. L. Beveridge 'Approximate Molecular Orbital Theory' McGraw-Hill (1970)

26 K. Fueki, D. F. Feng, L. Kevan J. Amer. Chem. Soc. 95(5),1398,(1973)

27 K. Fueki, D. Feng, L. Kevan, R. E. Christoffersen J. Phys. Chem. 75,2297,(1971)

28 N. R. Kestner, J. Jortner J. Phys. Chem. 77(8),1040,(1973)

29 M. Natori, T. Watanabe J. Phys. Soc. Japan 21(8),1573,(1966)

30 P. M. Rentzepis, R. P. Jones, J. Jortner J. Chem. Phys. 59(2),766,(1973)

31 M. J. Bronskill, R. K. Wolff, J. W. Hunt J. Chem. Phys. 53(11),4201,(1970)

32 K. Kawabata, H. Horii, S. Okabe Chem. Phys. Lett. 14(2), 223, (1972)

33 G. Nilsson J. Chem. Phys. 56(7),3427,(1972)

34 A. von Hippel, D. B. Knoll, W. B. Westphal J. Chem. Phys. 54(1),134,(1971)

35 R. P. Auty, R. H. Cole J. Chem. Phys. 20(8),1309,(1952)

36 T. Kajiwara, K. Funabashi, C. Naleway Phys. Rev. A.6,808, (1972)

37 M. Tachiya, Y. Tabata, K. Oshma Chem. Phys. Lett. 19(4), 588,(1973)

38 K. Kawabata J. Chem. Phys. 55(8),3672,(1971)
K. Kawabata, S. Okabe, S. Taniguchi J. Chem. Phys. 57(7) 2855,(1972) K. Kawabata, H. Horii, S. Okabe, Chem. Phys. Lett. 14(2),223,(1972)

39 H. Hase, L. Kevan J. Chem. Phys. 54(3),908,(1971)

40 D. R. Hartree 'Calculation of Atomic Structures' Wiley (New York)

41 G. Kuper, G. D. Whitfield 'Polarons and Excitons' (Plenum, New York)

42 K. I. Zamaraeu, R. F. Khairutdinov Chem. Phys. 4,181,(1974)

43 J. R. Miller J. Chem. Phys. 56(10),5173,(1972)

44 J. R. Miller, J. E. Willard J. Phys. Chem. 76(18),2641(1972)
J. R. Miller Chem. Phys. Lett. 22(1),180,(1973)

45 J. L. Magee J. Amer. Chem. Soc. 73,3270,(1951)
A. H. Samuel, J. L. Magee J. Chem. Phys. 21(6),1080,(1953)
A. K. Ganguly, J. L. Magee J. Chem. Phys. 25(1),129,(1956)

46 A. Mozumder, J. L. Magee Rad. Res. 28,203,(1966)
J. L. Magee, M. Burton J. Amer. Chem. Soc. 73,523,(1951)
H. A. Schwarz J. Phys. Chem. 73(6),1928,(1969)

47 G. C. Abell, K. Funabashi J. Chem. Phys. 58(3),1079,(1973)

48 K. Kawabata J. Chem. Phys. 55(8),3672,(1971)

49 I. A. Taub, K. Eiben J. Chem. Phys. 49(6),2499,(1968)

50 N. V. Kassen, H. A. Gillis, G. G. Teather J. Phys. Chem. 76(25),3847,(1972)

51 J. B. Gallivan, W. H. Hamill J. Chem. Phys. 44(3),1279,(1966)

52 J. R. Miller, J. E. Willard J. Phys. Chem. 76,(16),2341,(1972)

53 D. R. Smith, J. J. Pieroni Can. J. Chem. 43,876,(1965)

54 D. Shooter, J. E. Willard J. Phys. Chem. 76(22),3167,(1972)

55 W. M. McClain, A. C. Albrecht J. Chem. Phys. 44(4),1594,(1966)

56 L. Kevan J. Phys. Chem. 76(25),3830,(1972)

57 C. D. Jonah, E. J. Hart, M. S. Matheson J. Phys. Chem. 77(15),1838,(1973)

58 R. K. Wolff, M. J. Bronskill, J. E. Aldrich, J. W. Hunt J. Phys. Chem. 77(11),1350,(1973)

59 D. Eisenberg, W. Kauzmann 'The Structure and Properties of Water' (O.U.P. New York, 1969)

60 G. Kenney-Wallace, D. C. Walker J. Chem. Phys. 55(1),447,(1971)

61 K. Fueki, D. F. Feng, L. Kevan J. Phys. Chem. 78(4),393,(1974)

62 M. Falk, T. A. Ford Can. J. Chem. 44,1699,(1966)

63 T. A. Ford, M. Falk Can. J. Chem. 46,3579,(1968)

64 J. E. Bertie, H. J. Labbé, E. Whalley J. Chem. Phys. 50(10),4501,(1969)

65 J. W. Schaaf, D. Williams J. Opt. Soc. Amer. 63(6),726,(1973)

66 A. H. Samuel, J. L. Magee J. Chem. Phys. 21(6),1080,(1953)
R. Schiller J. Chem. Phys. 43(8),2760,(1965)
R. Schiller J. Chem. Phys. 47(7),2278,(1967)

67 R. A. Holroyd, B. K. Dietrich, H. A. Schwarz J. Phys. Chem. 76(25),3794,(1972)

68 D. R. Bates (Ed.) 'Atomic and Molecular Processes' Academic Press (New York)

69 H. S. W. Massey, E. H. S. Burhop 'Electronic and Ionic Impact Phenomena' Vols. 1 & 2 Clarendon Press

70 L. G. Christophorou, J. G. Carter Chem. Phys. Lett. 2(8), 607,(1968)

71 K. Fueki, D. F. Feng, L. Kevan J. Phys. Chem. 74(9),1976, (1970) K. Fueki, D. Feng, L. Kevan, R. E. Christoffersen J. Phys. Chem. 75,2297,(1971)

72 L. G. Christophorou J. Phys. Chem. 76(25),3730,(1972)
L. G. Christophorou, R. P. Blaunstein Chem. Phys. Lett. 12(1),173,(1971) K. G. Mothes, E. Schultes, R. N. Schindler J. Phys. Chem. 76(25),3758,(1972)

73 T. B. Truong, A. Bernas, J. Roncin J. Phys. Chem. 78(9), 867,(1974)

74 A. Bernas, D. Grand, T. B. Truong J. Chem. Soc. Chem. Comm. 759,(1972)

75 W. B. Fowler 'Physics of Colour Centres' Academic Press(1968)

76 W. B. Fowler Phys. Rev. 135,1725,(1964)

77 P. J. Dyne, O. A. Miller Can. J. Chem. 43,2696,(1965)